An investigation of secondary flow in a turbine blade with end wall profiling

Punitha Jayaraman

An Investigation Of Secondary Flow In A Turbine Blade With End Wall Profiling

by

P.Jayaraman

School of Engineering

University of Durham

1999

This Thesis is submitted to satisfy the partial fulfilment of the requirements for the M.Sc.(Research).

Acknowledgement

I would like to express my gratitude to my supervisor, Dr. David Gregory-Smith for his advise, guidance and assistance. His constructive comments during the writing of this thesis were most appreciated. His encouragement and criticisms have also been most helpful. He has been a constant source of new ideas and suggestions throughout this project, which has made it very interesting and challenging. I would also like to acknowledge the financial support from Rolls Royce plc. and University of Durham.

I would also like to thank the staff of the School of Engineering and the technicians in the mechanical and electrical workshop as they have been of constant assistance throughout the duration of my course. In particular, I thank Mr. Allen Swan for his great help on the manufacturing of the end wall profile, Mr. Gary Parker and Mr. Ray Mand for their assistance during the installation of the cascade.

I am also grateful to Dr. Neil Harvey and Dr. Martin Rose and other members of the Turbine Aerodynamics Design group from Rolls Royce plc. for their informative discussions and suggestions.

I am indebted to my parents and my brothers for their support, motivation and sponsorship. Lastly, but not least my colleague A.Gkiouvetsis for being a great source of motivation, competition and information.

Punitha Jayaraman

December 1999

Abstract

Secondary flows have been long recognised as a significant form of loss mechanism in turbomachinery. They have a major influence over the performance of the blade rows since they cause unsteadiness in the mainstream flow. This consequently affects not only the mechanical integrity of the blades but also causes extra loss.

This research is aimed to reduce secondary flows using a novel method; end wall profiling. Profile 2 end wall was designed by Rolls Royce plc. with improved design features compared to its predecessor, Profile 1 end wall. Profile 2 end wall was manufactured and tested using the test facility available at the University of Durham. The flow was measured at two different axial positions, together with end wall static measurements and flow visualisation. The inlet flow conditions were also checked for consistency. These results were analysed and compared to Profile 1 and Planar end wall profile results, which have been studied previously by Hartland [1999]. Profile 2 end wall achieved better secondary flow reduction compared to the Planar end wall. However Profile 1 end wall still proved to be better compared to both Profile 2 and the Planar end wall.

This project has provided a thorough understanding of the various flow mechanisms in turbines and the available techniques in eliminating secondary flows. The application of end wall profiling has still shown potential in being a reliable method. It is also important that the flow physics is understood in detail to determine the shape of the end wall profile that will be effective.

Contents

Nomenclature

C	Blade true chord
C_{ax}	Blade axial chord
C_{TU}	Total pressure loss coefficient
C_{PS}	Static pressure coefficient
C_{SKE}	Upstream total pressure
C_{Snet}	Net secondary loss coefficient
C_{Pinlet}	Total pressure loss coefficient at inlet
C_{Pmid}	Mid span profile loss coefficient
$C_{TU\infty}$	Mixed-out total pressure loss coefficient
$\overline{C_{TU}}$	Pitch averaged total pressure loss coefficient
$\overline{\overline{C_{TU}}}$	Mass averaged total pressure loss coefficient
$\overline{C_{SKE}}$	Pitch averaged secondary kinetic energy coefficient
$\overline{\overline{C_{SKE}}}$	Mass averaged secondary kinetic energy coefficient
α_m	Vector mean angle
α_{mid}	Mid-span angle
$\overline{\alpha}$	Pitch averaged yaw angle
$\overline{\overline{\alpha}}$	Mass averaged yaw angle
h	Blade half span
P_{TL}	Local total pressure
P_{TU}	Upstream total pressure
P_{SL}	Local static pressure
P_{SU}	Upstream static pressure

r	Radius of curvature of boundary layer
R	Radius of curvature of mainstream flow
s	Blade pitch
v	Boundary layer velocity
V	Mainstream flow velocity
V_U	Upstream velocity
V_{TR}	Secondary velocity
V_1, V_2, V_3	Mean velocity components
x, y, z	Streamwise co-ordinates
ρ	Density
ξ_{sec}	Secondary vorticity
ξ_n	Normal vorticity
ε	Turning angle of the flow

Chapter 1 Introduction

The designs of modern turbines are characterised by high pressure turbines having low aspect ratio stages or by low pressure turbines having high aspect ratio with strongly varying end wall geometries. Pressure losses in such machines arise primarily from viscous effects, resulting from the interaction of boundary layers, which develop on the blade and end wall surfaces. The portion of the total pressure loss that is attributable to the nominally two-dimensional blade surface boundary layer is called profile loss of the blade. There is also a tip leakage loss due to the clearance between the tip of the blades and the casing. Convention has relegated the remainder of the loss as secondary flow loss. This flow is associated with a velocity field not in the primary flow direction. Research in the past and present has repeatedly showed that secondary loss is a major constituent of the total blade row loss.

The existence of secondary flows has been recognised since the 1950's and investigations have been undertaken to understand this phenomenon and its effects. As a consequence, it is now possible to pinpoint the main design parameters that influence the growth of secondary flows. With this information, various researchers have focussed their work into inhibiting the generation or growth of secondary flows by manipulating the related design variables in a turbine. Many methods have been introduced and analysed with experiments carried out to validate its efficiency to control the three-dimensional flow. These methods include boundary layer fences and trips, radial slots, leaned blades and even blowing and suction of the inlet boundary layer. However the results of these investigations have been inconclusive.

Fortunately, end wall profiling is a promising technique that has been given much attention by many researchers. It involves influencing the flow field through a blade passage whether a rotor or a stator by contouring the wall of the casing or the hub between the blades, shown in Figure 1.1. In order to develop the optimum profile shape, it is first necessary to understand the flow characteristic and the influence of pressure gradient on the flow. This is then followed by carefully introducing curvatures whether convex or concave or both, to influence the pressure field. This in the past this has been pursued through trial and error with thorough experiments together with supporting correlations to study each profiled end wall. More recently with the advancement of computing technology, computational fluid dynamics (CFD) has been more popular since it consumes far less time to compute multi-variable equations. However, CFD is still at its infancy stage and requires more improvement before it could be totally relied upon for predicting the flow evolution in the blade passage.

In this investigation, secondary flows are studied in a rotor blade row in a linear turbine cascade. The work is aimed to influence and reduce the secondary flows in the blade row through end wall profiling. The design of the end wall has been analysed and produced using CFD at Rolls Royce plc. Hence, this research involved manufacturing the profile, followed by experimental investigation to understand the influence of the curvature of the end wall on the flow field.

The work previous to this has been carried out by Hartland [1999]. He first investigated experimentally the end wall proposed by Rose [1994] with modification for the low speed linear cascade. Once the results had been

compared with the CFD predictions so as to assess the reliability of the CFD technique, a new end wall profile (Profile 1) was created. Profile 1 end wall has been tested and evaluated with respect to CFD predictions. With further understanding of the flow physics and the effects of the end wall contouring, another end wall profile was designed. This new profile (Profile 2) is the profile that was tested experimentally using the Durham linear cascade for this investigation.

This thesis will first begin with a general description of secondary flow in turbines including the related vortices along with a review of its origin and generation. This chapter also covers the prediction and reduction methods emphasising on end wall profiling. Chapter 3 gives a detailed description of the experimental apparatus and techniques. It also includes the Profile 2 manufacturing procedure and also the definitions of the quantities calculated which are presented in Chapter 4. This chapter discusses the measurements that have been taken and presents the experimental results. The next chapter will discuss the results in general and finally some conclusions and recommendations for further work are given in Chapter 6.

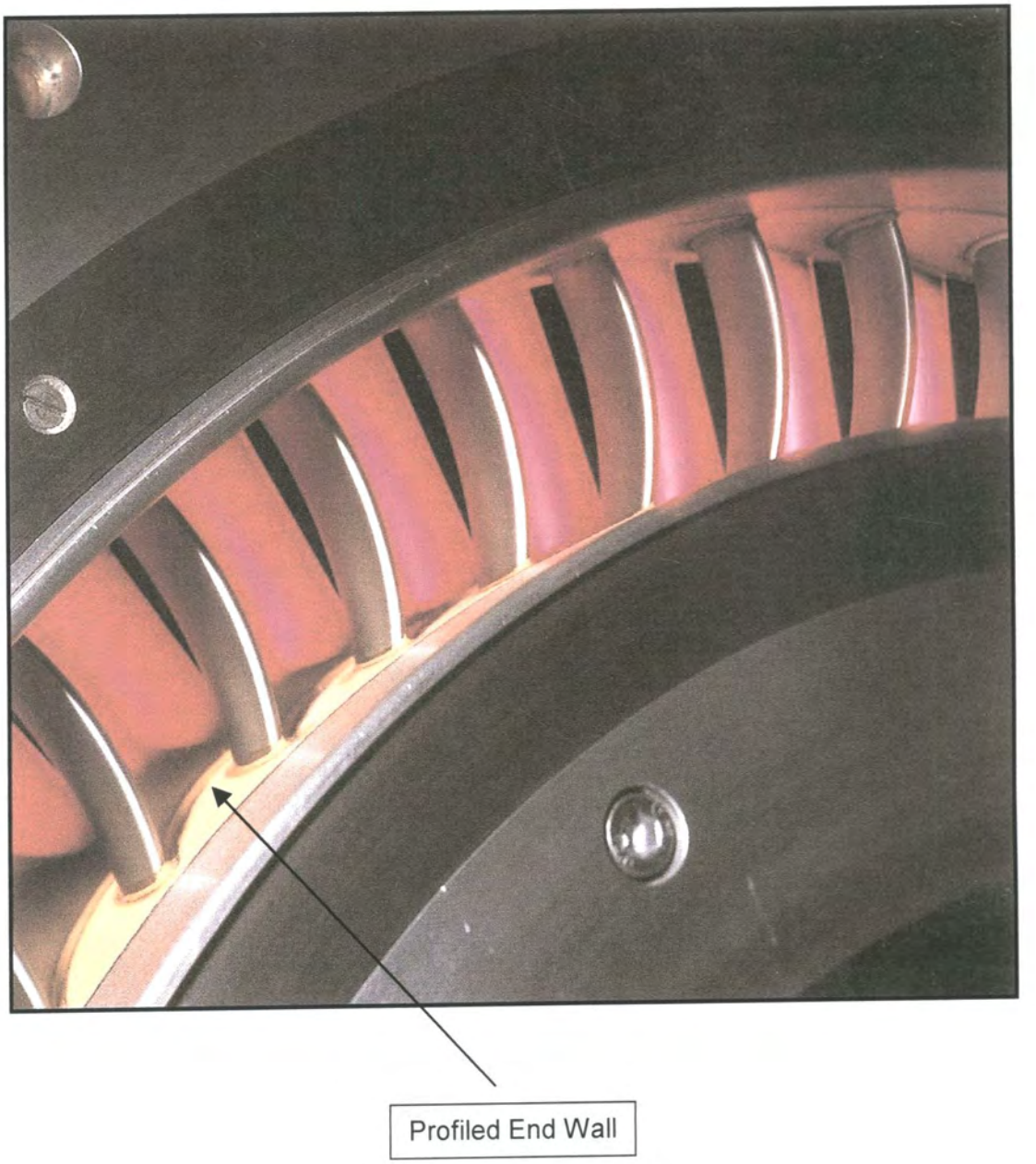

Figure 1.1 A Profiled End Wall

Chapter 2 Secondary Flows And Reduction Methods

This chapter reviews the experimental investigations of the flow through a turbine blade row and methods available to reduce secondary flows. The main flow features, the loss generation mechanisms and the distribution of secondary flows are discussed. This discussion is restricted mainly to the simplified flow found in linear cascades and briefly on the differences of the flow found in a real turbine and a linear cascade. This chapter is aimed to highlight the areas of flow that are important with respect to loss production and those that require detailed investigation. The various techniques available for the reduction of secondary flow will also be discussed with emphasis on end wall profiling.

2.1 Definition Of Secondary Flow

In an axial turbomachine when the flow is turned through an angle, the flow far from the end walls, hub or casing, may often be considered a two-dimensional flow. However near the end wall region, the boundary layer at inlet contains a spanwise velocity gradient. Transverse velocities are produced when this boundary layer is turned. This three-dimensional flow is called the secondary flow. The reason for the formation of secondary flow can be understood with reference to Figure 2.1 by Gregory-Smith [1997].

The primary flow sets up a pressure gradient across the blade passage from the pressure to suction surface. This causes the slower moving boundary layer, which is subjected to this same pressure gradient to flow from the

pressure to the suction surface. This relationship between the pressure gradient and the radius of curvature is given below.

$$\frac{\delta P}{\delta R} = \frac{\rho V^2}{R} = \frac{\rho v^2}{r} \qquad \text{Equation 2.1}$$

where ,

$\frac{\delta P}{\delta R}$	=	pressure gradient
V	=	mainstream velocity
v	=	boundary layer velocity
R	=	radius of curvature of mainstream
r	=	radius of curvature in the boundary layer

Since the velocity in the boundary layer is smaller than that in the mainstream, then the radius of curvature will also follow the same trend. The action of the boundary layer fluid having to follow a tighter radius of curvature causes over-turning of the flow. Hence, the flow on the end wall is directed from the pressure surface to the suction surface. In order to preserve continuity, there is a back flow away from the end wall, which causes under turning of the flow, as illustrated in Figure 2.2. Squire and Winter [1951] were the first to point out the importance of the turning angle on the secondary flow. They showed that (see Equation 15 of the paper) the secondary vorticity is twice the normal vorticity times the difference between the inlet and the outlet angle i.e.

$$\xi_{sec} = -2\,\xi_n\,\varepsilon \qquad \text{Equation 2.2}$$

It is important to note that although the inlet boundary layer on the end wall is produced by the act of viscosity, the phenomenon of secondary flow is an

inviscid effect. It is actually produced by the action of pressure and inertia forces with the presence of the sheared flow, and the direct action of viscous forces on the secondary flow is of minor importance. Secondary flows also occur when a developed pipe flow enters a bend, or when a boundary layer meet an obstacle normal to the surface over which it is flowing.

In turbomachinery, the performance is highly dependent on the secondary flows especially for those with low aspect ratio blades where secondary loss could probably be the most significant loss mechanism. The secondary flow structure both convects low momentum fluid from the boundary layers to the free stream and causes radial non-uniformities in the blade row exit angle. Both of these may have a detrimental effect on the performance of the following blade row, further reducing efficiency. This increased unsteadiness of the flow may also affect the mechanical design of the blades. Furthermore, transfer of heat may be enhanced by the secondary flow in the blade row, in turn making film cooling less effective.

2.2 Flow Features In A Turbine

Turbomachinery secondary flow has been studied in detail by a number of authors, for example; Marchal and Sieverding [1977], Langston, Nice, Hooper [1977], Gregory-Smith and Graves [1983] and Denton [1993]. Sieverding [1985] carried out a comprehensive review of the existing work to hand where he presented a detailed description of these flow structures and their effect on the boundary layers and loss growth. Denton [1993] also reviewed the current knowledge of losses in turbomachinery. The main aspects of the secondary flow

are described below and the structure of the flow is shown in Figure 2.3 taken from Binder [1985].

Passage Vortex

As fluid is turned through the blade channel, a cross channel pressure gradient is set up. This pressure gradient causes an over-turning of the low momentum fluid in the end wall boundary layer in the passage. This in turn causes the fluid to migrate from the pressure surface to the suction surface. When this boundary layer fluid reaches the suction surface, it moves radially outward up the blade surface away from the end wall and towards the mid span. New fluid moves radially towards the end wall to replace the old boundary layer, and hence a large vortex structure is formed near the suction surface. This is known as the passage vortex.

The passage vortex grows in size and migrates towards the suction surface as it progresses through the blade passage. This vortex is at first centred near to the end wall of the cascade after which it begins to move away (Gregory-Smith and Cleak [1990]). Gregory-Smith and Graves [1983] has also described the passage vortex movement as shown in Figure 2.4. The movement was understood to be caused by the mutual convection of the vortex by its mirror image in the end wall. The amount of movement is believed to be linked to the strength of the vortex. The movement is smaller and the vortex stands closer to the end wall in a low turning nozzle passage than in a high turning rotor blade.

Horseshoe Vortex

As the end wall boundary layer upstream of the blade row meets the blade leading edge, it rolls up to form a horseshoe vortex. This vortex is formed around the leading edge in the same way as around any blunt body such as a cylinder with its axis perpendicular to the wall. In a turbine blade, the horseshoe vortex consists of two legs, which flow around both sides of the leading edge of the blade. The pressure surface leg of the horseshoe vortex quickly moves away from the blade pressure surface and migrates across the end wall where it is believed to merge with the passage vortex (Langston et. al. [1977]). While crossing the blade passage, this leg rolls up most of the inlet boundary layer which is then discharged from the blade row in the form of a loss core on the suction surface a small distance from the end wall. This pressure side leg rotates in the same sense as the passage vortex. This is shown diagrammatically in Figure 2.3.

The suction side leg of the horseshoe vortex is convected up the blade suction surface and it rotates in the opposite sense to the passage vortex. Moore and Smith [1984] contributed an essential piece of information, which measured the flow trajectories by ethylene detection on the exit plane. The authors found that the ethylene injected at the location of the suction side branch of the horseshoe vortex near the blade leading edge was convected around the passage vortex core, while ethylene injected into the pressure side branch of the horseshoe vortex was found in the centre of the vortex. Research carried out by Marchal and Sieverding [1977] using smoke visualisations shows that the suction side vortex rotates on the mid span side of the passage vortex as in

Figure 2.3. However Langston [1980] sees the suction side leg of the horseshoe leg continuing in the suction side end wall corner. He concluded that the final location of this vortex was thought to depend on the rotational speed of the passage vortex, which in turn depends on the cascade geometry and the overall flow conditions.

Counter Vortex

A new highly skewed boundary layer is formed on the end wall downstream of the pressure side leg of the horseshoe vortex. As this strong cross flow meets the suction surface, a small counter vortex is formed in the corner. It is formed by a stagnation process similar to that which forms the horseshoe vortex. This counter vortex reduced over turning in line with the trailing edge and increases loss as it moves downstream.

Vortices Downstream Of Blades

The passage vortex is seen as the dominant feature downstream of the blade exit together with the effect of the corner counter vortex. Also evident downstream is streamwise vorticity shed from the trailing edge of the blades. This is in the form of vortex sheet and is illustrated in Figure 2.5 taken from Sieverding [1985]. There are two component of trailing vorticity which are not two separate physical phenomena but arise through mathematical modelling using the classical secondary flow theory by Came and Marsh [1974]. The two components are called 'trailing shed vorticity' and 'trailing filament vorticity'. The first arises from the circulation variation along the blade, and the second from the

stretching of the vortex filaments around the blade. In reality, the vortex sheet rolls up into discrete vortices between the passage vortices. As the flow proceeds downstream, the effect of viscous action slowly dissipates the vortices. However in a real turbine, little dissipation takes place before the flow enters the subsequent blade row.

2.3 Loss Origin And Generation

Analysis of the vortex structures and their effects on the end wall boundary layer gives a fairly clear idea about the factors contributing to the generation of loss through the turbine cascade. Sieverding [1985] has identified seven origins of loss in a turbine blade row. These are listed below.

- Stagnant separation bubble in the leading edge region between the separation lines.
- Growth of new boundary layers behind the separation lines.
- Corner losses in both pressure side and suction side end wall contours, the latter being more important.
- Shear stress effects along all three-dimensional separation lines.
- Losses due to the shear action of the passage vortex on the blade suction side and the mixing process between the cross flow and the blade surface flow along the three-dimensional separation lines. This line is caused by the suction side leg of the horseshoe vortex.
- Dissipation of all vortices and mixing of the non-uniform outlet flow downstream of the cascades.

Denton [1993] in his review on loss mechanisms in turbomachines defined loss in terms of entropy increase. He summarised by saying that there are several mechanism that contributes to entropy increase in turbines. The major contribution to loss comes from the entropy generation in the annulus boundary layers within, upstream and downstream of the blade row. Another contribution is the loss associated with the secondary kinetic energy produced during the mixing process and shock waves, where shock waves occurs in supersonic turbines. The final component is the heat transfer across temperature gradients in the flow.

The overall loss occurring in the blade row may be conveniently subdivided into three component losses, each component loss being influenced by variables defining both the aerodynamic and geometry of the blade. Generally, these categories are profile loss, secondary loss and tip leakage loss. Profile loss is the loss due to the shear friction or separation, which takes place in a uniform two-dimensional flow across a cascade of blades. It includes the loss generated in the blade boundary layers on the suction and pressure surfaces and extra loss arising at the trailing edge.

Secondary losses at end wall are the losses due to the secondary flows generated in the end wall region of a blade row and finally, tip leakage loss arises from the flow through any clearance gap between the blades and the end wall. According to Denton [1993], the relative magnitude of each of these three component losses depends on the blading design, but are approximately equal in most machines.

2.4 Real Turbines

Flows in low speed linear cascades vary much from those in real turbines. Probably the most obvious difference is that in a real turbine, the blades are arranged radially in an annulus and alternate rows rotate. This leads to radial pressure gradient between the hub and the casing. In a rotating blade row, the boundary layer fluid on the blade experiences an outward centrifugal force due to the rotation. This causes the low energy fluid to migrate along the suction surface of the blade towards the casing. In a stationary blade, the migration will be inwards due to the higher pressure on the casing caused by the swirling of the flow. This causes a significant change to the secondary flows and increased losses at the hub. Flows in a low speed cascade also do not experience high-speed flow phenomena such as shock waves, which usually occurs in transonic turbines.

In passing from the stationary frame of reference to a rotating one means that the inlet boundary layer will be skewed. Gregory-Smith and Walsh [1985] simulated this effect in a linear cascade with the skew produced by a moving end wall. They found that for a turbine the direction for this skew enhances the secondary flow and increases the loss, they also found that by moving the end wall in the opposite direction so as to simulate movement for a compressor, there was a significant reduction of secondary flow and losses.

Another consequence of the relative motion is that the non-uniform flow that exits from one blade row produces unsteadiness at inlet for the next row. Investigation on a single stage turbine by Binder et. al. [1985] showed that a

sudden increase in turbulent energy occurred when a wake portion of the incoming fluid entered a rotor. The stator secondary vortices were cut off by the rotor blades and caused turbulence in the vortex region. It was thought that the breaking up of the vortical motion near the pressure side of the rotor blade led to turbulence in the flow, which in turn could significantly affect the boundary layer behaviour on the pressure side.

Mitchell et. al. [1993] has also investigated this complex three-dimensional flow through experimental study in a two-stage low speed axial flow turbine. His results indicate that the exit flow from the second stator row is different from the first stator row, attributed to the non-uniform inlet flow conditions that exist at the inlet for the second stator. The exit flows of the rotors however were found to be only slightly different. He showed that there is substantial interaction between the shroud leakage flow and the mainstream flow downstream of the two rotors. This in turn generates a different secondary flow field downstream of the blade rows. This phenomenon is impossible to be simulated in a linear cascade.

2.5 Secondary Loss Prediction Methods

Predicting secondary loss in turbomachinery is particularly important for the design engineer since it has direct influence on the machine efficiency. For design work therefore simpler methods have to be used, relying largely on the correlation of empirical data. There have been numerous experimental data on secondary losses and also a large number of correlations developed for this purpose.

As mentioned above a number of correlations have been developed using available cascade data. Dunham [1970] made a significant attempt to review and compare the various correlations available to predict secondary losses. These correlations show which parameters may be the important factors that effect the magnitude of loss. Hence secondary losses can be reasonably predicted if blading parameters such as flow angles, aspect ratio, Reynolds number, Mach number and blade geometry including pitch, chord, and thickness are known. He found that those methods were best which were based on the Ainley-Mathieson [1951] loading parameter, Z defined as follows.

$$Z = \left(\frac{C_L}{s/c}\right)^2 \frac{\cos^2 \alpha^2}{\cos^3 \alpha_m} \qquad \text{Equation 2.3}$$

where C_L = Lift coefficient

s = Blade pitch

c = True chord

α_m = Vector mean angle

Similarly, Denton [1973] has conducted a survey and compared the methods available for predicting profile loss and secondary loss for turbine blades. He compared the correlations produced by various authors against a collection of cascade data obtained from literature survey. He concluded that the basic philosophy of any correlation method is that the loss is mainly dependent upon the blade angles and is not greatly influenced by the detailed blade shape. His work has showed large differences between the predictions of different

methods and poor agreement with cascade results, which suggests that the approach is incorrect.

There are also another group of researchers who have attempted to predict through modelling the physics of the flow rather than on overall correlations. Gregory-Smith [1982] proposed that the secondary loss could be separated into three components;

- The upstream boundary layer which is shed as a loss core
- The new skewed boundary layer growing on the end wall
- An 'extra' secondary loss due other secondary vortex and its interaction with the end wall and blade boundary layers.

He added a loss model to the secondary flow calculation of Glynn and Marsh [1980] and obtained reasonable agreement with the experimental results. Okan and Gregory-Smith [1995] have further developed this method of calculation by taking into account radial migration of loss due to pitch wise pressure gradients and buoyancy effects.

2.6 Reduction Techniques

Sieverding [1975] reviewed a number of ways by which the overall performance of a turbine cascade may be improved by influencing the secondary flow. He identified four different potential methods, by which achievement may be possible. These include aerodynamic optimisation of the blade height, turning angle and other blade parameters, changing the blade loading, the use of

boundary layer devices and finally end wall contouring. Some of these and other promising techniques are discussed below. Some of them would be difficult to apply to a turbine but the concepts have been tested on cascades.

Optimisation of the blade surface pressure distribution needs a careful balance between the combination of the blade height, turning angle and Mach number. By increasing the blade height, secondary flow and its interaction with the mainstream flow will become relatively less compared to the total pressure loss. Modifications to the blade shape in order to change the aspect ratio have also proved to reduce secondary flows. Work by Moore and Ransmayr [1984] involved changing the shape of the leading edge to reduce the horseshoe vortex since it is a part of the secondary flow phenomena. A smaller and weaker vortex was created when a less blunt leading edge was used. The thickness of the trailing edge causes more additional loss on the blade with thick boundary layers than with thin boundary layers.

Heinemann [1977] studied the effects of turning angle and Mach number on secondary flow on a high turning rotor cascades. He found that the inlet angle is the most sensitive parameter, which is to be expected since the angle through which the flow is turned is the most important factor in determining the strength of secondary vortex. He also showed that at low inlet angle, there is a small span wise variation of the flow and more than 50% of the blade height near the end wall showed uniform flow. As the angle was increased, the two-dimensionality was poorer at mid span and about 40% of the blade height had uniform flow.

The effect of incidence angle on the blade has been predicted by Ainley and Mathieson [1951]. Since then several researchers have conducted experiments and found that since positive incidence angles lead to greater turning, this gives higher blade loading and hence greater secondary flows and losses. This has been demonstrated by Hodson and Dominy [1986] who tested a rotor blade with design inlet angle of 38.8^0 and exit angle of -53.9^0. They found secondary loss coefficient of 0.0137 at -20.8^0 incidence, 0.0259 at design and 0.0360 at 8.6^0 incidence. They have also investigated the effect of the pitch to chord ratio and found that by increasing this ratio, the secondary flow and losses increase for a given turning. In terms of Reynolds number, Hodson and Dominy also showed a slight reduction in secondary loss with increasing Reynolds number as would be expected from a turbulent flow situation. As for Mach number effect, the loss rises towards transonic Mach number, then decreases and rises further in the supersonic regime.

Investigations have also been done by various other workers (Han et. al. [1994], Wang et. al. [1999], Harrison [1990]) to study the effect of non-radial stacking or blade lean in attempt to reduce the secondary flow. The application of blade lean was shown to have a marked effect upon blade loading, on the distribution of loss generation and on the state of boundary layers on the blade suction surface and end walls. Wang et. al. [1999] showed that the dominant effect of blade lean is the radial component of blade force giving rise to a radial pressure gradient. So if the blades are leaned so as to increase the pressure at the hub in an annular cascade, this would oppose the radial flow and so may reduce losses. However Harrison [1990] found from his experiment on a linear cascade, that this geometry reduced velocities and hence loss generation

substantially at one end wall but increased them at the opposite wall. He also tested the idea of compound lean whereby the blades are stacked on a circular arch inclined at 30^0 from perpendicular to the end wall at each end. It was found that the end wall losses were reduced but at the expense of increased losses at mid span. On the whole, since the application of compound lean blades generates more uniform flow at exit, it might improve the overall efficiency in a turbine. At present this method is the most common way to reduce secondary loss in turbines.

In a linear cascade, boundary layers are built up on the side walls leading to a reduced effective flow area behind the cascade. Since the inlet boundary layer is the main factor that affects the growth of secondary losses, suction may seem to be the most efficient way to eliminate the boundary layer. Gustafon [1977] carried out his observations from a low speed cascade. He described this effect in terms of axial-velocity-density ratio, which is the ratio between the exit axial velocity and density and the inlet axial velocity and density. He found that increasing this ratio (increasing suction), the streamlines of the suction surface was straightened out. On the pressure surface, the flow has a velocity component towards the wall which is secondary flow effect due to the boundary layer cross flow. Although this experiment proved successful, the suction method requires additional power making it inapplicable in practice.

Another technique of influencing the boundary layer is by blowing tangentially in the upstream boundary layer. This was studied by Biesinger and Gregory-Smith [1993]. With low blowing the inlet boundary layer was first thickened and produced higher secondary loss. Then as the blowing was

increased a counter streamwise vorticity was generated which in turn weakens the passage vortex. This has successfully produced a reduction in loss but when the energy for the inlet blowing is included, no net gain was achieved. This is due mainly to the mixing loss of the injected air. This method would also be difficult to implement on a real turbine.

The method of using radial slots can also be applied to reduce secondary flow where the pressure surface and the suction surface is connected (Kawai et.al.[1989]). The aim is to modify the blade suction side pressure distribution such as to reenergize the boundary layer at the suction surface to suppress the corner stall in a compressor. However it is not possible for turbine blades because the boundary layer on the suction surface is quite thin, and thus an injection from the pressure side wall makes the boundary layer thicker on the suction side, causing more loss.

Prumper [1988] tested other methods including boundary layer fences in the form of metal sheets fixed onto the end wall, which are aimed to correct the flow direction. Fences are meant to reduce the migration of the cross-flow to the suction surface and hence reduce the mixing losses. However it is not practical to use these metal sheet fences because of their weak mechanical strength.

In general, many investigations have been carried out through implementation of new ideas by various researches. Some of these workers have achieved loss reductions in specific geometries in cascades, but these reductions are often counter balanced by the increased profile loss or higher inlet losses. These kinds of effects may not be realised in a machine environment.

For example tests in an annular cascade by Boletis [1985] show that the effects of optimisation on the following blade row may produce the most benefits. It appears that part of the problem is appreciating the full three dimensional effects and understanding the flow characteristics.

2.7 End Wall Profiling

Many researchers accept that the growth of the passage vortex is responsible for most of the secondary losses, which develop within the blade passage. Therefore, methods which attempt to reduce the secondary losses, should concentrate upon ways to influence the passage vortex development by changing the end wall pressure distribution. End wall profiling is a potential method that has been given attention since the early sixties.

In a blade passage, the reduction of velocities take place at the most curved region, where secondary flows develop intensely. As the flow experiences the strong pressure gradient across the channel, where the high pressure is at the pressure surface and low pressure at the suction surface, the flow accelerates from the pressure surface to the suction surface. Through this acceleration process, the passage vortex migrates and stretches as it moves to the suction surface. The high turbulence that is generated when this vortex interacts with the suction surface counter vortex, is a source of secondary losses downstream of the blades.

Therefore, it is necessary to influence the passage vortex by increasing the velocity at the pressure surface and reducing that at the suction surface. This is

done by introducing a convex curvature at the pressure surface to reduce the local pressure and a concave curvature at the suction surface to increase the pressure there. This idea of non-axisymmetric profile is a fairly recent idea while previous work has been more focussed on axisymmetric profiles.

Axisymmetric profiling was introduced by Deich et.al. [1960] who carried out extensive tests on different end wall geometries on both linear and annular cascades, optimising the position of maximum curvature and contraction ratio. He showed that the blade shape should be reduced in height using a similar profile shape to that shown in Figure 2.6 for the tip end wall, while the maximum curvature for the beginning of the 'kink' should be situated just behind the position of maximum channel curvature. The optimum contraction ratio can be referred from Figure 2.7. Using the optimum profile, stage efficiencies could be increased by up to 3.5% with an aspect ratio of 0.2. The curvature of the end wall reduces the velocity along the blade suction surface, reducing the cross channel pressure gradient by almost half at the point of maximum channel curvature, in addition shifting the maximum acceleration at the end walls towards the trailing edge of the blade passage. This significantly reduces the development of secondary flow and the associated losses. However, it is not applicable to have such a low aspect ratio in many turbines. This work was continued by Morris and Hoare [1975] where they optimised the dimensions of the profiles developed by Deich and experimented with them in a linear cascade. The profiles achieved a fluid velocity reduction over the front of the blade where turning is greatest, and therefore a secondary loss reduction was expected. However these beneficial affects were annulled by the increase in adverse pressure gradients over the rear of the blade suction surface. This caused the

flow to move from the end wall towards the suction surface with extensive three-dimensional disturbance to the flow.

Atkins [1987] et. al, tested five different axisymmetric end wall contours in a linear turbine cascade. One of the configurations had an outlet to inlet ratio of one while the other four had a converging outer wall. Comparing the results between the four end walls in cascades with a converging outer end wall, a reduction of 10% in the cascade loss (total loss minus inlet loss) was achieved. In the case with the cascades with the same span at the trailing edge and leading edge, there is an increase of loss by 4%. The four profiles had a common feature of reduced blade span from the leading edge to the trailing edge plane. As a result, the streamlines were forced closer together and the pressure drop in the streamwise direction was increased. This favourable condition has reduced the growth of the blade surface and end wall boundary layers, and also reduced their tendency to separate. Atkins concluded that another possible advantage of incorporating contraction through end wall profiling is that, the flow into the next blade row downstream will be more uniform because the loss cores will be closer to the end walls.

More recently, Duden et al [1998] tested an axisymmetric end wall in a highly loaded turbine cascade with no changes in the axial area ratio. His experiments showed improvements concerning the radial extent of the secondary flow and a decrease in secondary loss of 26 %. Unfortunately this reduction was counterbalanced by increased profile losses and higher inlet losses due to increased blockage, but with significant reduction of the exit flow angle deviations connected with the secondary flow.

Many other researchers have carried out experiments using axisymmetric profiles and their results have not produced reduction in secondary loss and in crease in overall performance. Most of the researchers except that this is due to the redistribution of pressure and hence loading of the blade near the end wall, resulting in weaker secondary flows and less migration of low momentum fluid from the boundary layers to the free stream. However, they agree that the loss reduction gained on the profiled end wall has been counter balanced by extra loss on the flat end wall making the axisymmetric end wall less efficient.

With the development of prediction techniques using computational fluid dynamics (CFD), some workers have used CFD to design end wall profiles. Atkins [1987] is one of the few researchers who have attempted to use non-axisymmetric profiles, designed using CFD. He used a combination of CFD and experiment, with the former guiding the latter, and in turn being validated through experiments. He tested two non-axisymmetric profiles, where both are designed with a bump adjacent to one blade surface and reducing to a flat profile near the opposite surface. It was intended to reduce the maximum pressure at the pressure surface and the minimum pressure at the suction surface. However both profiles resulted in an overall increase in losses due to the adverse effects of the flow near the profiled end wall causing a strong twist of the blade wake.

Rose [1994] used CFD to design a profiled end wall for a nozzle guide vane aimed to reduce the circumferential non-uniformities of static pressure to reduce disc coolant flow leakage. He found that the mean flow was hardly affected by the profiling although the objective was achieved. More recently, Yan

et. al. [1999(1)] designed various non-axisymmetric end walls for a turbine nozzle row with the aim of reducing the cross passage pressure gradient on the wall. These were evaluated using CFD and the most optimum profiled end wall was chosen and tested. Yan et. al. [1999(2)] later showed that the selected profile achieved an overall loss reduction of 6.6%.

Due to the large number of geometric options in end wall profiling, it is difficult to make use of the results by the various researchers to optimise the design of end wall of a turbine blade. Moreover, the designs of different authors are not in complete agreement and the loss reduction for a particular end wall cannot be predicted with high accuracy. Therefore, according to Boletis [1985], the only way to evaluate the potential benefits of a particular contouring is to support an analysis of the three-dimensional flow field, and determine the actual losses through experimental testing.

2.8 Research By Jonathan Hartland (1999)

Jonathan Hartland is a student pursuing his PhD at the University of Durham. His research is aimed at reducing the losses caused by secondary flows in turbine blading through end wall profiling. However his approach of designing and testing of the profile must be considered. He utilised both CFD and experiments to yield the necessary understanding of the three-dimensional effects in order to develop a design methodology. This work was in collaboration with Rolls Royce plc.

Hartland first investigated experimentally the end wall design proposed by Rose [1994], with slight modifications for the low speed linear cascade. This is necessary because the end wall profile designed by Rose was for an annular nozzle row as opposed to a linear rotor row. Detailed measurements were taken of the profiled end wall, including the inlet and exit traverses. These experiments were carried out using the large-scale low speed Durham linear cascade and have been reported in Hartland et.al. [1998]. He then studied the results obtained by past investigations of the secondary flow by previous researchers from the same linear cascade. Using this information, CFD codes were developed.

In order validate the codes, CFD predictions and assessment of flow physics were carried out for the results obtained from the testing of the initial end wall. The CFD methods were incorporated into an inverse design method, as described by Harvey et. al. [1999]. Further new end wall profiles were designed out of which only one was selected and manufactured. This new profile is named Profile 1 end wall.

In order to understand how this new profile affects the secondary flow, it is necessary to compare the results of this profile with an end wall without any profiling. This is the flat end wall or referred to as the Planar end wall in this thesis. This Planar end wall was also manufactured the same way as Profile 1, using the same techniques and machining procedures but using a Perspex plastic as the material. Both the Planar and Profile 1 end wall were tested and were both evaluated with respect to CFD predictions and experimental results.

The results of the experimental validation has been published by Hartland et. al. [1999].

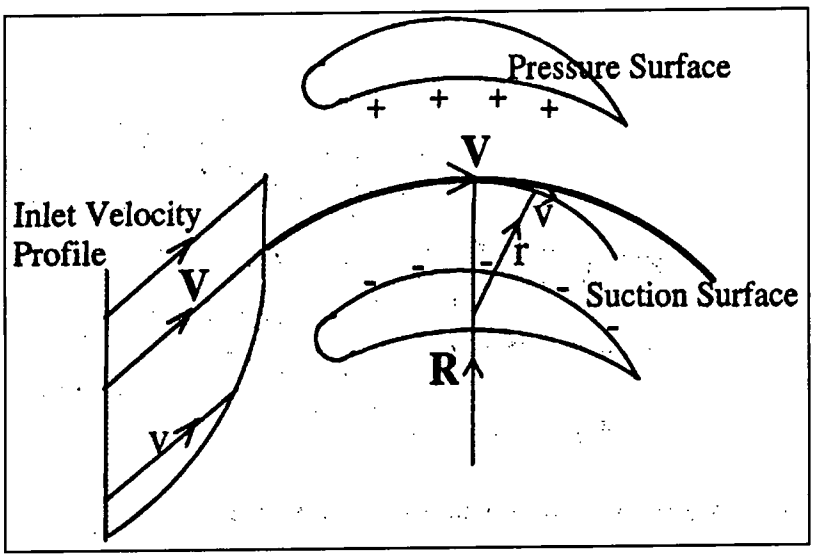

Figure 2.1 Turning Of End Wall Boundary Layer

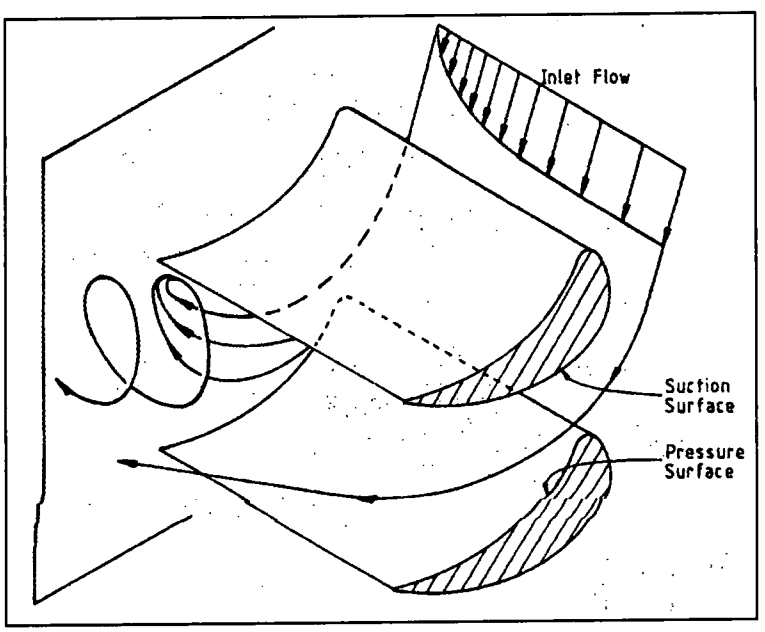

Figure 2.2 Secondary Flow In A Blade Passage

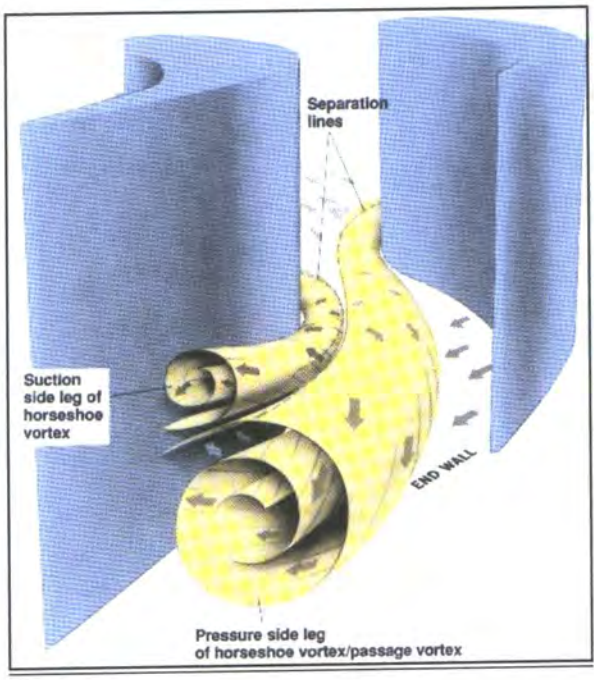

Figure 2.3 Secondary Flow Structure

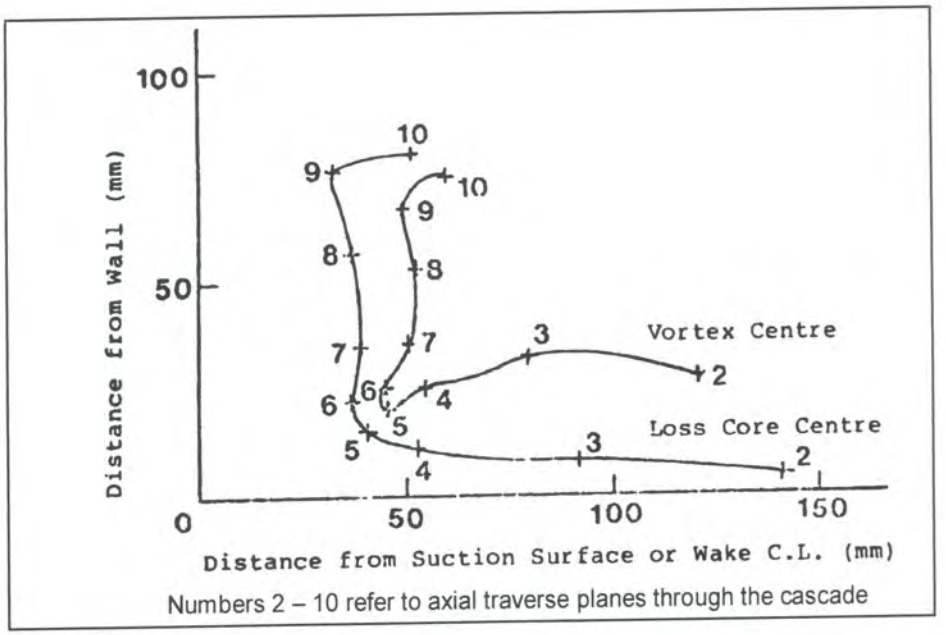

Figure 2.4 Passage Core Centre And Loss Core Movement

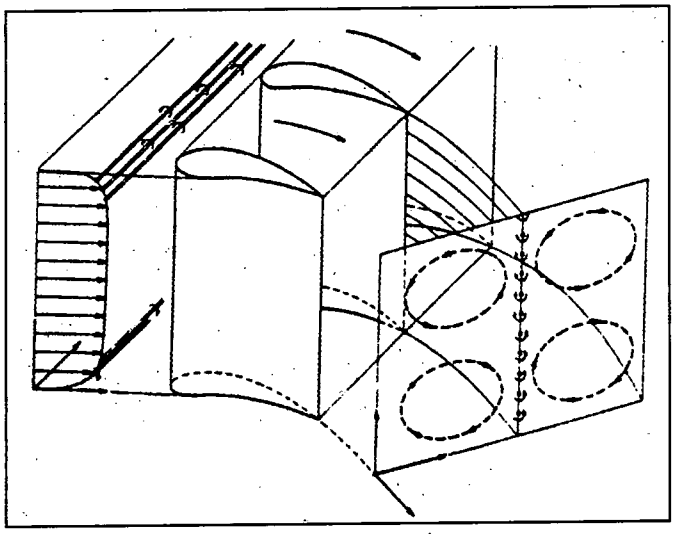

Figure 2.5 Vortices Downstream Of Blades

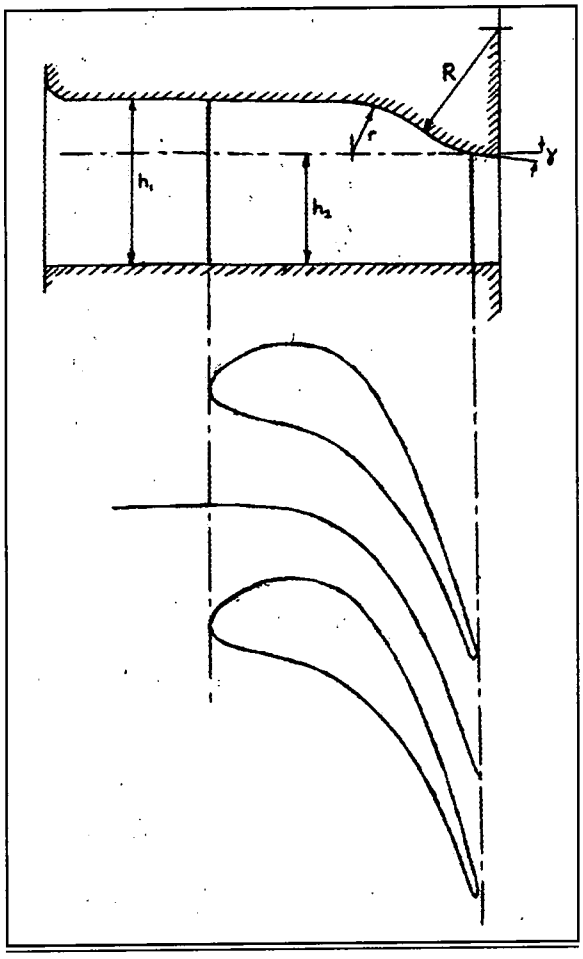

Figure 2.6 Contraction Shape By Deich

Chapter 3 Experimental Apparatus And Profile 2 End Wall Manufacture

The first part of this chapter describes the test facility, instrumentation and the technique use to obtain the experimental data presented in this thesis. The current work is a continuation of past research in turbomachinery flows at Durham University. As such, much of the apparatus has been used and described by previous workers. Biesinger [1993] investigated a novel secondary flow reduction method through air injection tangentially into the end wall boundary layer. Moore [1995] conducted experiments to test the validity of turbulence and transition models for a turbine cascade. More recently, Hartland [1999] tested various profiled end walls, which were designed using CFD.

Throughout the years of experimental work, various alterations have been done to the apparatus to fulfil the various research requirements. However, since the current work is similar to that carried out by Hartland, most of the apparatus, and data-acquisition software are exactly the same. Modifications were only done to the programs and calculation spreadsheets to accommodate a different set of data.

The second part of the chapter will describe the process involved in manufacturing Profile 2 end wall. This will include the conversion of data from a grid to a format acceptable to the CNC machine for manufacturing and the making of the pressure tapping holes.

3.1 Durham Wind Tunnel

The Durham cascade is a large scale, low speed linear cascade, of high aspect ratio. This is the main piece of apparatus and is mounted at the exit of a large wind. The air is supplied by a double entry centrifugal fan (Keith Blackman Series 28) driven by a variable speed motor. The fan and motor is enclosed in a housing, where three of the walls contain six 457 mm square Vokes general purpose filters. These are fitted to remove dirt and other particles from air, which might contaminate any instruments used. Air from the fan passes through a parallel wall section and then enters a large chamber through a diffuser. The flow is then accelerated through a contraction, to produce a uniform high speed flow, and then past a honeycomb flow straightener before entering the test section.

The working section is shown diagrammatically in Figure 3.1. It is 700 mm high and 460 mm wide upstream and 400 mm downstream of the tunnel. One side of the cascade is used for the end wall testing while the opposite side provides access for the instrumentation. This difference of 60 mm in width of the tunnel provides a clearance between the end wall and the upstream wind tunnel side wall. This is located approximately 1250 mm upstream of the blade leading edge where it is used to bleed off the upstream boundary layer. This creates a working section that is slightly asymmetric.

As shown in the diagram, there is also a turbulence grid located just upstream of the bleed section. This was previously designed by Cleak [1989] to generate turbulence levels similar to those experienced in an actual gas turbine. It is made out of 25 mm diameter bars 80 mm spaced from each other, with an

additional 8 mm diameter bar located 25 mm from the end wall. The smaller diameter bar is required at the end wall location to hinder a jet effect flow at the end wall. The grid was set parallel to the leading edge at an angle of 42.75^0 so that it is has a constant distance of 1400 mm from the blades. The large distance between the location of the grid and the blades provides sufficient time to allow the strong jet flow of the air past the bars to thoroughly mix out and consequently producing isotropic turbulence.

In addition to this, there are three slots located 172 mm upstream of the blades. These slot are each 250 mm long and 12 mm wide and are aligned parallel to the working section. They are located at different positions relative to the bars of the turbulence grid. Their locations were chosen to allow measurements to be taken at one axial chord upstream of the blades, to define the inlet flow conditions. Their different alignment relative to the turbulence grid is to check for uniformity of the turbulence.

3.2 Durham Linear Cascade

At the exit of this wind tunnel is where the cascade is fitted as mentioned earlier. It consists of six high pressure turbine rotor blades designed to give a similar aerodynamic behaviour at low speed as the RT60 model turbine profile gives at transonic speeds. These rotor blades were cast in epoxy resin from an aluminium master using a technique similar to that of Gregory-Smith and Marsh [1971]. Table 3.1 gives the design detail of the cascade.

Inlet Flow Angle	42.75^0
Blade Exit Angle	-68.7^0
Blade Chord	224 mm
Blade Axial Chord	181 mm
Blade Pitch	191 mm
Blade Half-Span	200 mm
Reynolds Number (Axial Chord and Exit Velocity)	4.0×10^5
Exit Mach Number	0.1

Table 3.1 Cascade Design Details

Figure 3.2 shows the location of the eleven tangential slots through which the probe may enter for pressure measurements. As can be seen, four of the slots are located outside the blade passage and cover slightly more than one pitch. The slots are filled with wooden inserts that fit firmly and closely to the inside of the end wall when not in use. During a traverse, the slot in use is covered using a thin strip of a flexible brush to reduce leakage of air while still allowing for probe movement. On the opposite side is where the profiled end wall is fitted.

It is necessary to ensure that this low speed cascade is operated at a constant Reynolds number. This is achieved by using a "standard day" atmospheric condition, which is given in the table below. Variations from these conditions are corrected by adjusting the upstream dynamic head and corrections to all measurements relative to this.

Ambient Temperature	19.0^0 C
Dynamic Viscosity	1.814×10^{-5} Ns'm^2
Air Density	1.179 kg/m^3

Table 3.2 "Standard Day" Conditions

3.3 Instrumentation

3.3.1 Traverse Equipment

The traverse unit, which was originally constructed by Graves [1985], consists of a pair of linear slides, A4012Q1 unislides from Time and Precision Ltd. Each side is 304 mm in length where one is mounted on the other perpendicularly as shown in Figure 3.3. The fixed slide provides motion along the slots, which is the tangential movement of the probe while the other provides movement along the radial direction. Both slides are of the lead screw type with a 1 mm pitch and is driven by a McLennan HS23 stepper motor. These motors produce 200 steps per revolution giving a linear step size of 0.005 mm. A motorised rotary stage is mounted on the spanwise traverse to hold the probe in place. This motorised stage (Time and Precision A375TP) is driven by a 200 steps per revolution stepper motor with a 90:1 gear ratio giving an angular resolution of 0.02^0.

3.3.2 Probes

A pitot-static probe is installed at mid-height, 700 mm upstream of the leading edge. It is used to measure the upstream static and total pressure. To

measure the flow field however, a five-hole cobra shaped probe was used. A flattened pitot probe was used for taking measurements of the inlet boundary layer. The dimensions of the five-hole probe and the flattened pitot probe are shown in Figure 3.4 and Figure 3.5 respectively. The five-hole probe was mounted on the rotary stage, which is free to slide tangentially, radially and be rotated about its axis by the traverse. The probes were calibrated using the same method as that of Treaster and Yocum [1979]. The probe was tested at a similar Reynolds number as that produced in the wind tunnel. Since a variable speed pump was used for the calibration it was adjusted to provide a flow of 40 meters per second. An example of a calibration map produced for the five-hole probe is shown in Appendix C. The calibration was carried out at a step of 5.0^0 angular change in both pitch and yaw direction.

The only limitation to this probe is that its diameter restricts the probe from getting close to the blade surface. This is particularly severe near the trailing edge where the blade surface is at an acute angle to the traverse slots. At closest to the blade surface, the probe is still tens of millimetres away measured in the tangential direction from the blade surface. This results in a large gap between the measured data and the blade surface when presenting results on an axial plane.

3.3.3 Traverse Control

A computer model 386DX with an AT-bus controls both the traverse and the data-acquisition system. Each stepper motor is driven by a four phase

bipolar driver board (RS 342-501) which is in turn controlled by a 48 channel Input/Output board, Amplicaon Liveline PC14AT, installed in the computer. The motors are driven in half step mode and are accelerated and decelerated slowly to ensure accuracy of movement.

There are in total five transducers used for the measurements. These are standard commercial pressure transducers that produce an electronic signal due to the change in capacitance of a bending metal diaphragm, which in turn is linearly dependent on the measured pressure. These transducers (CMR CONTROLS 200-008 P-sensor) are able to measure a pressure range of 0 to 2000 Pascal with 0 to 10 Volt linear output. One transducer is connected to the central hole of the five hole probe and to the total pressure connection of the upstream pitot static probe. The other four transducers are connected to the other four holes of the probe and the static pressure connection of the upstream static probe. There is also an additional transducer, which links the upstream pitot-static probe to the computer to monitor the upstream dynamic head. The connections between the transducer, computer and the probe are shown in Figure 3.6. All the transducers are calibrated by the manufacturer before any testing were done.

The overall inaccuracies can be attributed to several sources, particularly calibration of the probe, initial positioning of the probe and the readings from the pressure transducers. These are estimated to be $\pm\ 0.1^0$, $\pm\ 1.0^0$, and $\pm$ 0.5 Pa respectively. The initial positioning of the probes used has an estimated error of $\pm$ 0.1mm but it is deflected slightly by the flow so the error in the axial and

tangential directions could be up to ± 0.5 mm. The error in the total pressure coefficient is estimated to be ± 0.005.

3.4 Data Acquisition

The output signal of the transducers is recorded by one of two Analog to Digital (A/D) converters. Both have 12-bit resolution and take a ± 5V input. The standard card (PC-LabCard PCL-812PG) samples 16 channels at speeds up to 30 kHz. Normally only six of the channels are used, one to monitor the inlet dynamic head and the other five to take readings from the five hole probe.

To control the traverse gear and collection of data, a set of C programs was written formerly by Moore [1995], and later modified by Hartland [1999]. As mentioned earlier, experiments are carried out at the same Reynolds number to ensure consistency. Adjustments are made to the upstream dynamic head to correct to the "standard day" conditions once the current atmospheric conditions are inserted during a question and answer interface. Once the working conditions of the wind tunnel reaches the required state, the computer is programmed to start taking the measurements according to a grid specified for every slot. A typical traverse takes between three to five hours depending on the number of measurement points to be taken.

During a traverse, the sampled data is only processed as far as it is necessary to reduce memory requirements of the computer. This process usually involves converting a set of A/D readings to pressure readings, and

recording of the dynamic head to an output file. These values are then saved to a hard disk and transferred to a workstation for further processing. The data is then analysed using a FORTRAN program written by Hartland to calculate the yaw and pitch angle, local velocity, total pressure and static pressure for every traversed point on the specified grid.

3.5 Presentation of Results

In order to study the three-dimensional flow on Profile 2, area traverses were done at two different slots, Slot 8 and Slot 10. The results for Slot 8 and 10 will be presented in contour, vector and pitch averaged plots with the suction surface being on the left and the pressure surface on the right. These slots are actually axial positions in the cascade, and the locations of the slots are given in the Table 3.3.

For each slot, there are four area plots which includes secondary velocity vectors, total pressure loss coefficient contours, secondary kinetic energy contours and the yaw angle contours. The secondary velocity at any position is obtained by resolving along and normal to the local mid span flow direction at that pitch wise position. The plotted secondary vector is that projected onto the axial viewing plane as shown in Figure 3.7.

Slot Number	Axial Position		Slot Number	Axial Position	
	mm	%Cax		mm	%Cax
1	-197.0	-9.0	6	-52.0	71.0
2	-170.0	6.0	7	-24.0	87.0
3	-141.0	22.0	8	-5.0	97.0
4	-112.0	38.0	9	29.0	116.0
5	-81.0	55.0	10	51.0	128.0

Table 3.3 Location Of Traverse Slots

The total pressure loss coefficient, C_{TU} is the difference between the local and the upstream total pressure value made dimensionless with respect to upstream dynamic pressure, given below.

$$C_{TU} = \frac{P_{TU} - P_{TL}}{0.5\rho V_U^2} \qquad \text{Equation 3.1}$$

Similarly, the static pressure coefficient, C_{PS} is the difference between the local and upstream static pressure made dimensionless with respect to upstream dynamic pressure. This is represented by the equation below.

$$C_{PS} = \frac{P_{SL} - P_{SU}}{0.5\rho V_U^2} \qquad \text{Equation 3.2}$$

The secondary kinetic energy coefficient, C_{SKE} is the ratio of the sum of the secondary and radial kinetic energy to the upstream kinetic energy, which then reduces to the ratios of velocities as given below.

$$C_{SKE} = \frac{V_{TR}^2 + V_3^2}{V_U^2} \qquad \text{Equation 3.3}$$

where V_3 = Radial component of flow

and V_{TR} = $V_2 \cos \alpha_{mid} - V_1 \sin \alpha_{mid}$

with V_1 = Axial component of flow

V_2 = Tangential component of flow

α_{mid} = Mid-span angle

The pitch averaged total pressure loss coefficient is the mass averaged loss across one tangential pitch and is defined by the equation given below. Mass averaged total pressure loss coefficient shows the growth of mass averaged aerodynamic loss through the blade passage and is calculated at each axial plane of measurement. Since the experiment is carried over low Mach numbers, the density is assumed to be uniform in the plane.

$$\overline{C_{TU}} = \frac{\int_0^s C_{TU} V_1 dy}{\int_0^s V_1 dy} \qquad \text{Equation 3.4}$$

Similarly, calculations of mass averaging across a tangential plane are carried out for the secondary kinetic energy and yaw angle. These are represented by Equation 3.5 and 3.6. It can be seen from Equation 3.6 that the pitch averaged yaw angle is given by the mean tangential velocity, $\overline{V_2}$ and the mean axial velocity, $\overline{V_1}$. The mean tangential velocity and the mean axial

velocity are the velocities corrected to give the same tangential momentum and mass flow, as the real flow respectively. This is represented by Equation 3.7.

$$\overline{C_{SKE}} = \frac{\int_0^s C_{SKE} V_1 dy}{\int_0^s V_1 dy} \qquad \text{Equation 3.5}$$

$$\bar{\alpha} = \tan^{-1}\left(\frac{\overline{V_2}}{\overline{V_1}}\right) \qquad \text{Equation 3.6}$$

$$\bar{\alpha} = \tan^{-1}\frac{\int_0^s V_2 V_1 dy.s}{\left(\int_0^s V_1 dy\right)^2} \qquad \text{Equation 3.7}$$

The mass averaged total pressure coefficient is defined by the equation below. It is a value that is obtained by mass averaging the pressure coefficient over the whole measurement area.

$$\overline{\overline{C_{TU}}} = \frac{\int_0^h \int_0^s C_{TU} V_1 dydz}{\int_0^h \int_0^s V_1 dydz} \qquad \text{Equation 3.8}$$

Calculation of the secondary kinetic energy and yaw angle of the flow downstream is also mass averaged over the measurement area, represented by Equation 3.8 and 3.9.

$$\overline{\overline{C_{SKE}}} = \frac{\int_0^h \int_0^s C_{SKE} V_1 dydz}{\int_0^h \int_0^s V_1 dydz} \qquad \text{Equation 3.9}$$

$$\overline{\overline{\alpha}} = \tan^{-1} \frac{\int_0^h \int_0^s V_2 V_1 dydz.s.h}{\left(\int_0^h \int_0^s V_1 dydz\right)^2} \qquad \text{Equation 3.10}$$

The mixing loss that occurs downstream of the blade passage is calculated by applying momentum and continuity equations to a control volume at infinity. Here the flow will have mixed out to give a uniform velocity and pressure field, and so the mixed out total pressure loss coefficient may be calculated. The detailed derivations are given in Appendix A.

3.6 End Wall Profile 2 Manufacture

The information regarding the shape and curvatures of Profile 2 was provided by Rolls Royce plc. in form of a CFD grid. This information was then transformed into a format that can be read by the machining equipment. This required detailed programming procedure for the preparation of the grid file. This is summarised and explained in Appendix B which includes an example of a grid file used.

A ball ended cutter was used in the CNC machine since this gives a good surface finish, and does not cause any problems when machining internal curves in the vertical plane. A 10 mm radius cutter was used for surfaces that are flat and a 5 mm radius cutter was used for the curvatures. This is because the smaller the radius the surface finish would be finer, but is a compromise with time since it will take twice as much to cover the same area compared to the 10 mm radius cutter. This is because the smaller radius is required to give an accurate profile where it is curved. Programming instructions to the CNC machine took account of the cutter radius.

The end wall is manufactured in 6 separate parts or panels which when put together covered the 5 rotor blades on the cascade. The end wall is manufactured out of Necuron® 100, which is polyurethane foam specially formulated for prototyping and rapid machining. A number of tests was first carried out using the CNC setup and different diameter ball cutters to verify the reliability of the system and the quality of the surface finish. The surface was first machined using a 5 mm square grid, traversing the cutter in the pitch wise direction. This gave a very coarse surface in the axial direction especially on the hump at the pressure surface. Then it was tested again at a finer resolution of 2 mm grid and the surface finish was satisfactory. Once all the necessary adjustments and selection of the appropriate cutter had been done, the end wall was then manufactured from panel to panel with each panel covering one blade passage. The manufacture of each panel took approximately 8 hours.

Once the manufacture of the 6 panels was complete, one was selected to be the tested profile, in which pressure tapping holes were made. The pressure

tapping holes were made using the same CNC machine but with a 0.75 mm radius cutter. There are 16 axial rows with 10 holes in each row, which were spaced systematically over the panel, emphasising the location near the leading edge and the beginning of the curvature. The grid is created using a coordinate system that was based on the distance around the blade suction surface from the trailing edge and the distance from the end wall. Each of the holes was inserted with a plastic tube approximately 5 cm long. During experiments when the static pressure tappings are not in use, it is necessary to avoid any leakage of air from the plastic tubes. This is prevented by connecting the tubes to each other at the back of the end wall using tubes of larger diameter. This larger tube connects every two pressure tapping tubes together on each end. This is just a simple measure to ensure that there is no change on the end wall static pressure. The sizes of the two tubes are given in the table below and its position with respect to the end wall is shown in Figure 3.8.

Tubes	Internal Diameter	External Diameter
Pressure Tapping Tubes	0.76 mm	1.22 mm
Connecting Tubes	1.14 mm	1.57 mm

Table 3.4 Tube Sizes

All six panels were then varnished using a mixture of acid and formaldehyde in equal proportions. The panels were painted with several coats to give a clear finish. It must be noted that the tubes in the pressure tapping holes were left proud of the surface while being varnished. The tubes were cut off flush with the surface only after varnishing was complete. This panel together

with the five others was given a smooth finish by sanding the surface using commercial sandpaper. Finally the panels were then assembled and fixed onto the cascade.

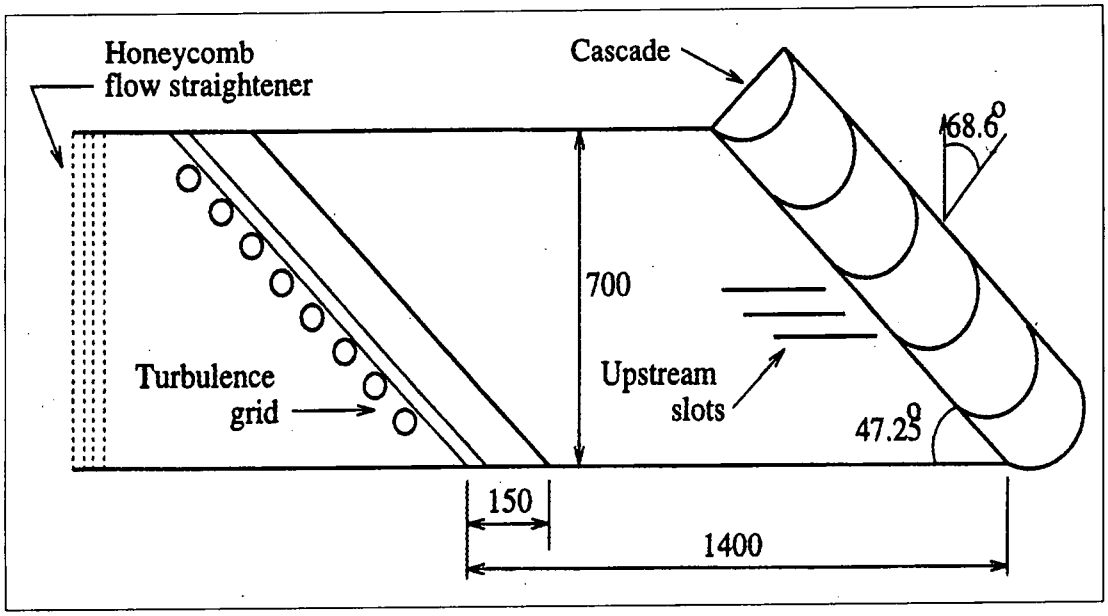

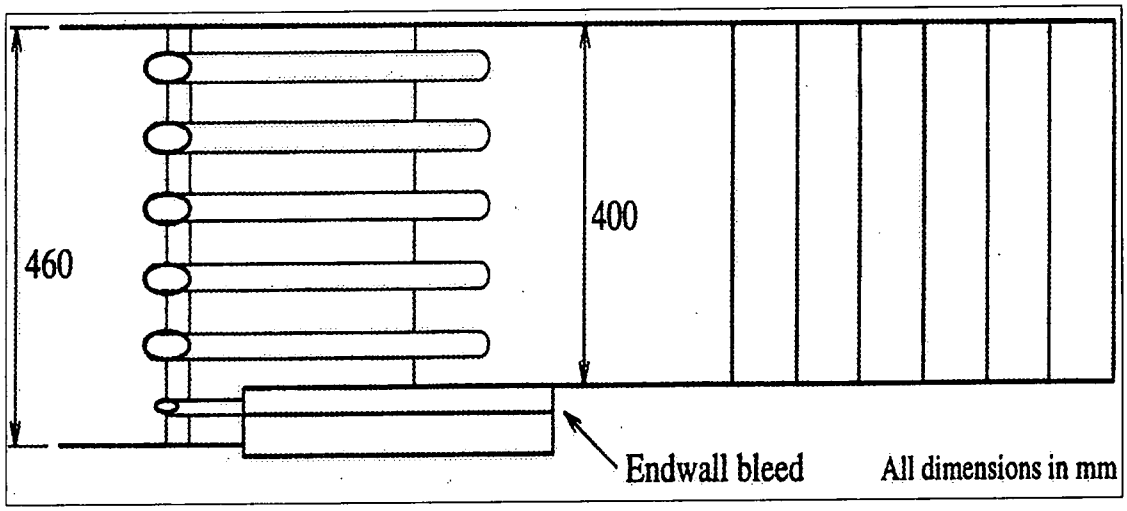

Figure 3.1 Durham Wind Tunnel Construction

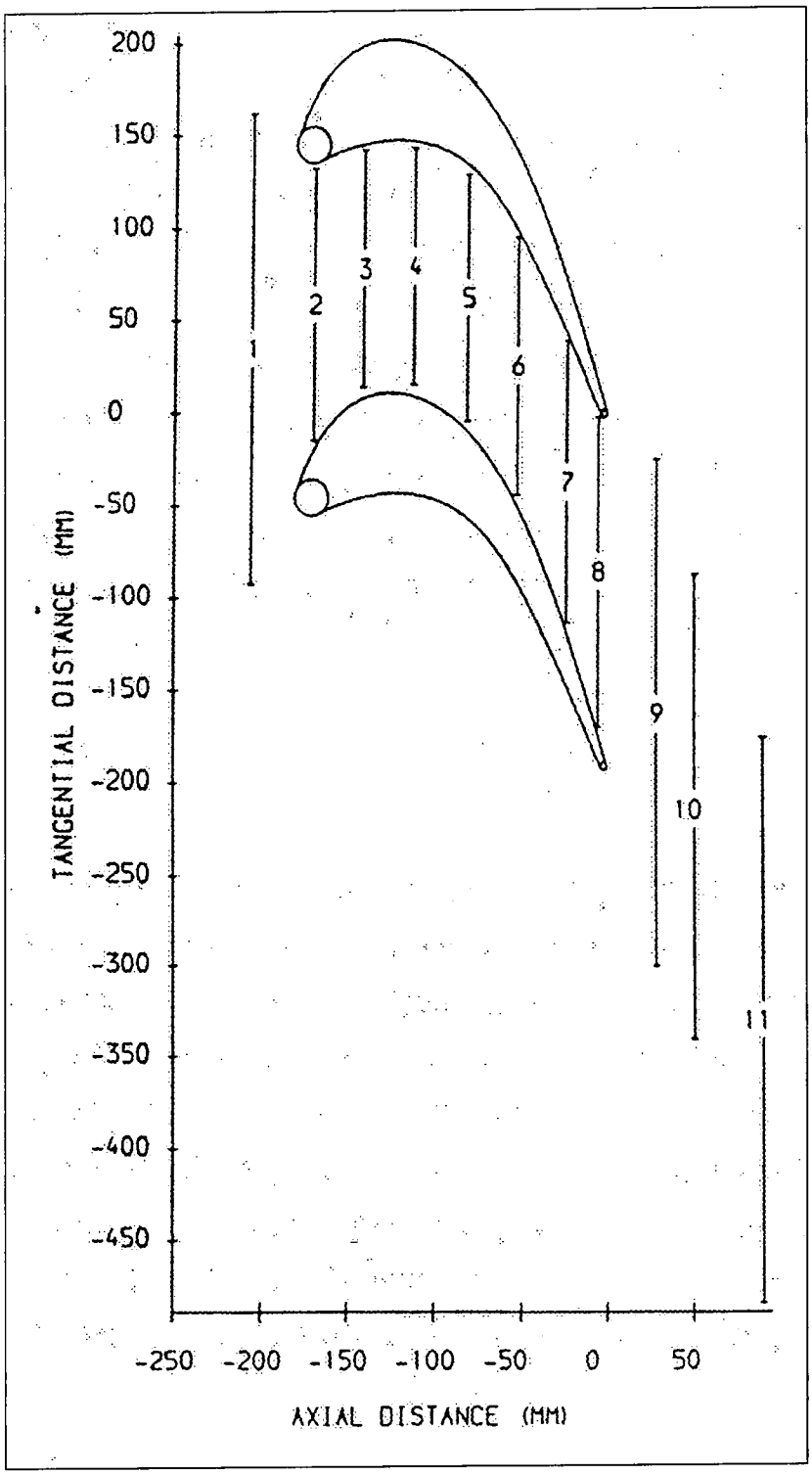

Figure 3.2 Positioning Of Tangential Slots

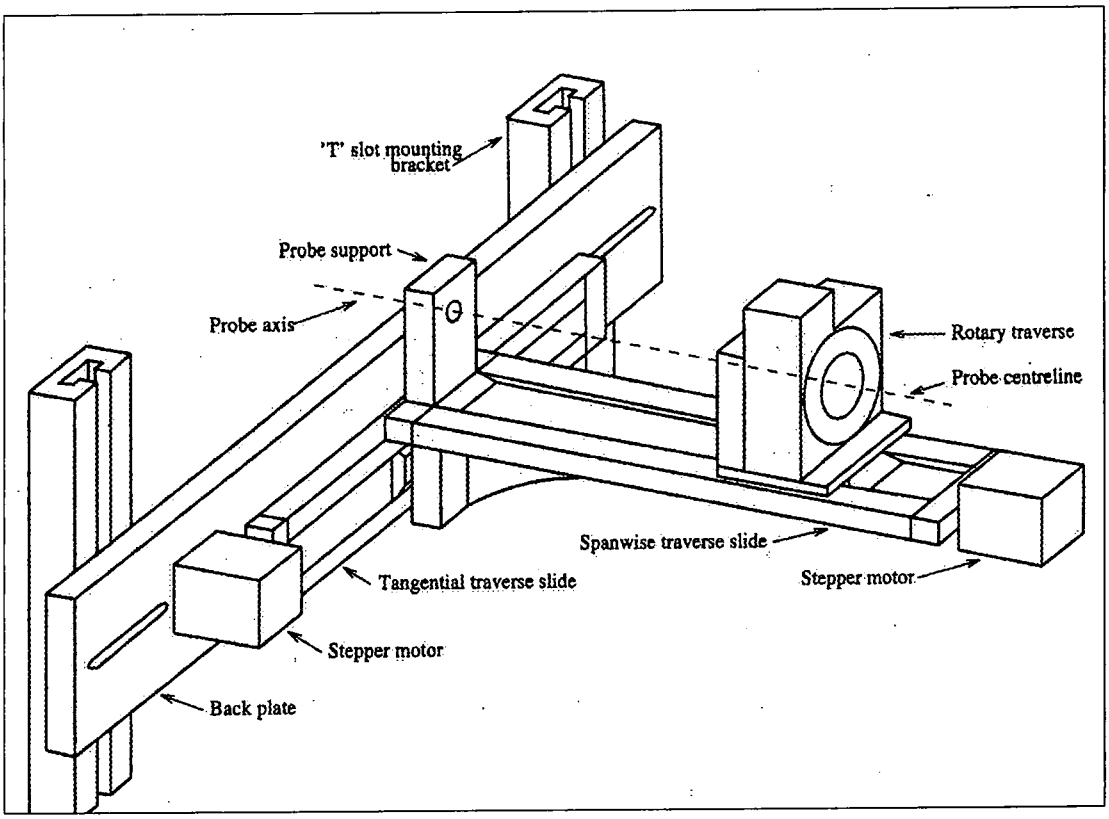

Figure 3.3 Traverse Gear

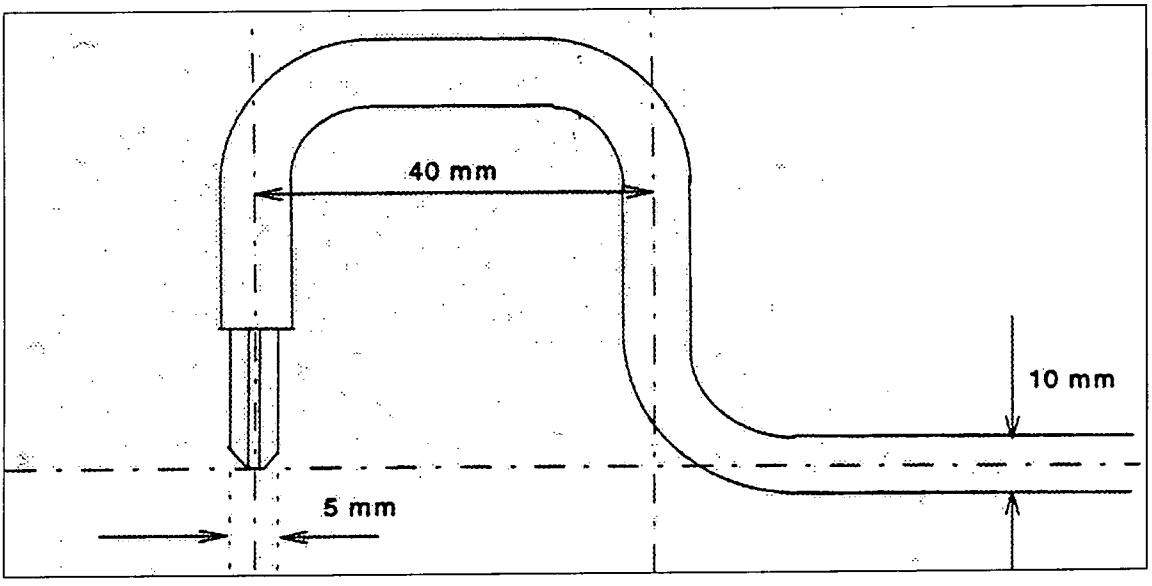

Figure 3.4 Dimensions Of The Five-Hole Probe

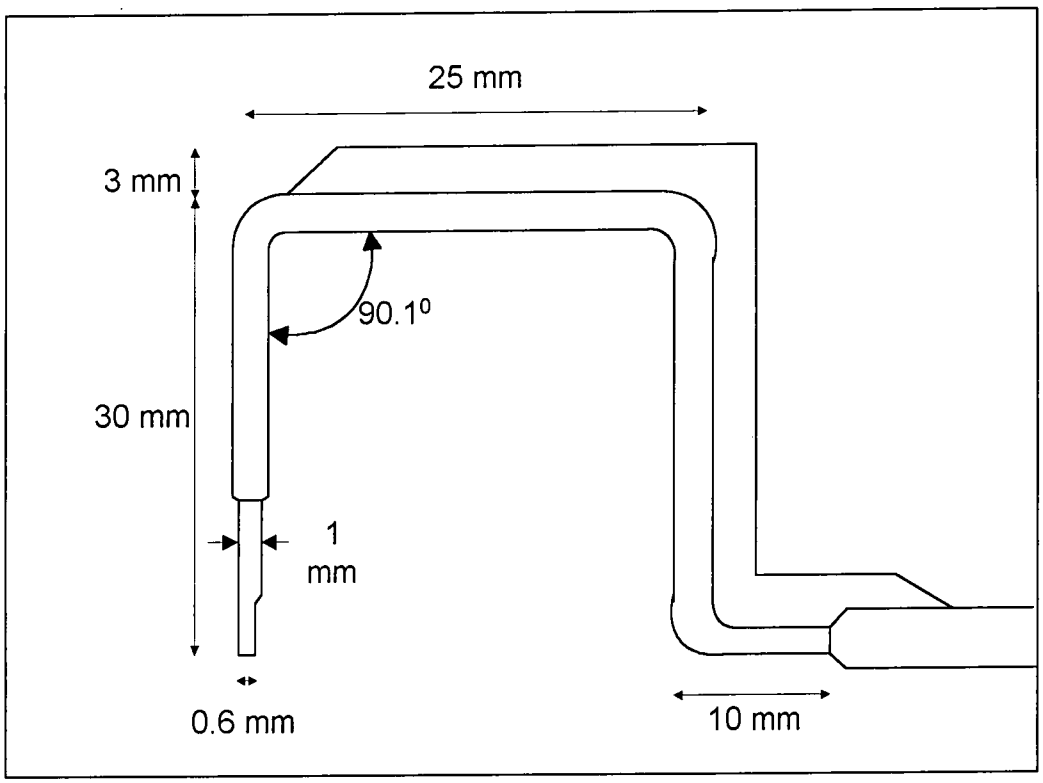

Figure 3.5 Dimensions Of The Flattened Pitot Probe

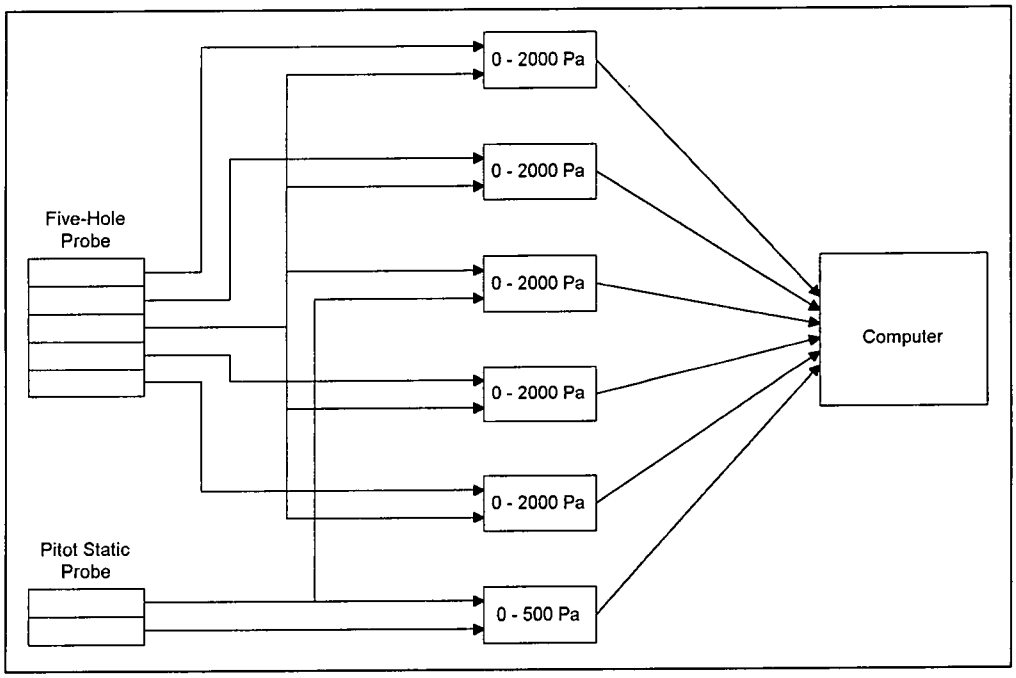

Figure 3.6 Connections Between Transducer, Computer and Probe

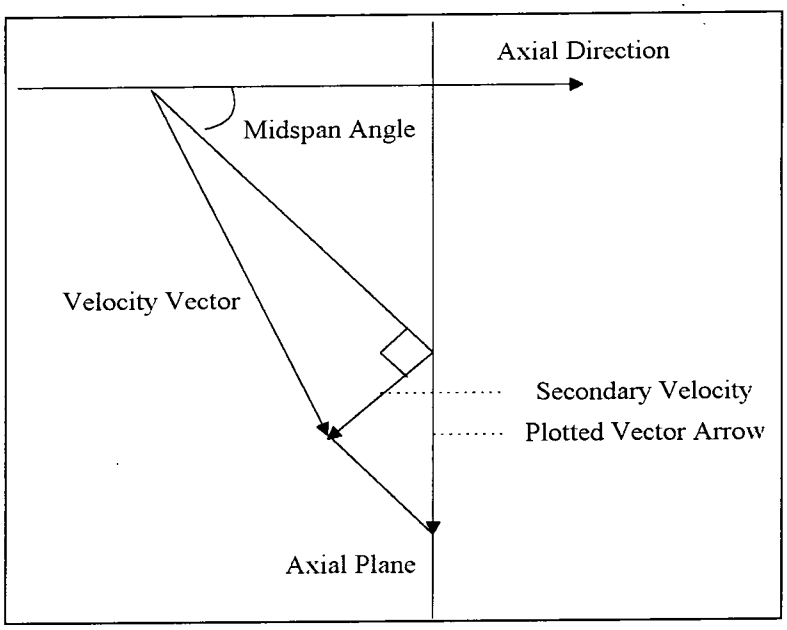

Figure 3.7 Flow Trajectories

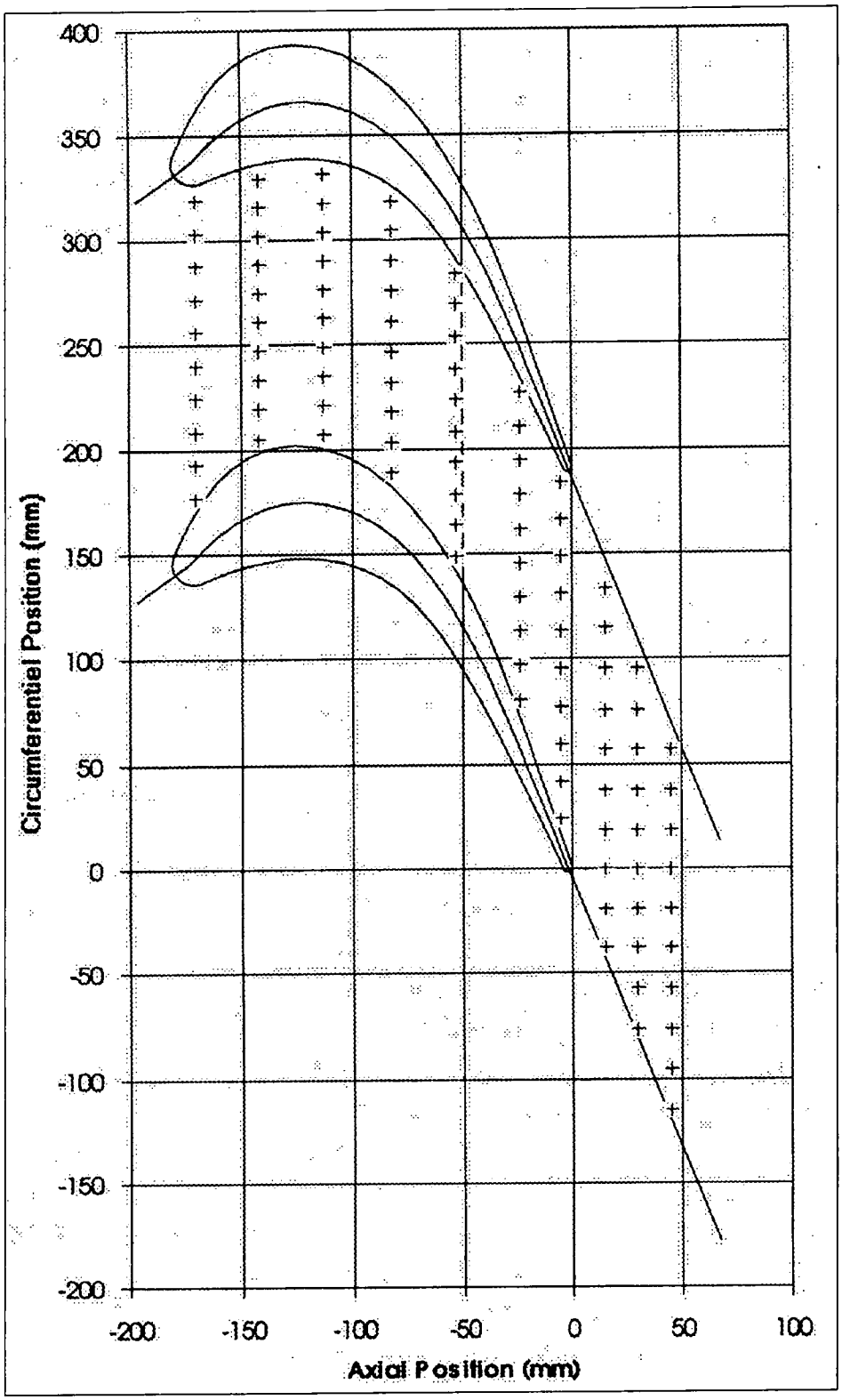

Figure 3.8 Static Pressure Tapping Holes

Chapter 4 Experimental Results

This chapter will discuss the results of the analysed data obtained from the experiment. These values are then plotted depending on their form for discussion. A brief section will be dedicated to explain the difference in features between Profile 1 and Profile 2 end wall. Testing for each slot for Profile 2 has been repeated at least three times to ensure consistency of results. Measurements were also taken to produce end wall static pressure contour maps to give a better understanding of the end wall characteristics. This would give an indication of the effect of the profile shape on the fluid flow in the blade passage. Finally flow visualisation was carried out, which involved short strands of thread. This will be explained in detail in section 4.6.

Comparisons will be first made for the end wall static pressure contours for the Planar, Profile 1 and Profile 2 end wall. This will be followed by the analysis of the contour maps and secondary flow vectors and the related pitch averaged and area averaged results for Slot 8. Results for Slot 10 will be discussed in a similar manner, and will also include the mixed out loss results

4.1 Profile 1 and Profile 2 End Wall

As mentioned in Chapter 1, Profile 1 end wall refers to the end wall profile tested by Hartland et. al. [1999]. Profile 2 end wall refers to the current end wall profile. It must be remembered that both these profiles have been manufactured using the same material and tested in the same large-scale cascade in Durham.

Profile 1 end wall is designed with a curvature that begins upstream of the leading edge and terminates downstream of the trailing edge. It has a significant convex curvature at the pressure surface that stretches up to the trailing edge and a concave curvature that is more significant near the suction surface. In Profile 2 end wall however, the curvature is restricted to the blade passage, after which it is planar beyond the trailing edge. This is to make it more realistic for application to a real turbine. Profile 2 end wall is designed with this improved feature with the same aim of reducing the losses caused by secondary flows. Figure 4.1 shows the height contour plot for Profile 1 end wall while Figure 4.2 shows Profile 2 end wall with emphasis on the curvatures on the pressure side. It can be clearly seen that the ridge located near the trailing edge in Profile 1 end wall has been removed in Profile 2 end wall.

Once Profile 2 end wall was manufactured, it was then fixed onto the cascade firmly to ensure no irregularities on the wall of the cascade. Measurements were taken principally using an automated traversing system at Slots 8 and 10, which are 97%, and 128% axial chord respectively. These traverses were carried out using the 5-hole pressure probe. Due to the size of the probe which prevented traversing closer to the end wall, measurement were taken 5mm from the end wall for all 3 profiles for both Slot 8 and 10. The data obtained after traversing was then processed as mentioned earlier in Chapter 3. The final results were the plotted to give the respective contour and pitch averaged plots.

4.2 End Wall Statics

Analysis of the end wall static pressure was done on the Profile 2 and was compared with the Planar and the Profile 1 end wall. The pressures were measured on an inclined multi-tube manometer, which was set at 30^0. The contours are of static pressure coefficient C_{PS}, which is the difference between the local and the upstream static pressures divided by the upstream dynamic head. This has been previously defined in Chapter 3. Thus a negative value on the contour would signify low local pressure while a positive value indicates high pressure. Figure 4.3 shows contour plots for the Planar, Profile 1 and Profile 2 end walls. It should be noted that due to the contour plotting routine, only the central passage should be studied as the contours are misleading in the upper and lower half passages.

In general it can be seen from Figure 4.3, that in all three contour plots that there is a high pressure region near the pressure surface and a low pressure region near the suction surface. Thus in the presence of a strong pressure gradient caused by the mainstream flow, the low momentum boundary layer will sweep across from the pressure surface to the suction surface of the end wall. Since the secondary flow is largely influenced by this cross passage pressure gradient, it is important to influence the local velocity by changing the end wall pressure distribution. Thus the idea of a non-axisymmetric end wall profile in both Profile 1 and Profile 2 was to influence the local pressure field. The convex curvature near the pressure surface is aimed to reduce the static pressure while the concave curvature at the suction surface is aimed to increase the local pressure.

From the Planar contours, it can be seen that there is a very high pressure region at the pressure surface which is identified by the 0.75 contour line. This is not seen in both Profile 1 and Profile 2. This clearly shows that the convex curvature has significantly reduced the static pressure in both the profiled end walls at the pressure surface.

Between Profile 1 and Profile 2, it can be seen that the high pressure region is more widespread at the pressure surface in Profile 1 than in Profile 2. However, the peak of the highest pressure is located approximately 20 mm from the blade pressure surface in Profile 2, whereas it is much closer to the pressure surface in Profile 1. It would appear that the convex curvature in Profile 2 end wall has a different characteristic from that in Profile 1 end wall. This difference is not only in terms of location from the pressure surface but also the shape of the convex hump which is more rounded in Profile 2 end wall than in Profile 1 end wall. On the suction surface however, Profile 1 seem to generate much lower pressures compared to Profile 2 end wall. Therefore due to the higher pressures at the suction surface in Profile 2 end wall compared to Profile 1 end wall, the velocities in the suction surface would be significantly reduced in Profile 2 than in Profile 1 end wall. The effects of curvature on the static pressure magnitude are much greater near the suction surface because the velocities are higher there.

Following the –2.00 contour, it can be seen for the Planar end wall that it begins at 210 mm from the pressure surface and ends 195 mm on the suction surface with reference to tangential position. It ranges 15 mm in circumferential position and almost 80 mm in axial position. A similar pattern is observed for Profile 1 where it occupies 5 mm in circumferential position and 80 mm in axial

position. As for Profile 2 end wall, it only covers 25 mm in axial position but a larger circumferential position of approximately 100 mm. In other terms the –2.00 contour line is more vertical than in the other two profiles. This trend is observed to begin from the –1.00 contour line onwards. This clearly shows that there is a rapid pressure decrease on the suction surface for Profile 2 that takes place further downstream compared to the Planar and Profile 1 end wall. Hence the more uniform pressure across the blade passage in Profile 2 end wall should reduce the cross passage flows.

4.3 End Wall Boundary Layer

Measurements of the end wall boundary layer profile have been made at a slot located –108% axial chord upstream of the leading edge. This traverse consists of 42 radial points starting 2 mm from the end wall up to 190 mm from the end wall. It was measured using a flattened pitot probe, which measures only the total pressure. This value is then made dimensionless with the upstream dynamic head and plotted to give the total pressure coefficient graph.

The boundary layer profile for the Planar, Profile 1 and Profile 2 end wall is presented in Figure 4.4 and it can be seen that they are very similar with respect to each other. Near the end wall, Profile 2 appears to have the lowest loss from 2 to 10 mm from the end wall but is somewhere between Profile 1 and the Planar end wall in the range of 15 mm and 80 mm from the end wall. In general the inlet boundary layer is not an ordinary one due to the hump in total pressure (negative loss) between 20 and 130 mm in circumferential position seen in Figure 4.4. This is believed to be due to the turbulence grid, which is located 150 mm upstream of

the end wall bleed. A jet effect is produced between the bars that results in a non-uniform velocity profile further upstream at the end wall, and so distorts the inlet boundary layer shape. The extra bar fitted near the wall mentioned in Section 3.1 appears to be only partially successful in reducing the jet effect.

4.4 Slot 8 Results

Slot 8 that is located at 97% axial chord is just upstream of the trailing edge as demonstrated in Fig 3.2. The traversing grid for the Planar and the Profile 1 end wall carried out by Hartland [1999] differed from Profile 2. For the Planar and Profile 1 end wall, a grid consisting of 19 circumferential points and 30 radial points were used. Profile 2 end wall was tested using 21 circumferential points with 30 radial points. Measurements were taken over a range of 135 mm in circumferential position for the Planar and Profile 1 end wall and 131 mm for the Profile 2 end wall. Radially, both the Planar and Profile 1 end wall traverses occupied 150 mm in distance from the wall to the mid-span, whereas Profile 2 occupied 180 mm. For the purpose of comparison of results between the profiles, data for Profile 2 was only included up to 150 mm.

The results are presented in forms of contour plots and pitch averaged plots. It must be noted that the curves of the pitch averaged data represents only the measured data points and are not extrapolated through the boundary layers to the blade surfaces. On the pressure side, there is a circumferential distance of 26 mm before the point where measurements are taken. On the suction side, there is a distance of 20 mm from the point where the measurements end. It will be seen in the contour plots that there is a difference in the end wall shape

between Profile 1 end wall and Profile 2 end wall. This as mentioned earlier this is because Profile 1 has a curvature that stretches beyond the trailing edge while it is limited to the blade passage with Profile 2 end wall. Hence, the end wall is flat for Slot 8 for Profile 2 end wall but profiled for the Profile 1 end wall.

4.4.1 Secondary Vector Plots

Figure 4.5 shows the secondary vector plots for all three end wall profiles. It can be seen for the Planar end wall, there is a well formed passage vortex which is located far away from the end wall near the suction surface. Profile 1 end wall shows a weaker vortex, which has divided into two vortices. The larger but weaker vortex is centred close to the wall and nearer the pressure surface. The smaller vortex, which is stronger, is closer to the suction surface and further from the end wall. This process has been observed very closely by Hartland et. al [1999]. This smaller vortex seen in Profile 1 end wall is due to the ridge near the suction surface of the end wall. As for Profile 2, there are also two vortices. The larger vortex is located closer to the end wall while is the smaller vortex is located away from the end wall.

Compared to Profile 1, both the vortices are located closer to each other in Profile 2. The larger vortex appears to be weak while the smaller vortex appears to be stronger, as indicated by the strong radial flow near the suction surface on the left of the small vortex. In the region near the suction surface and approximately 65 mm from the end wall, there is a possibility of a weak counter vortex for both Profile 1 and Profile 2 end wall. It was not possible to traverse closer to the corner due to the size of the probe.

4.4.2 Total Pressure Loss

Total pressure loss coefficient, C_{PO} is defined as the ratio between the total pressure loss and the upstream dynamic head as defined in Chapter 3. With respect to this quantity which is shown in Figure 4.6, the Planar end wall shows that the rolling up of the inlet boundary layer is well advanced, thus forming a loss core away from the end wall. Profile 1 gives less rolling up the boundary layer and convection of high energy fluid. This is a result of the lower secondary flows compared to those in the Planar end wall. As for Profile 2 end wall, the inlet boundary layer has also rolled up causing the loss core to move away from the end wall but some what in between in terms of distance the Planar and Profiled 1 end wall. Also the loss levels in the core are higher in Profile 2 end wall than in Profile 1 or the Planar end wall.

4.4.3 Secondary Kinetic Energy

The secondary kinetic energy coefficient C_{SKE} is defined as the local secondary kinetic energy divided by the upstream mainstream kinetic energy. Figure 4.7 shows the secondary kinetic energy contours for the respective profiles. As expected, the Planar end wall demonstrates high energy in between the core of the vortex and the suction surface. The high energy fluid near the suction surface is clearly shown by the magnitude of the contours in that location which is approximately 0.24. Closer to the end wall, Profile 1 end wall has fluid of high secondary kinetic energy which is contributed by the passage vortex.

As for Profile 2 end wall, the high secondary kinetic energy values are clearly seen in position close to the smaller vortex. This peak core is stronger compared to both the Planar and the Profile 1 end wall. However, the region occupied by the high secondary kinetic energy fluid has been significantly reduced compared to the Planar or Profile 1 end wall.

4.4.4 Yaw Angles

Yaw angles represent flow in the circumferential direction. Comparing the yaw angle contour plots for the three profiles in Figure 4.8, the under-turning and overturning is seen to be highest in the Planar end wall. As for Profile 1 end wall, the degree of over over-turning and under-turning has been significantly reduced. Furthermore the angle variations are restricted closer to the end wall. For the Planar end wall, most of the over-turning takes place in close proximity to the vortex core and near the end wall. Approximately 65 mm from the end wall, the angle almost reaches -60^0 and about -75^0 near the end wall, which shows large angle variation. The close contour lines observed about 50 mm from the end wall reflects the vortex core. This is not observed in both the Profile 1 and Profile 2 end wall, which clearly show that the vortex is more intense in the Planar end wall compared to the other two profiled end walls.

As for Profile 2, less variation in angle is observed. The angle reaches approximately -63^o about 50 mm from the end wall and to about -72^o at the end wall. This shows smaller angle variation compare to the Planar or Profile 1 end wall. This characteristic will be seen more clearly in the pitch-averaged results.

4.4.5 Pitch Averaged Results

Figure 4.9 shows the pitch averaged plots for pressure loss coefficient, secondary kinetic energy and yaw angles for the three profiles. Looking at Figure 4.9(a), it appears that the total loss coefficient value dips to almost –0.05 between 60 to 80 mm in radial position for all three end walls. This is due to some high energy boundary layer fluid that did not migrate into the vortex, but instead remains in the mainstream flow as seen in the inlet boundary layer traverse in Figure 4.3.

It appears from Figure 4.9 (a), Profile 2 end wall has the highest loss compared to Profile 1 and the Planar end wall. The Planar end wall is somewhat in between in terms of loss compared to the profiled end walls. The peak for the Planar end wall is located approximately 50 mm from the end wall which corresponds to the core of the vortex seen in Figure 4.4 earlier. This loss approaches a constant value towards the mid-span, which shows that the flow towards the mainstream is mainly two-dimensional. This pattern is seen for both Profile 1 and Profile 2 end wall. Profile 1 end wall appears to have a higher loss closer to the end wall. This could be due to less convection of the boundary layer into the vortices near the end wall as shown in the secondary vector plots.

Profile 2 however appears to have a much higher loss than both the other profiles. It has a peak that is almost 77% higher than the Planar or Profile 1 end wall. This is because Profile 2 end wall has a very strong radial flow near the suction surface which gives rise to the loss. The peak again corresponds to the smaller but stronger vortex near the suction surface. This was demonstrated

earlier by the secondary vector plots. A similar trend is also seen for the pitch averaged secondary kinetic energy coefficients (Figure 4.9(b)) where the high values correspond to the two vortices seen earlier. However the yaw angle variations are lower for Profile 2 end wall than either of the Planar or Profile 1 end wall as seen in Figure 4.9 (c).

4.4.6 Area Averaged Results

For a more general quantitative comparison, the area-averaged values are calculated for three profiles. The area average value integrates the mass flow and the upstream velocities into its definition, as demonstrated in Section 3.5. There are three quantities defined in this way, total pressure loss coefficient, secondary kinetic energy and yaw angle. The table overleaf provides this information.

	Planar	**Profile 1**	**Profile 2**
Total Pressure Loss Coefficient	0.0213	0.0151	0.0590
Secondary Kinetic Energy Coefficient	0.0221	0.0118	0.0244
Yaw Angle	-66.1	-65.7	-65.8

Table 4.1 Area Averaged Values For Slot 8

In terms of the total pressure loss, Profile 1 has produced the least amount of loss compared to both the Planar and Profile 2 end wall. Profile 2 has produced almost three times as much loss than the Planar end wall. Both the Planar and Profile 2 end wall have about the same magnitude for the secondary kinetic energy coefficient but are both about twice that for Profile 1 end wall. In terms of

averaged angle, both Profile 1 and Profile 2 end wall have turned the flow slightly less compared to the Planar end wall but do not differ much compared to each other.

4.5 Slot 10 Results

Slot 10 is used to measure the exit flow, and is at 128% axial chord as shown in Figure 3.2. Hartland tested the Planar and Profile 1 end wall and measurements were taken over 267 mm in circumferential position and 200 mm radially. Profile 2 was tested over a region of 267 mm circumferentially and 180 mm radially. The traversing grid used for Profile 2 is the same as the one used for the Planar end wall. However, since the radial distance measured for Profile 2 is shorter than those in both the Planar and Profile 1 end wall, it was necessary to extrapolate the data for Profile 2 up to 200 mm for the mass averaged results.

4.5.1 Secondary Vector Plots

The secondary vectors as measured are shown in Figure 4.10 for all three profiles. The Planar end wall shows the passage vortex, which rotates in the clockwise direction with a shed vortex situated above to the left, rotating in the opposite direction. This counter vortex stems from the trailing vorticity from the blade. From Slot 8 to Slot 10, it would seem that the passage vortex has enlarged in size but is less intense, and has moved further away from the end wall. The rate of convection and the final position of the passage vortex downstream is a good indication of the strength of the secondary flows. It can also be seen on the

end wall about –320 mm and –125 mm circumferential position, that there is a small counter vortex caused by low cross flows there.

Profile 1 end wall has also a less intense vortex but slightly larger in size. It did not differ much in position from Slot 8. However, it appears that the cross flow near the end wall on the left of the passage vortex seem a little stronger. Apart from that, there is also a strong counter vortex seen on the end wall. It is located approximately –265 mm and –310 mm in circumferential position. This is due to the low pressure region on the ridge close to the suction surface near the exit.

Profile 2 end wall has very similar characteristics to the Planar end wall. It also has a large passage vortex but it has much reduced radial flow compared to that seen in Slot 8. The core of this vortex is situated closer to the end wall, approximately 50 mm from the surface, unlike for the Planar which is about 65 mm. However it appears to have a weaker counter vortex on the left of the passage vortex at the top compared to the Planar or the Profiled end wall. It also seems to have a small counter vortex on the end wall and a thicker boundary layer on the surface of the end wall.

4.5.2 Total Pressure Loss

The total pressure loss contour plots are shown in Figure 4.11. In general, it can be seen there are two high peaks in all three profiles, which have a coefficient value of 0.9. However they vary in terms of size and distance from the end wall and from each other. These would depend on the intensity and the location of the vortex core as has been observed from the vector plots earlier.

Profile 1 end wall shows a smaller extent of the peak of the loss core and generally closer to the end wall compared to the Planar end wall. Profile 2 shows that the peak of the loss cores are more extended than both the Planar and Profile 1 end wall.

With Profile 1 end wall, the loss associated with the strong counter vortex at the end wall is clearly shown. Looking at the Planar and Profile 2 end wall, there could also be a possibility of a counter vortex at the end wall although this is not so clearly visible. This is because measurements were taken 5 mm from the end wall. The distortion of the wake is less in Profile 2 compared to the Planar or Profile 1 end wall. This is due to the peaks that are located nearer the end wall in Profile 2 than in the Planar end wall. This feature generally results from lower secondary flow, which is more visible in Profile 1 than in Profile 2.

4.5.3 Secondary Kinetic Energy

The secondary kinetic energy contour plots are shown in Figure 4.12 for the three profiles. These plots show the location and the intensity of the high secondary kinetic energy fluid in the region. From the general look of the contour plots, it can be seen that the Planar end wall has the highest secondary energy coefficient value of almost 0.28, located in between of the two loss cores. Profile 1 and Profile 2 end wall appear to have much less high secondary kinetic energy fluid around the vortices. Profile 1 appears to have two regions of high energy fluid, where one is located between the vortices while the other is located near the strong counter vortex on the end wall surface.

4.5.4 Yaw Angle

The yaw angle contour plots for the three end walls are given in Figure 4.13. The Planar end wall appears to have the more under-turning at the vortex core compared to the profiled end walls. If the –64° contour line is followed, the Planar end wall occupies about 147 mm in circumferential distance. Profile 1 and Profile 2 end wall occupy approximately 103 mm and 79 mm respectively. This shows that the angle variations are larger in the Planar end wall, followed by Profile 1 and finally Profile 2 end wall. In Profile 1 end wall, there is also closely spaced contour lines that reflect the strength of the counter vortex on the end wall, and this is not the case for Profile 2 end wall.

4.5.5 Pitch Averaged Results

The pitch averaged plots for the three profiles are shown on Figure 4.14. The Planar end wall gives much lower loss while Profile 2 end wall give slightly lower loss when compared to Profile 1 end wall, at a distance between 5 mm and 30 mm away from the end wall. The high loss in Profile 1 near the end wall is an effect of the strong counter vortex at that location. This feature is clearly seen on both the total pressure loss and secondary kinetic energy coefficient plots. Further away from the wall (30 – 120 mm) the Planar end wall shows the highest and broadest lost peak, while Profile 1 shows the lowest and narrowest lost peak.

From the secondary kinetic energy plots, Profile 2 appears to give slightly higher kinetic energy compared to Profile 1 and this is largely situated between 25 mm to 80 mm from the end wall. This is due to the stronger passage vortex

seen in Profile 2 than in Profile 1. However it is clear that the Planar end wall has the highest peak compared to both the profiled end walls, which is an effect of the much stronger passage vortex in the Planar end wall.

In terms of yaw angle however, both the Planar and Profile 2 end wall give slightly less over turning near the end wall compared to Profile 1 end wall. Compared to Profile1, Profile 2 on the whole gives much less deviation in angle particularly lower under-turning. All three profiles give nearly no change in angle deviation towards the mid-span where the flow is two-dimensional.

4.5.6 Area Averaged Results

For a more general quantitative comparison, the area-averaged values are calculated for three profiles, the same as for Slot 8. The value integrates the mass flow and the upstream velocities into its definition. The three quantities, total pressure loss coefficient, secondary kinetic energy and yaw angle are provided in Table 4.2.

Compared to Slot 8 results in Table 4.2, Profile 2 end wall has now a total pressure loss coefficient value between the Planar and Profile 1 end wall but closer to the Planar end wall value. As for the secondary kinetic energy, Profile 2 end wall has a value much closer to Profile 1 end wall than the Planar end wall. Nevertheless, its average turning is slightly lower compared to both the Planar and Profile 1 end wall.

	Planar	Profile 1	Profile 2
Total Pressure Loss Coefficient	0.1355	0.1178	0.1289
Secondary Kinetic Energy Coefficient	0.0192	0.1001	0.0116
Yaw Angle	-67.5	-67.2	-66.7

Table 4.2 Area Averaged Values at Slot 10

4.5.7 Gross, Net And Mixed-Out Loss Results

Figure 4.15 (a) shows the gross losses at Slot 10. The mid-span loss is subtracted from the total loss to give the gross secondary loss. Between Profile 1 and the Planar end wall, there is a reduction of 23% in the gross total loss and 44% for the gross secondary loss. For Profile 2 end wall, there is only 5% reduction on the gross total loss and 10% in the gross secondary loss.

Further investigations have been carried out to understand the exit loss measured relative to the inlet loss at Slot 1. Figure 4.15 (b) shows the net losses at Slot 10. These values are obtained by subtracting the corresponding loss measured at Slot 1. Measurements at Slot 1 was carried out by Hartland for both the Planar and Profile 1 end wall and these gross values are given in Appendix D. The inlet loss values are negative due to a hump in the inlet boundary layer profile. Since testing has not been done at Slot 1 for Profile 2 end wall it is assumed here that the loss at the inlet is the same as for the Planar end wall. The Planar end wall is chosen instead of Profile 1 end wall because Profile 2 end wall

is flat upstream of the blade row which is the same as the Planar end wall. The net loss values are shown in Table 4.3 below.

	Total Loss	Profile Loss	Secondary Value	% Planar
Planar End Wall	0.1377	0.0598	0.0780	100
Profile 1 End Wall	0.1108	0.0557	0.0551	70.7
Profile 2 End Wall	0.1308	0.0587	0.0721	92.5

Table 4.3 Net Loss at Slot 10

The net secondary loss can be defined as the inlet loss coefficient at downstream and the mid-span profile loss subtracted from the downstream total pressure loss coefficient. This is given by the equation below.

$$C_{Snet} = \overline{\overline{C_{TU}}} - C_{Pinlet} - C_{Pmid\text{-}span} \qquad \text{Equation 4.1}$$

Compared to the Planar end wall, Profile 1 has achieved a net total loss reduction of 20% and net secondary loss reduction of 29%. The values for the secondary loss appear to be larger for the net loss values compared to gross loss values. This is because Profile 1 end wall gave a slightly lower loss at Slot 1. Profile 2 will have the same net loss reduction as the gross loss of 5% and 10% for the net total and secondary loss respectively.

Taking into consideration the assumption made for Slot 1, it would seem that Profile 2 has in fact has not performed as well as Profile 1 in reducing the secondary loss. However it is necessary to know if this new profile has achieved

better mixing throughout the blade passage. This would allow one to estimate the dissipation of the flow non-uniformities to the point of infinity. The definition of mixed-out loss is given in Chapter 3.

Figure 4.15 (c) shows the net total and secondary mixed-out loss at Slot 10. These values are obtained by subtracting mixed-out loss at Slot 1 from those at Slot 10. The values obtained are given in Table 4.4 below.

	Total Loss	Profile Loss	Secondary Value	% Planar
Planar End Wall	0.1588	0.0627	0.0961	100
Profile 1 End Wall	0.1345	0.0709	0.0636	66.2
Profile 2 End Wall	0.1458	0.0619	0.0839	87.3

Table 4.4 Net Mixed-Out Values at Slot 10

Taking the Planar end wall as the datum case, Profile 1 and Profile 2 achieved better mixing of the fluid throughout the blade passage. There is a reduction of almost 15% for the net total loss and 34% for the net secondary loss seen in Profile 1 end wall. As for the Profile 2 end wall, it has achieved a reduction of 8% and 13% for the net total and secondary loss respectively. However, Profile 1 has performed better than Profile 2 in terms of net mixed-out secondary loss, where there is almost 21% difference between the profiles. Nevertheless, it must be noted that Profile 2 has achieved better net and secondary loss reduction when calculated at the point of infinity compared to the values obtained at Slot 10. It showed an improvement of 3% for both the net and secondary loss reduction.

4.6 Flow Visualisation

A qualitative picture of the end wall flow is given by flow visualisation. This was initially done by using a mixture of dye and diesel, which is then painted on the end wall. Unfortunately, due to the porosity of the material used, the mixture was absorbed through the end wall rather than flowing on the surface through the action of the wind. Therefore, another method was used using small pieces of thread.

Short pieces of thread approximately 7cm long were inserted through the pressure tapping holes on the end wall. This thread was allowed to emerge on the end wall surface by only 1.5 cm and the rest of the length was used to tie knots to keep the thread in place at the back of the end wall surface. This was done to only 8 pressure tapping rows as shown in Figure 4.16. These rows are located just a short distance upstream and downstream of the leading edge, and also near the pressure surface where the convex wall curvature is present.

The aim of this flow visualisation to determine if there is any stagnant region just before the convex curvature. This would then suggest the possibility of flow separation, which in turn causes high turbulence in the blade passage and increased loss.

Once the wind tunnel was switched on, the short pieces of thread moves to the direction of flow. In areas where the flow is of low turbulence, the thread would not fluctuate but rather remain almost in a straight line. In regions where the flow is highly turbulent, the thread fluctuates in a violent manner. This

phenomenon has been recorded on a video cassette and was analysed more closely. The video images were then converted to normal Bitmap images as shown in Figure 4.17. A more quantitative analysis is given in Figure 4.18. The length of the thread has been greatly exaggerated for the purpose visibility. The fluctuations of the thread have been colour coded and the angle of fluctuation is defined here as the movement from left to right looking from a view normal to the end wall. This figure only shows the direction of flow and the intensity of turbulence based on the angle deviations from the flow direction.

Labelling the rows from upstream of the leading edge, Row 1 is clearly consisting flow with very little or no fluctuations. Most of the vibrations occur when the flow begins to move around the leading edge, which is clearly shown in Rows 3 and 4. However, the last pieces of thread of Row 3 and Row 4 appear to have directed away from the main field flow. This could be due to a small leakage of flow between one panel to the next. Close and above the convex curvature, the flow begins to move to the suction surface of the adjacent blade. This is represented by Rows 5 to 8 where the flow is now more uniform with less fluctuations. On the whole it would seem that the flow does not have any stagnant regions just before the concave curvature on the pressure surface near the leading edge. However the flow appears to be turbulent just before the convex curvature, perhaps suggesting a small separation.

Figure 4.1 **Height Contours for Profile 1 End Wall**

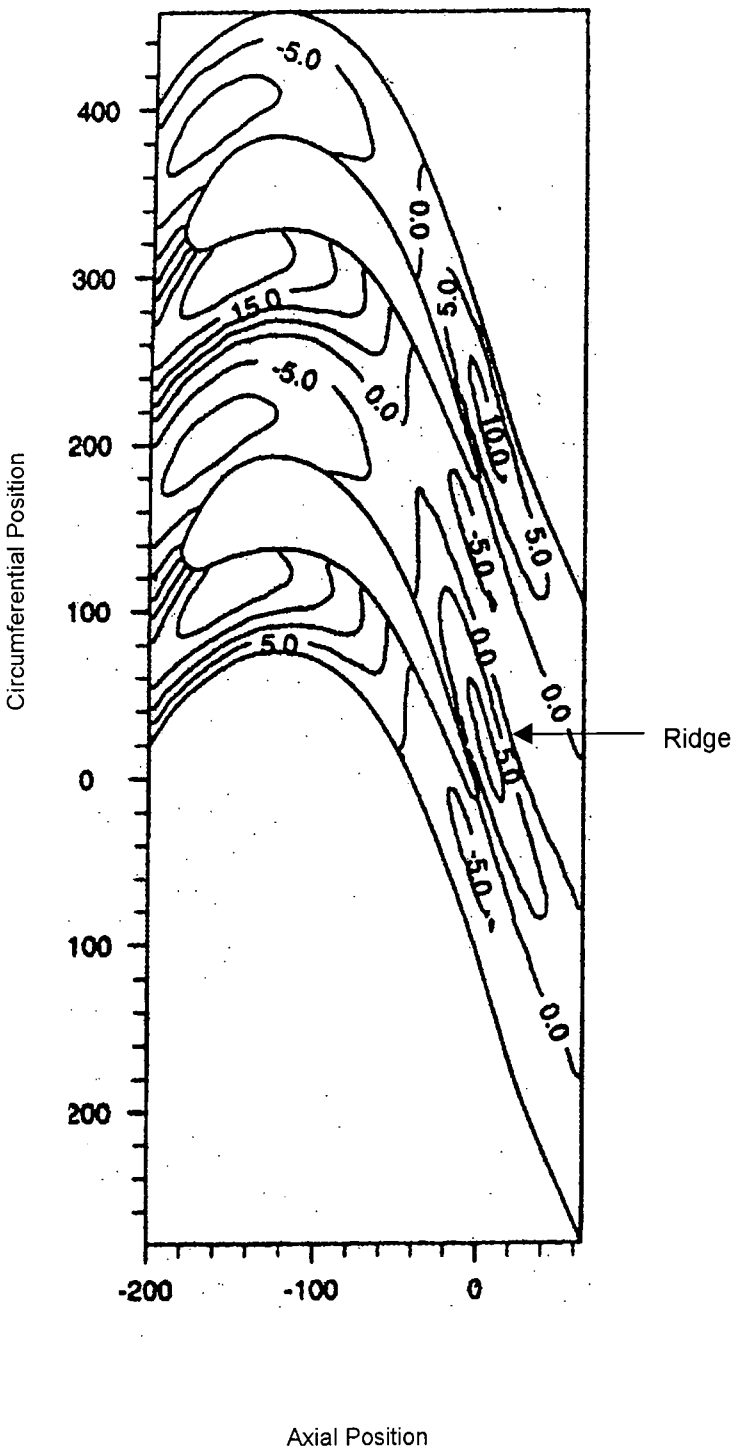

Figure 4.2 **Profile 2 End Wall Curvature**

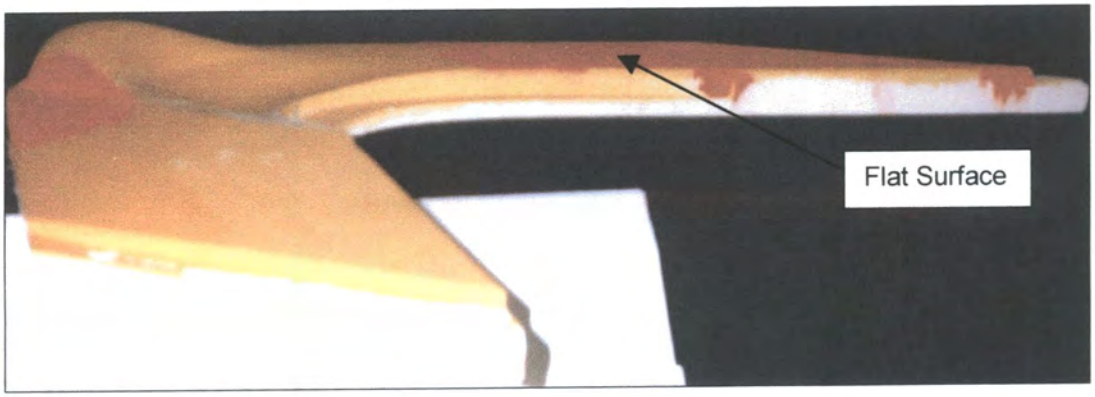

Side View of Profile 2 End Wall

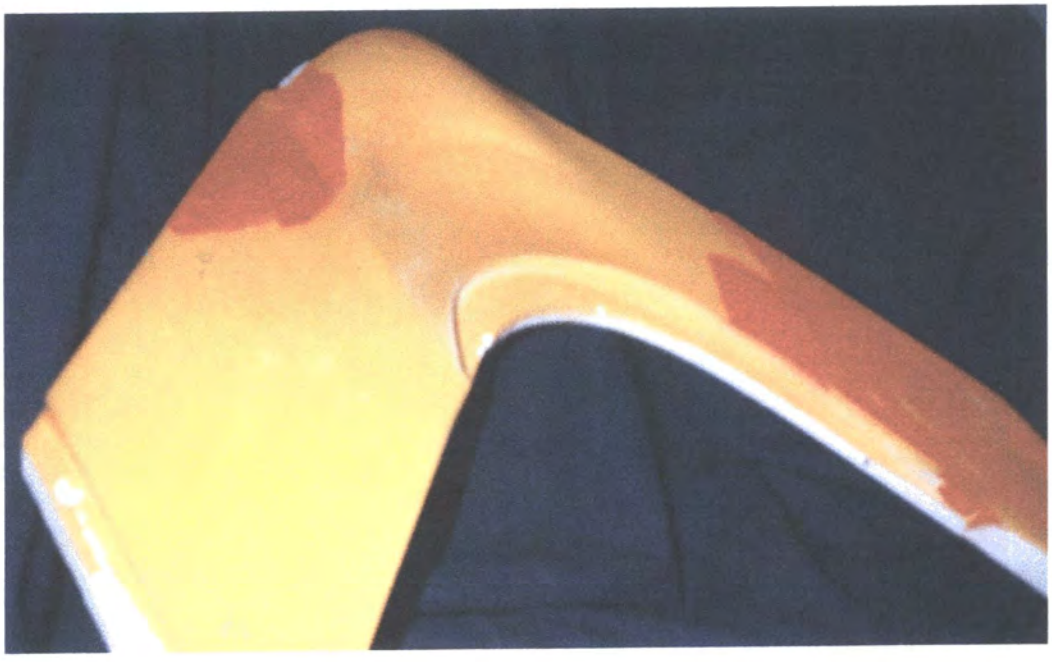

Top View of Profile 2 End Wall

Figure 4.3 End Wall Static Pressure Contour

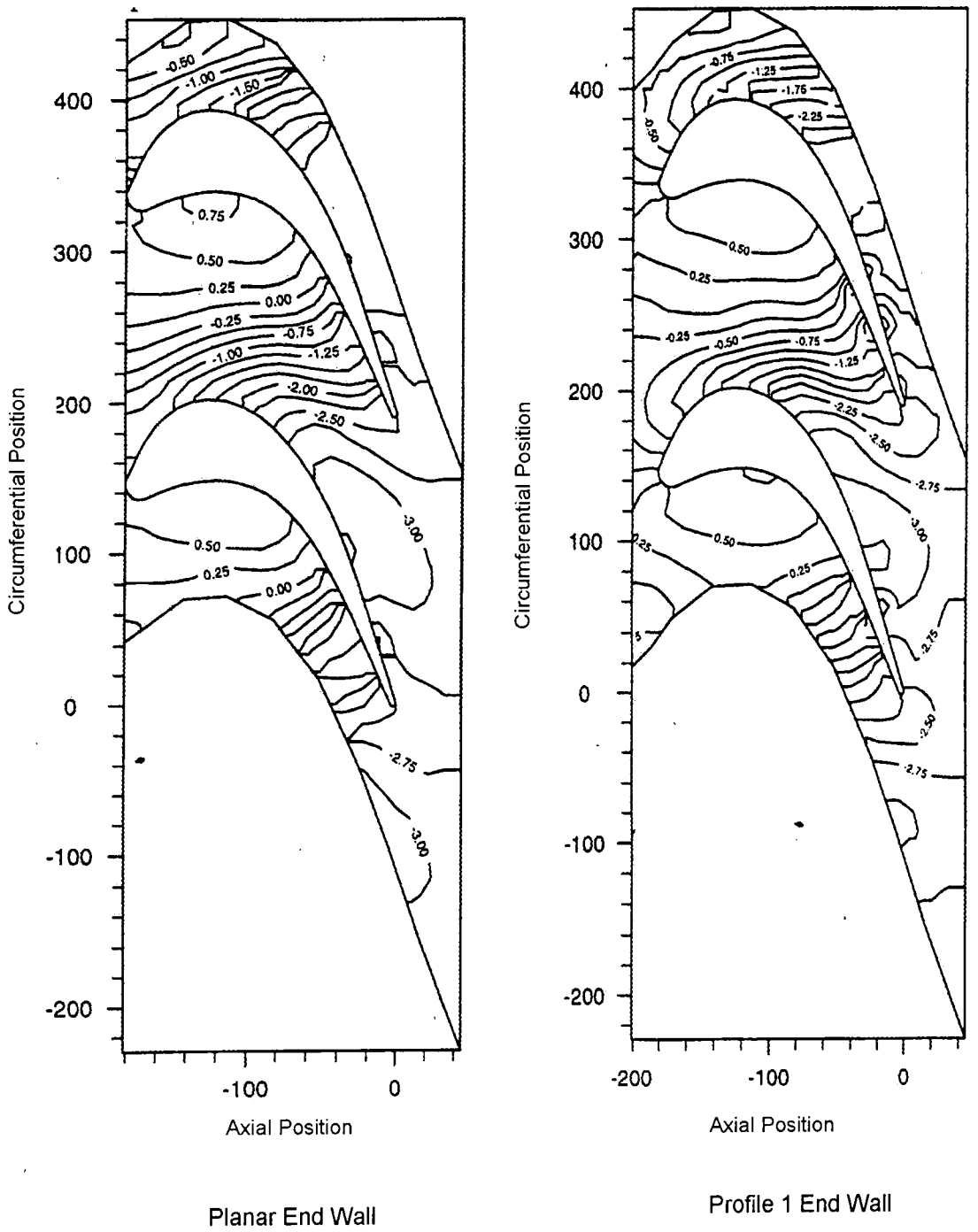

Figure 4.3 **End Wall Static Pressure Contours (cont.)**

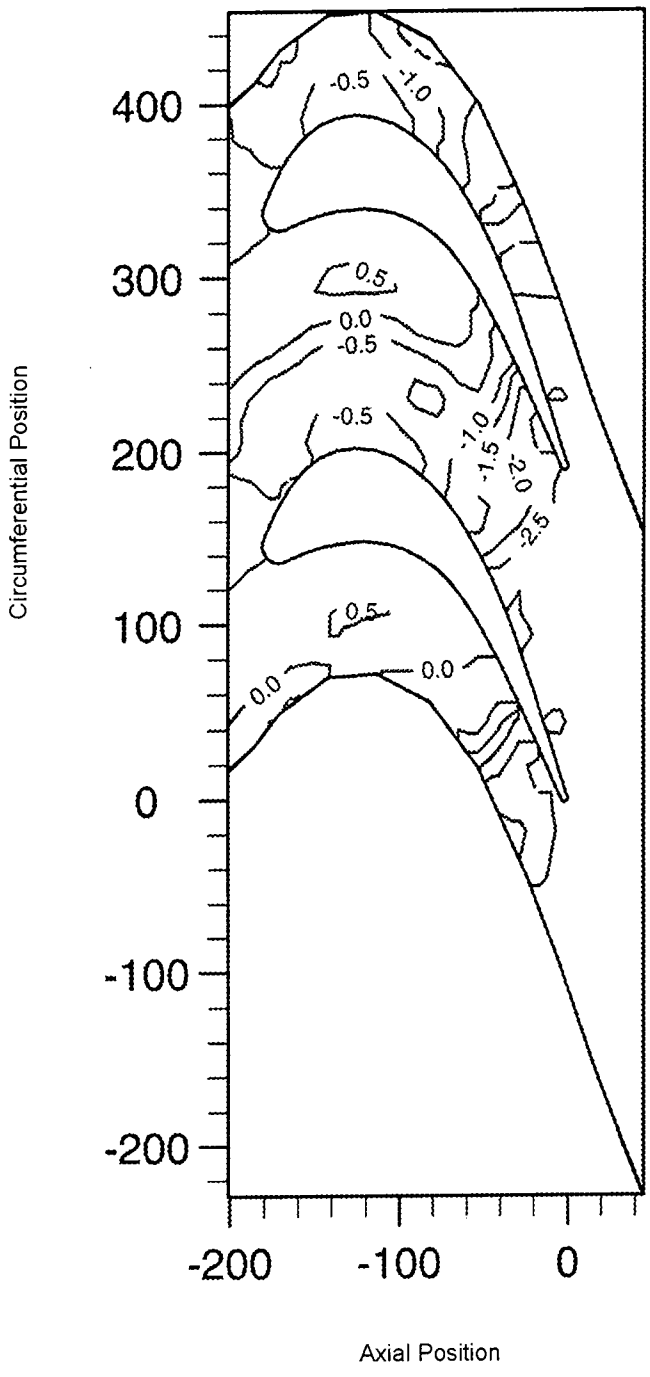

Profile 2 End Wall

Figure 4.4 **Total Pressure Loss Coefficient For The Inlet Boundary Layer**

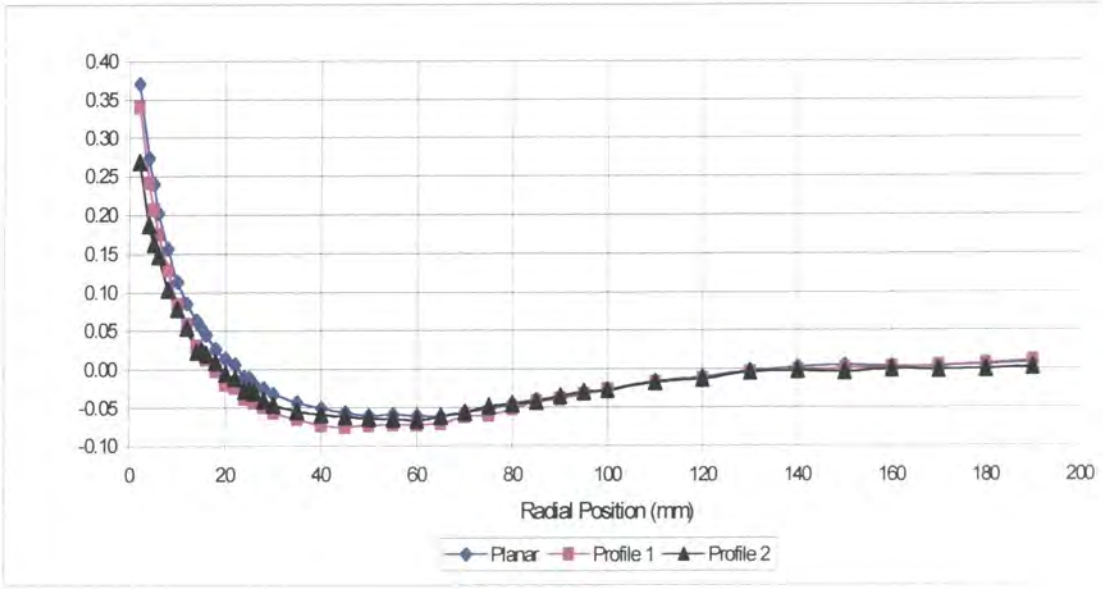

Figure 4.5 **Secondary Vector Plots For Slot 8**

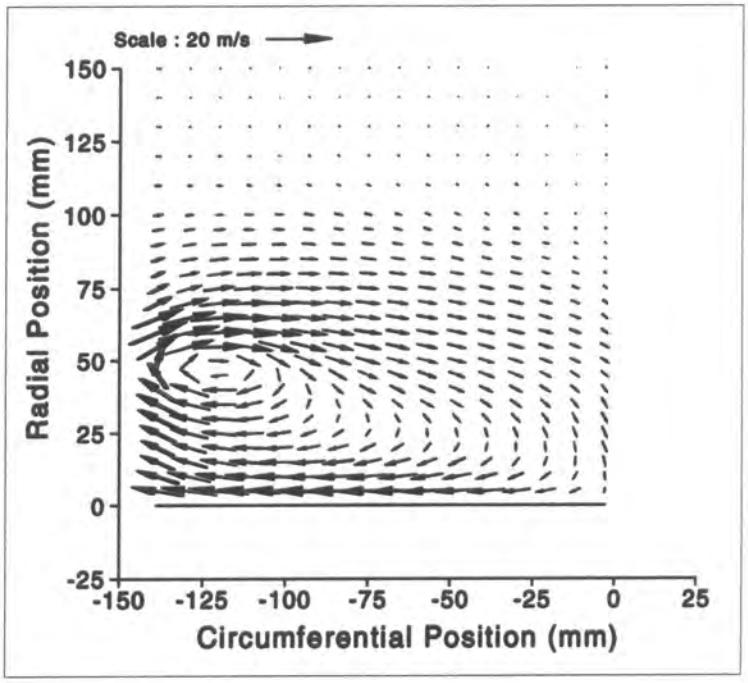

Planar End Wall

Figure 4.5 Secondary Vector Plots For Slot 8 (cont.)

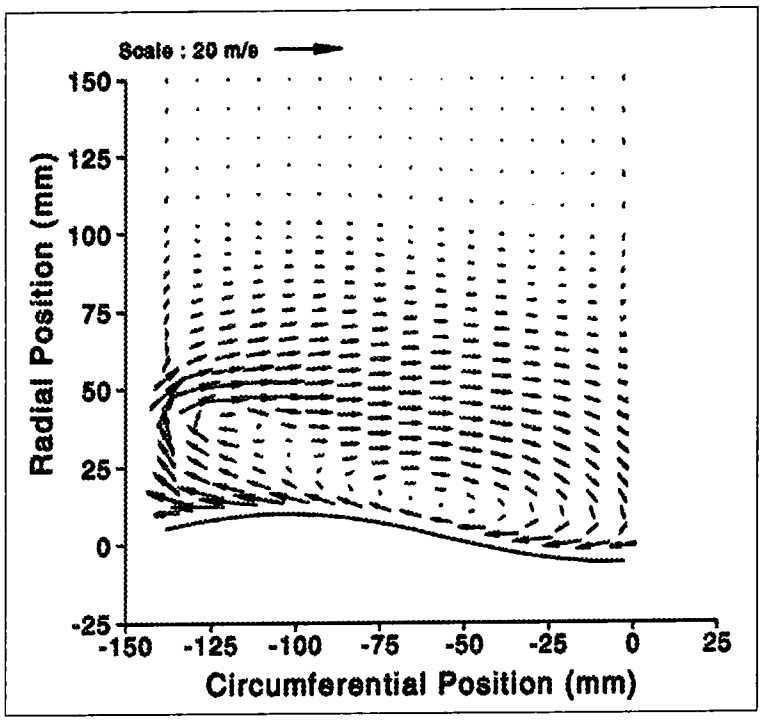

Profile 1 End Wall

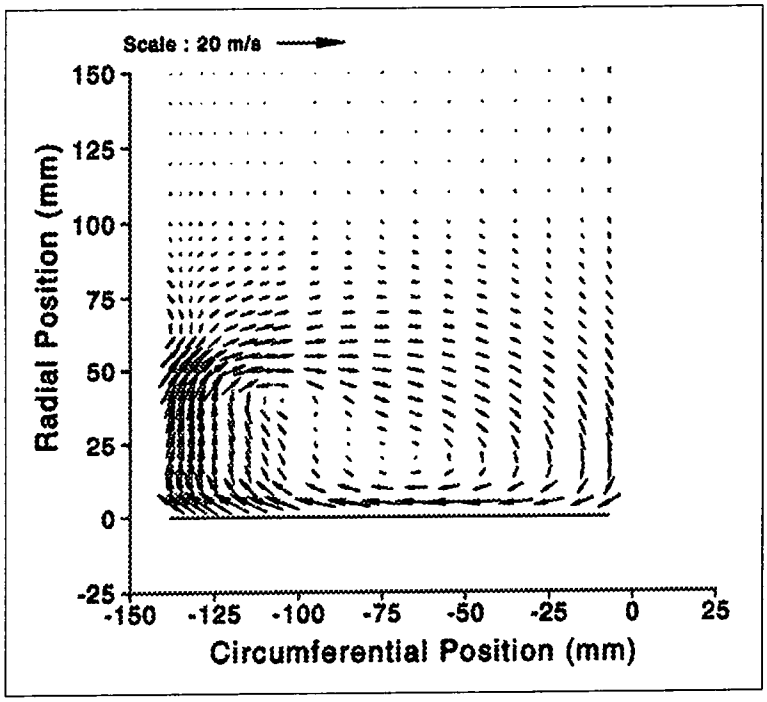

Profile 2 End Wall

Figure 4.6 **Total Pressure Loss Contour Plots For Slot 8**

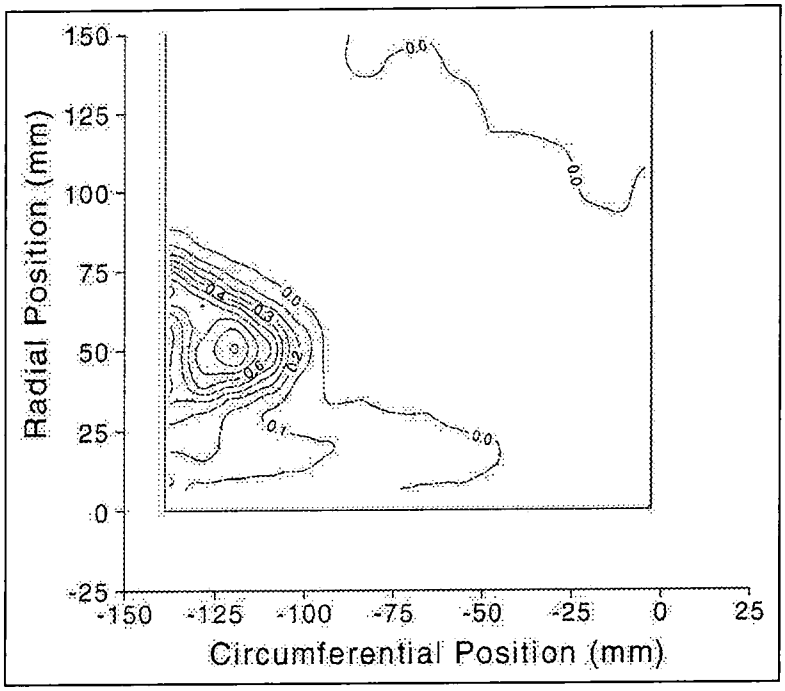

Planar End Wall

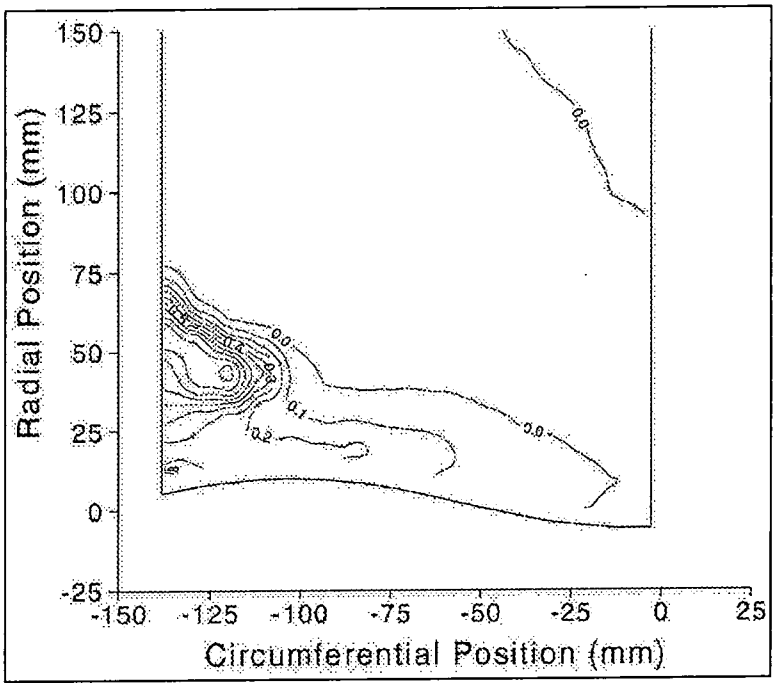

Profile 1 End Wall

Figure 4.6 Total Pressure Loss Contour Plots For Slot 8 (cont.)

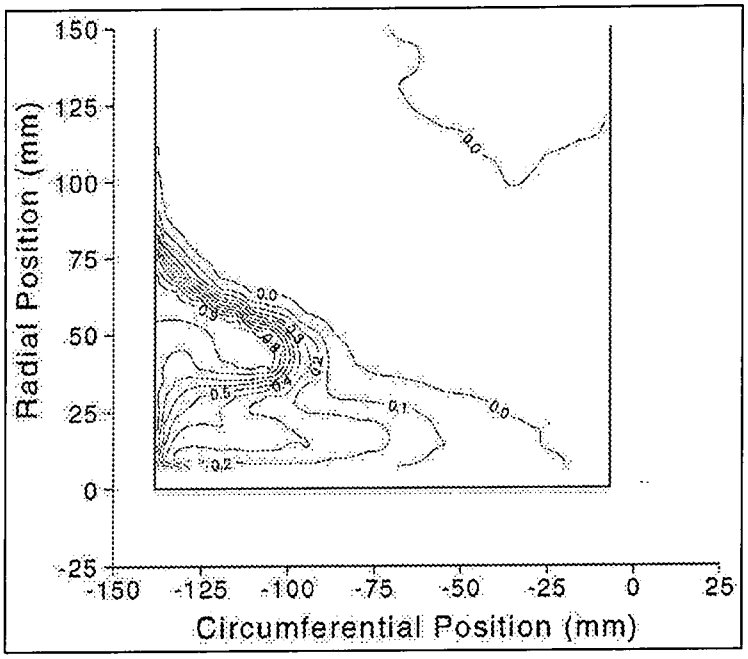

Profile 2 End Wall

Figure 4.7 Secondary Kinetic Energy Contour Plots For Slot 8

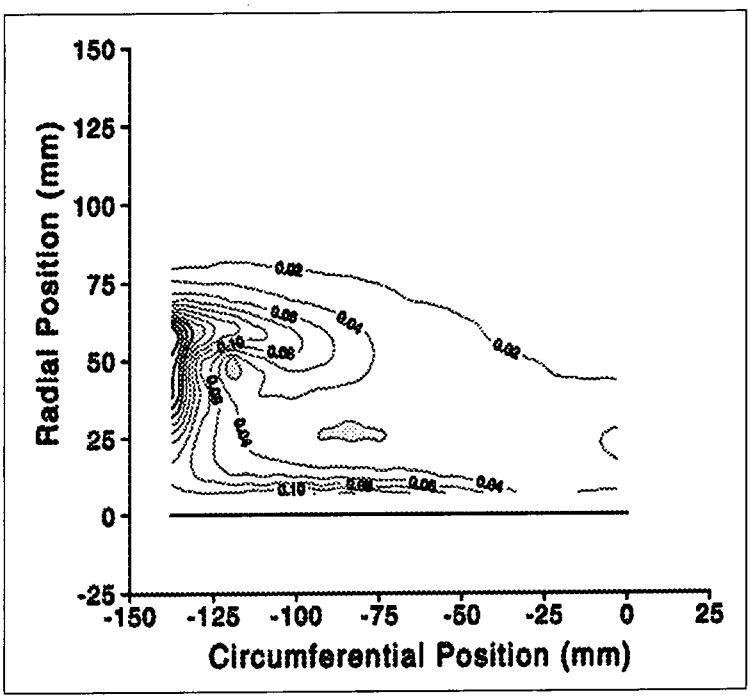

Planar End Wall

Figure 4.7 Secondary Kinetic Energy Contour Plots For Slot 8 (cont.)

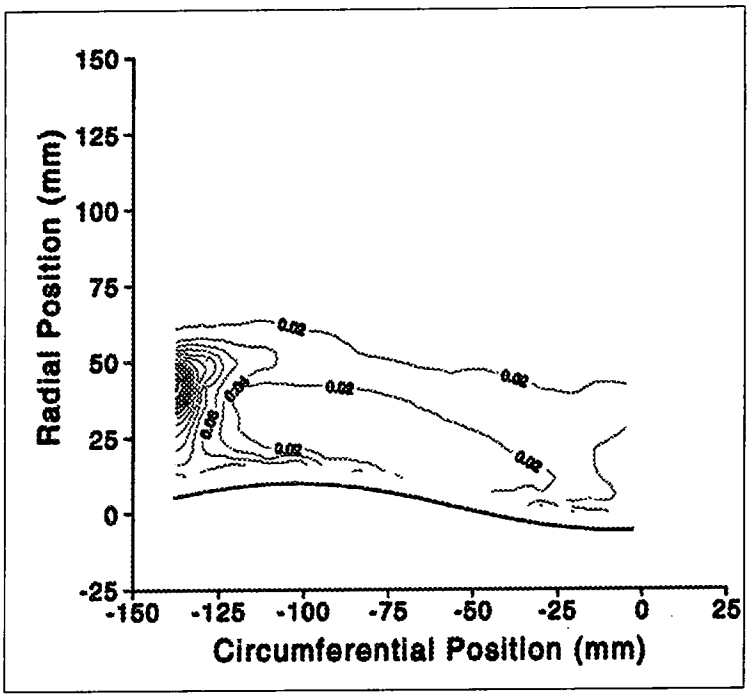

Profile 1 End Wall

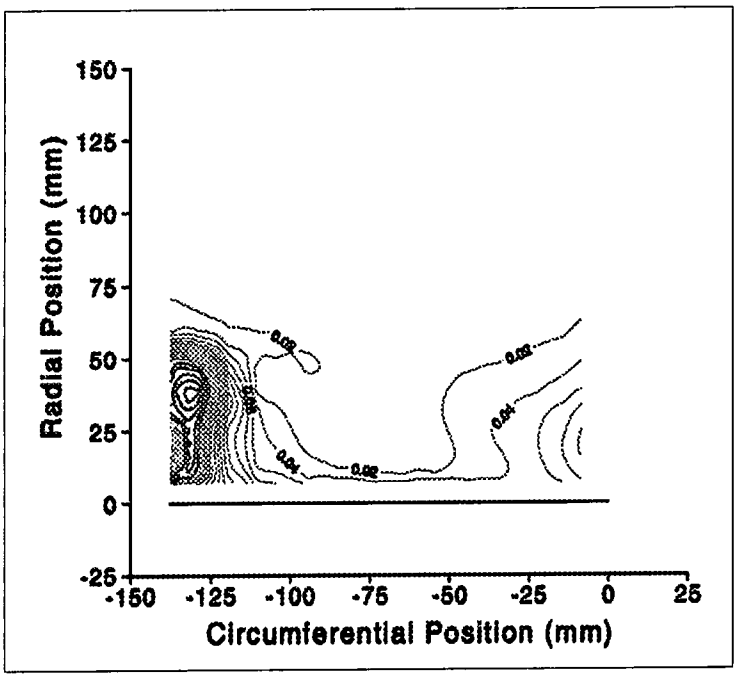

Profile 2 End Wall

Figure 4.8 Yaw Angle Contour Plots For Slot 8

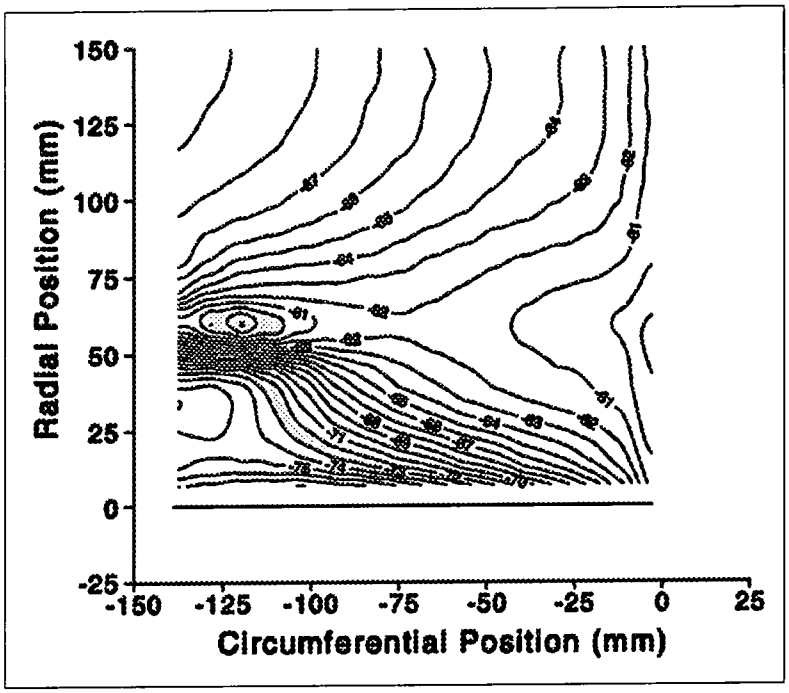

Planar End Wall

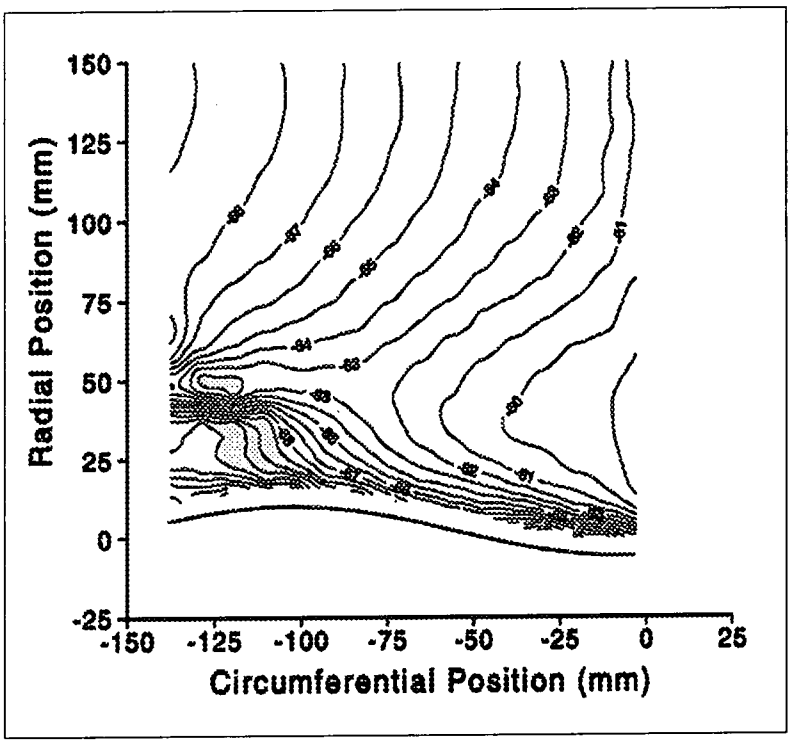

Profile 1 End Wall

Figure 4.8 Yaw Angle Contour Plots For Slot 8 (cont.)

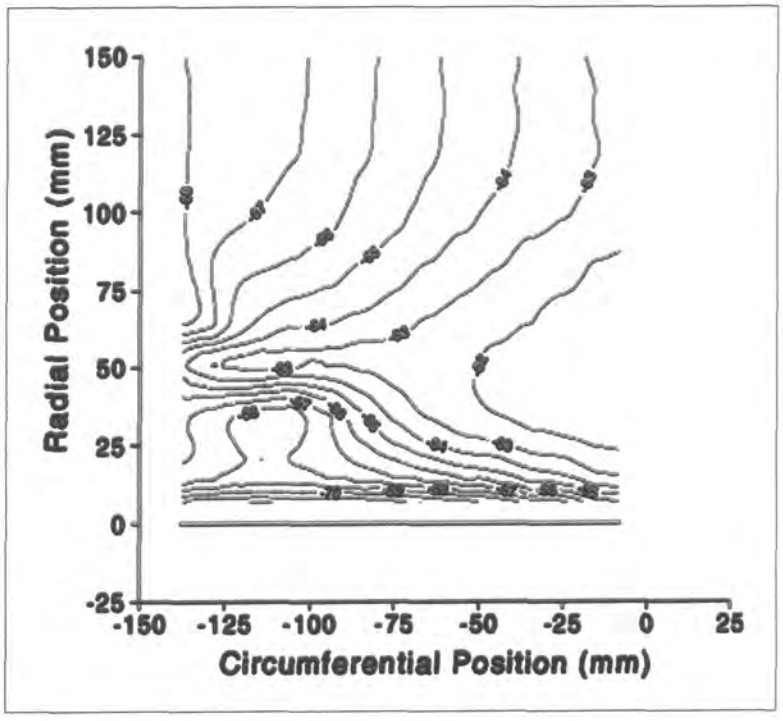

Profile 2 End Wall

Figure 4.9 Pitch Averaged Plots For Slot 8

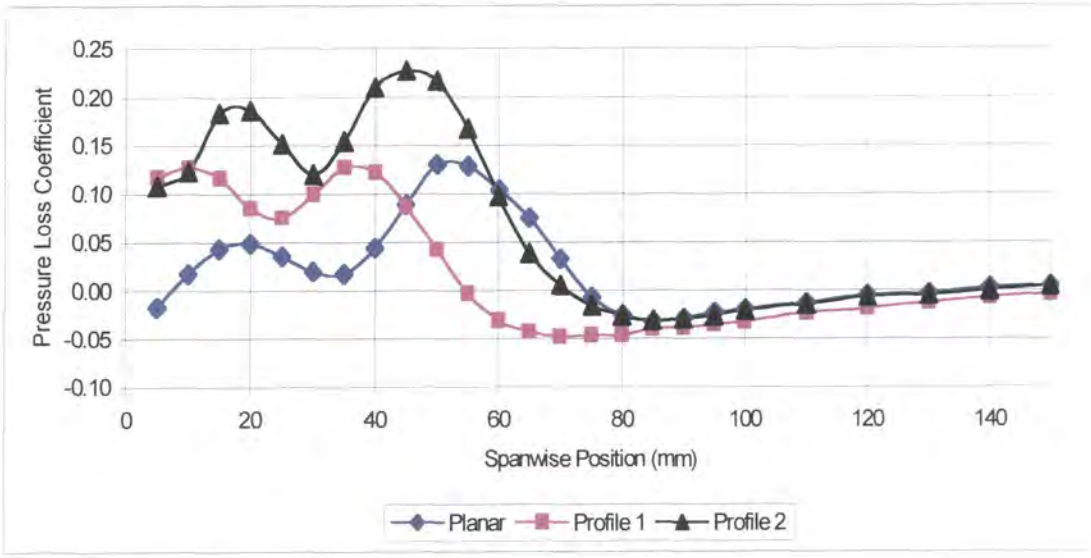

Figure 4.9 (a) Total Pressure Loss

Figure 4.9 Pitch Averaged Plots For Slot 8 Slots (cont.)

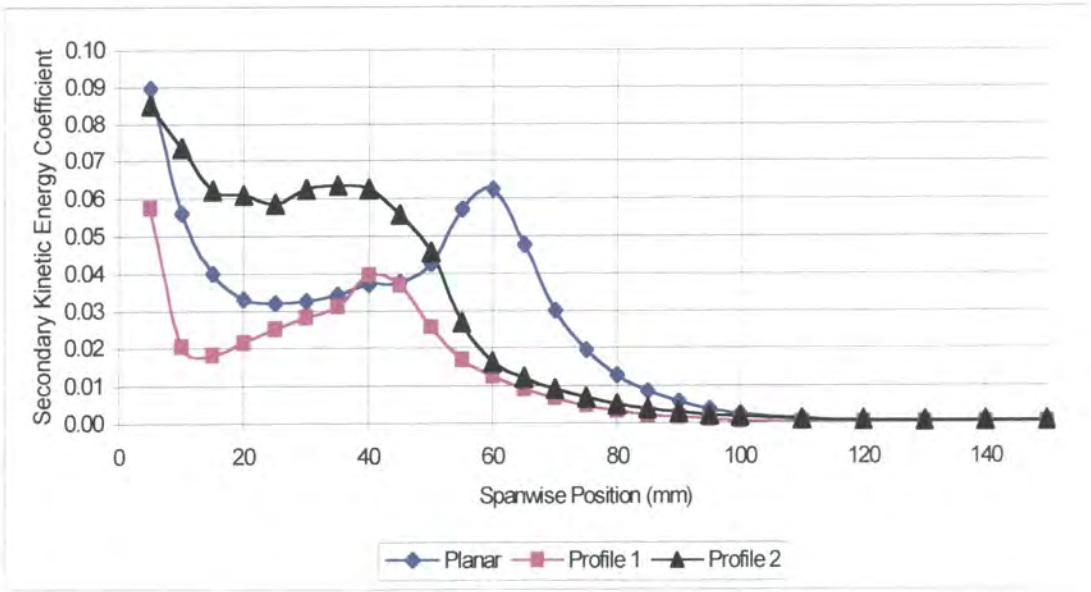

Figure 4.9 (b) Secondary Kinetic Energy

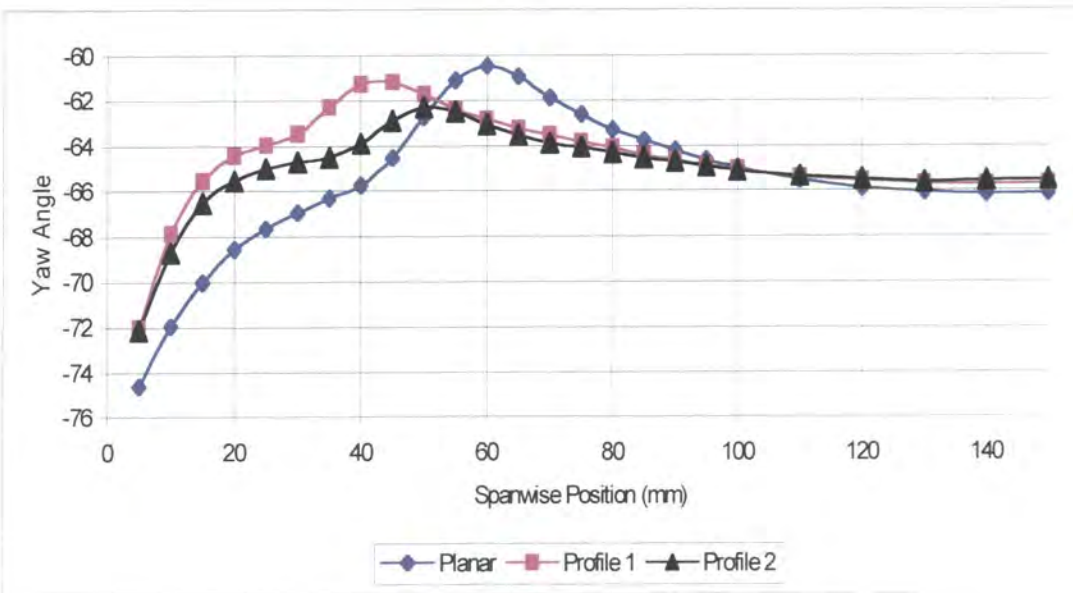

Figure 4.9(c) Yaw Angle

Figure 4.10 **Secondary Vector Plots For Slot 10**

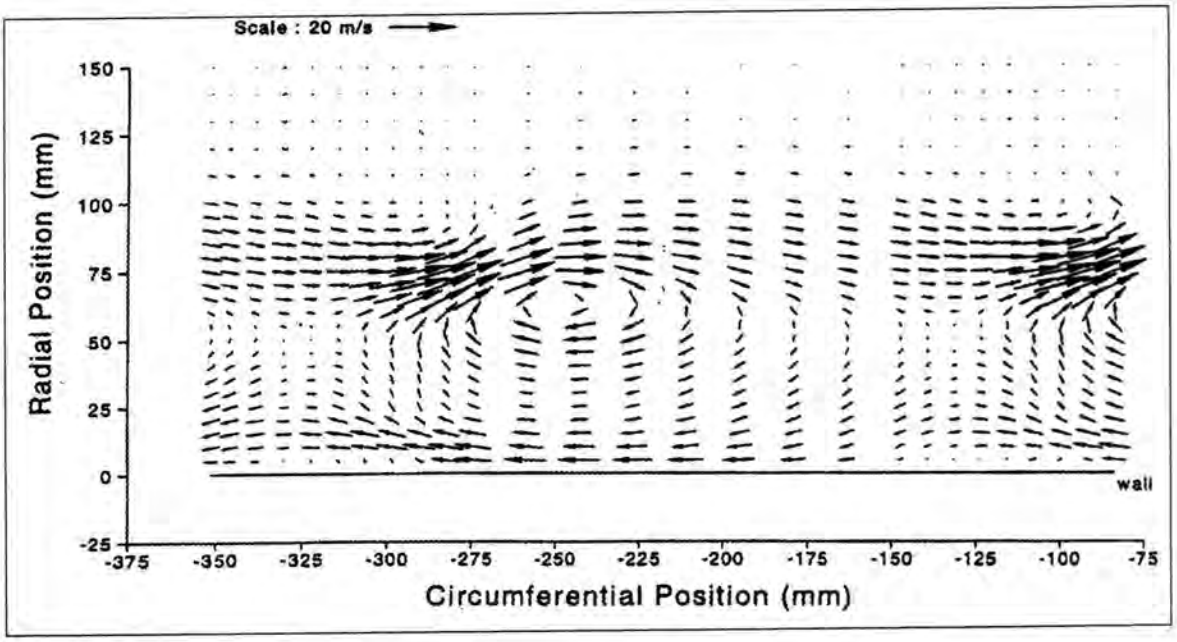

Planar End Wall

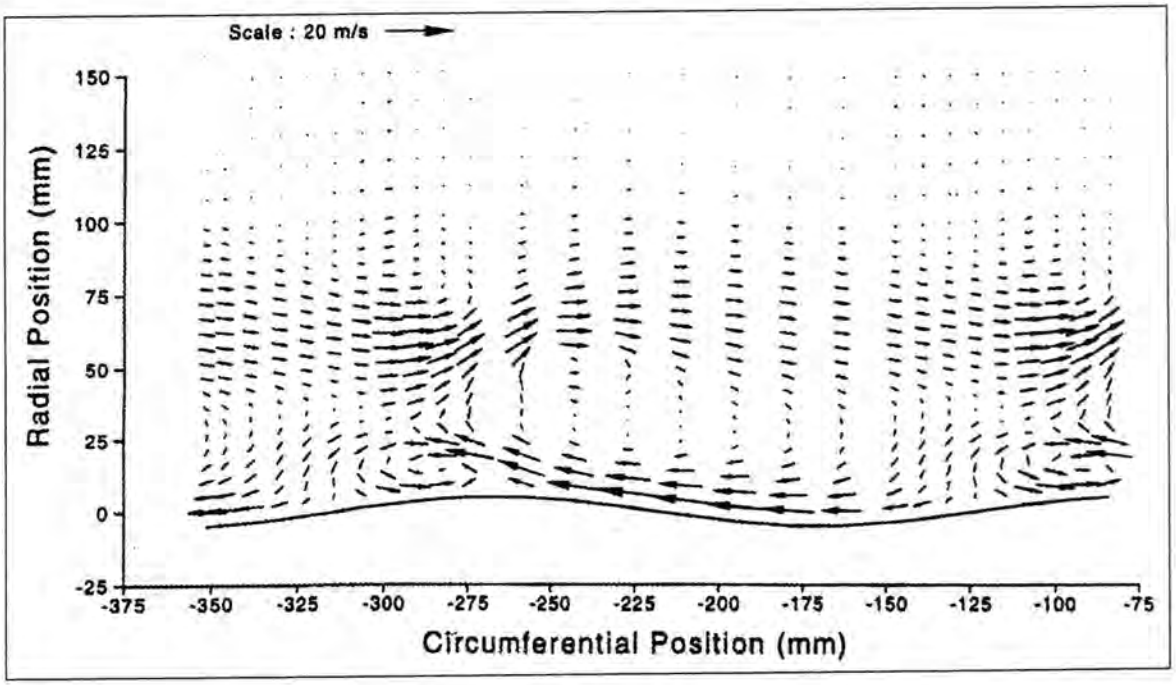

Profile 1 End Wall

Figure 4.10 Secondary Vector Plots For Slot 10 (cont.)

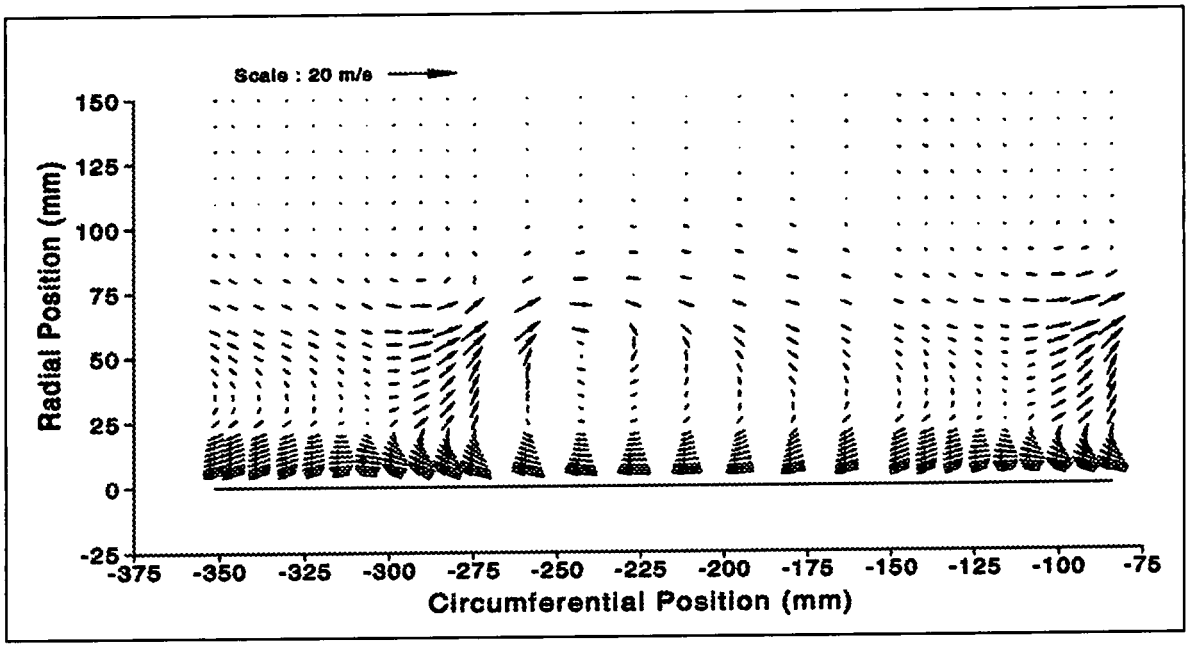

Profile 2 End Wall

Figure 4.11 Total Pressure Loss Contour Plots For Slot 10

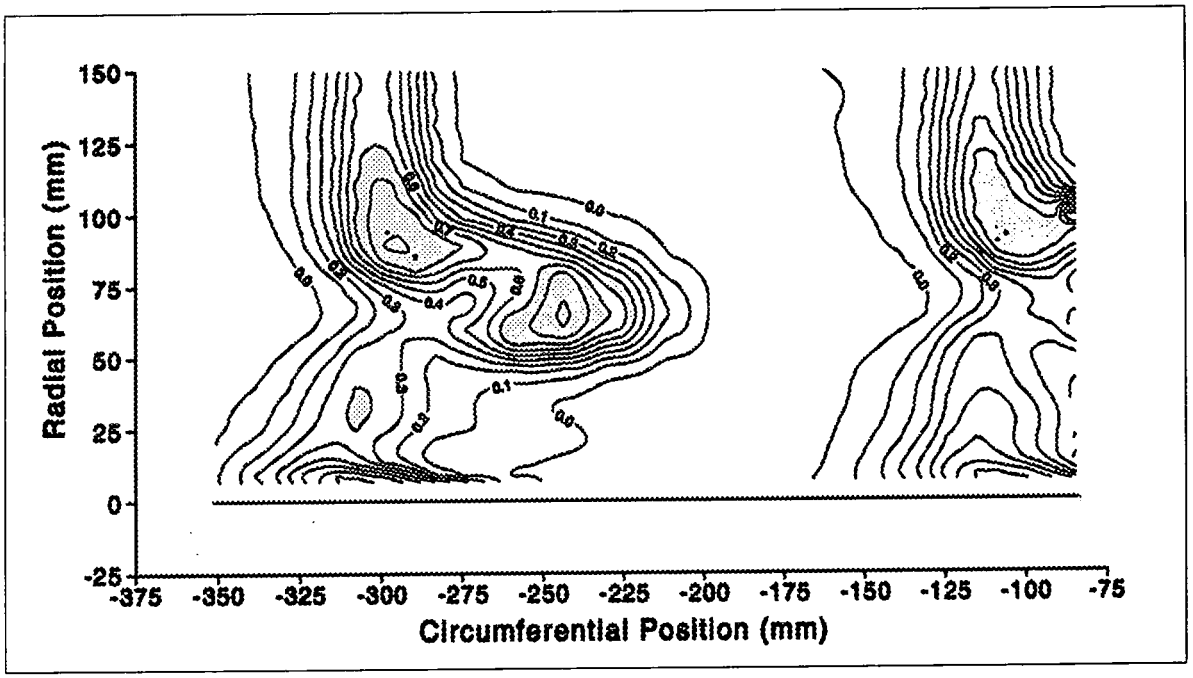

Planar End Wall

Figure 4.11 **Total Pressure Loss Contour Plots For Slot 10 (cont.)**

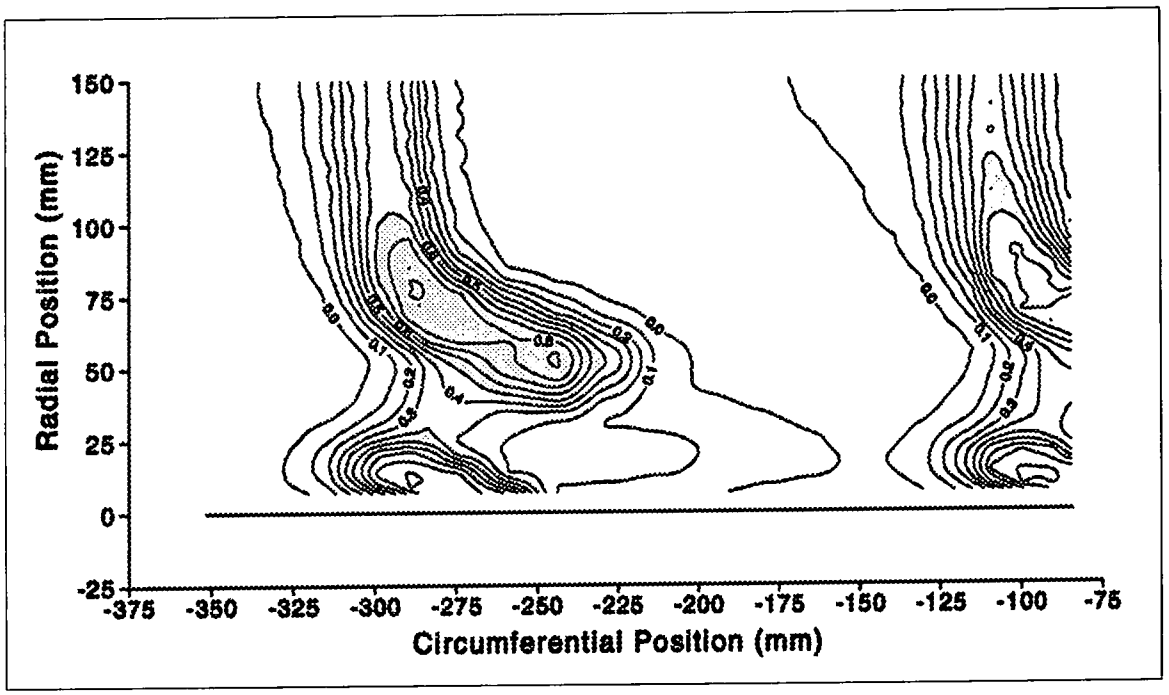

Profile 1 End Wall

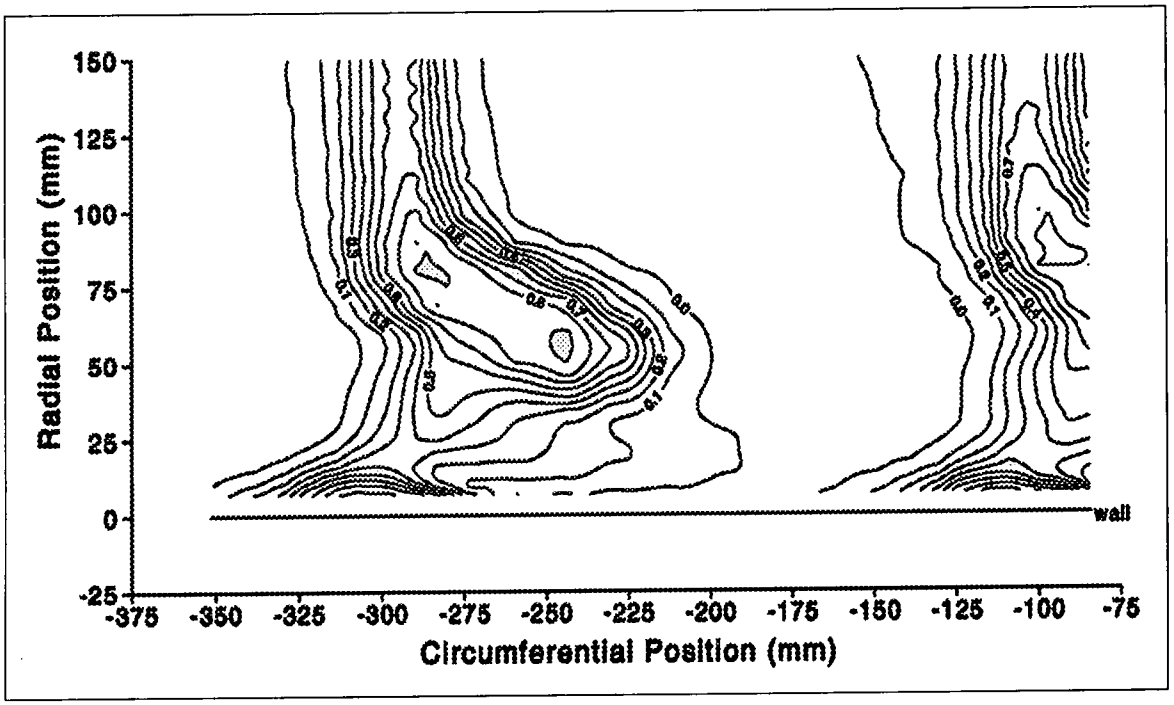

Profile 2 End Wall

Figure 4.12 Secondary Kinetic Energy Contour Plots For Slot 10

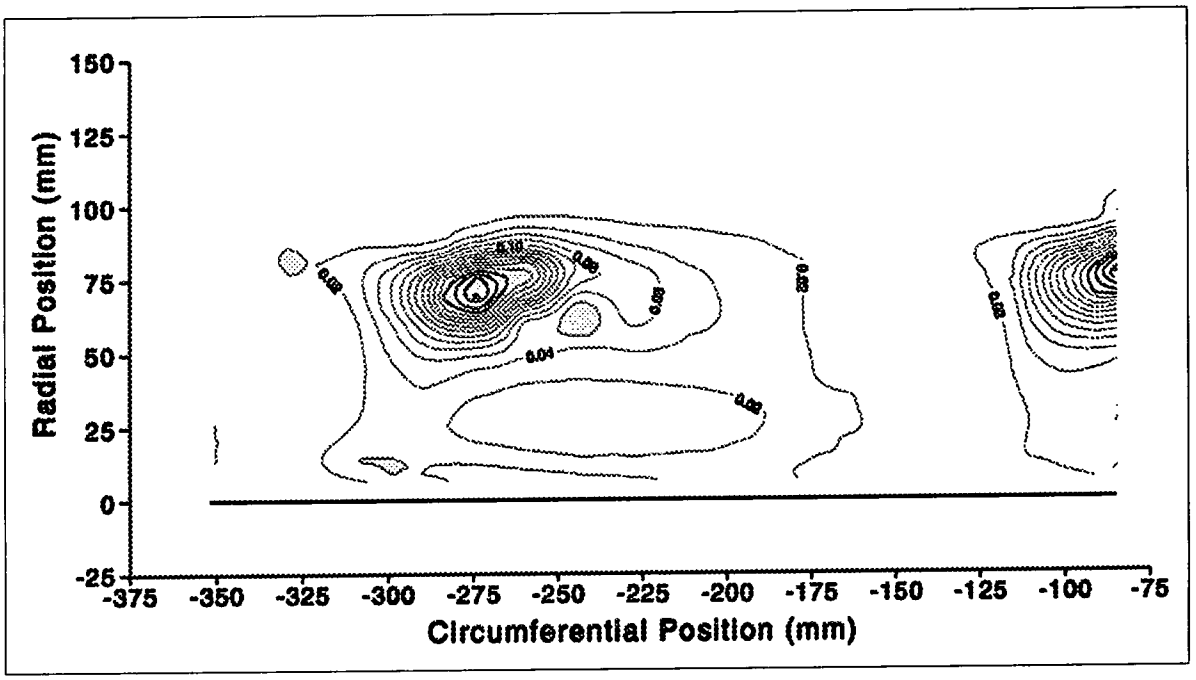

Planar End Wall

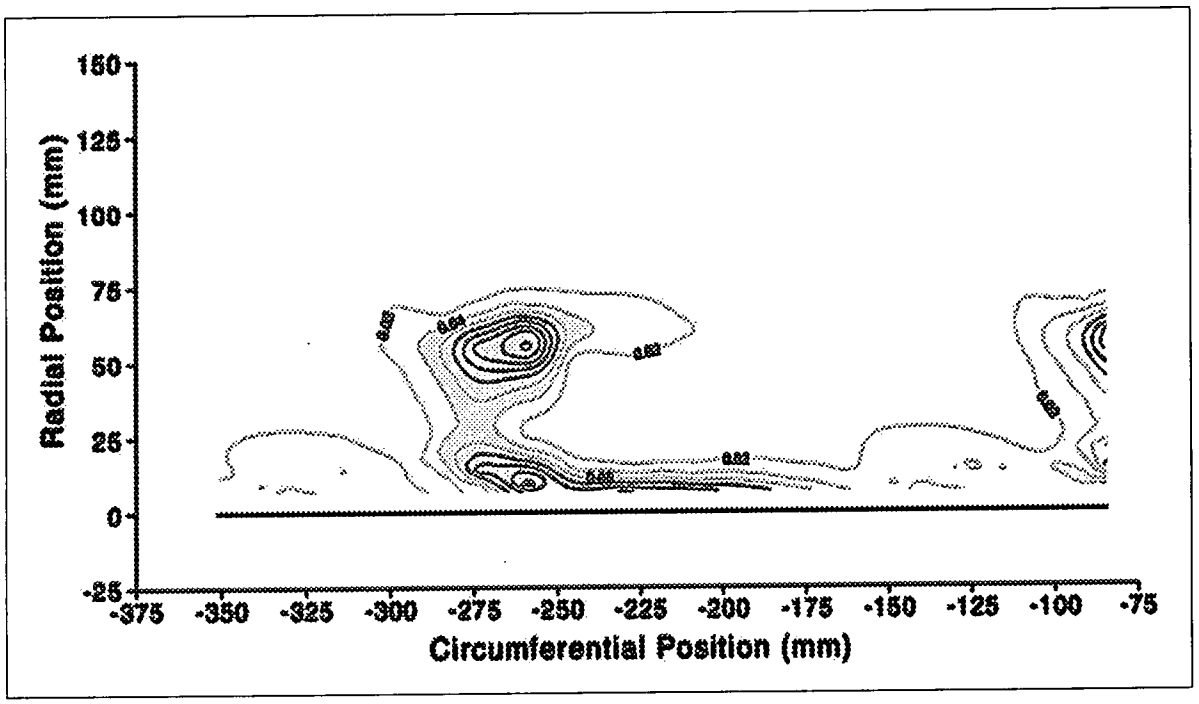

Profile 1 End Wall

Figure 4.12 Secondary Kinetic Energy Contour Plots For Slot 10 (cont.)

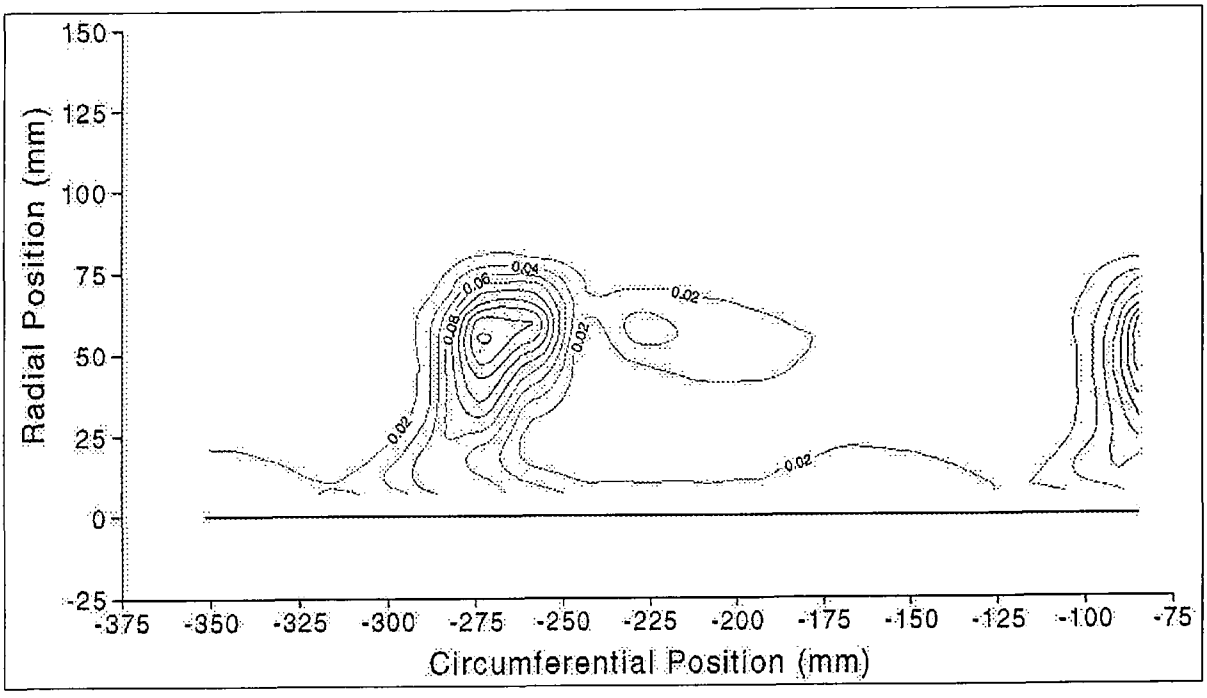

Profile 2 End Wall

Figure 4.13 Yaw Angle Contours For Slot 10

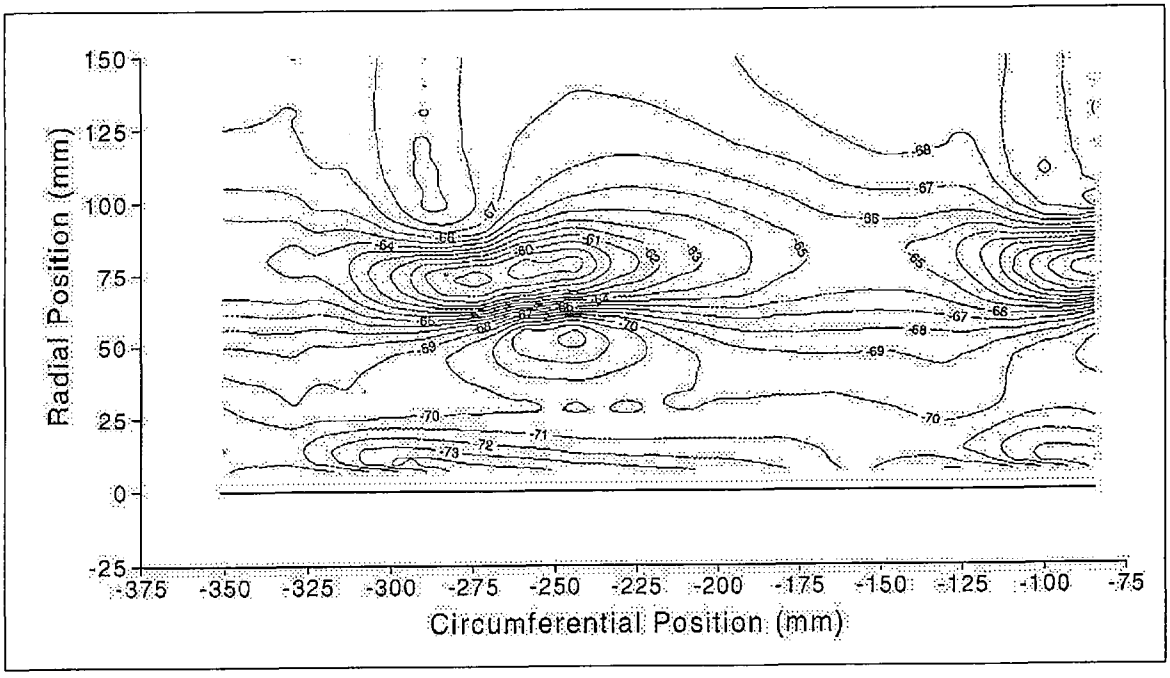

Planar End Wall

Figure 4.13 Yaw Angle Contours For Slot 10 (cont.)

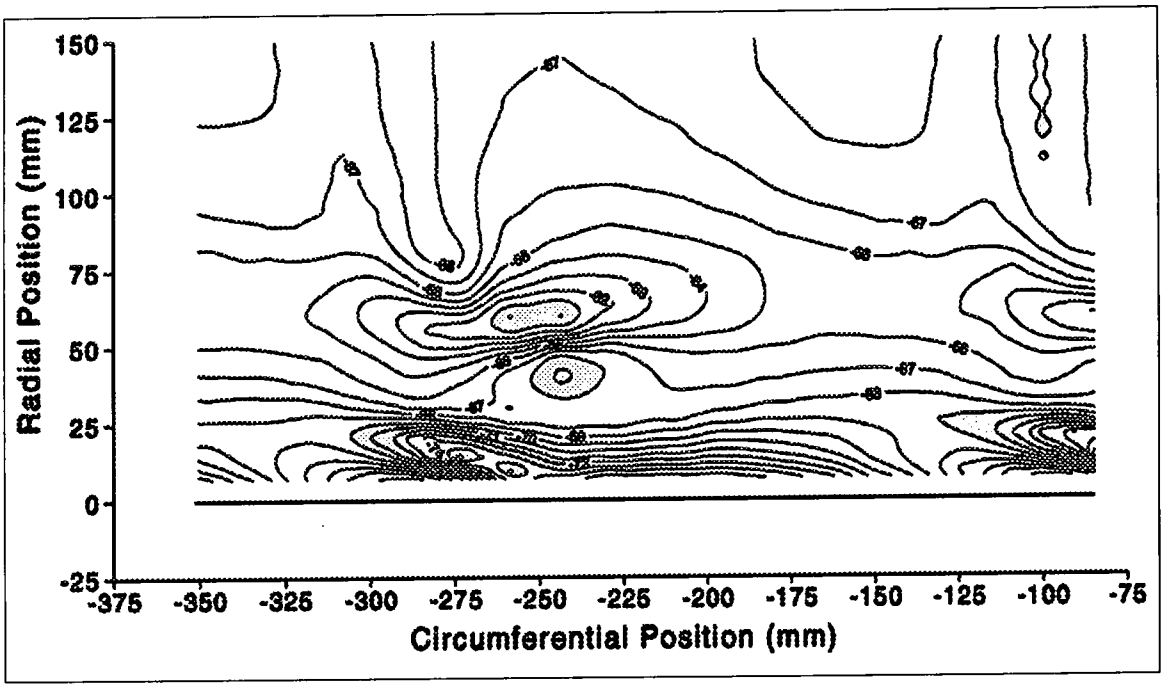

Profile 1 End Wall

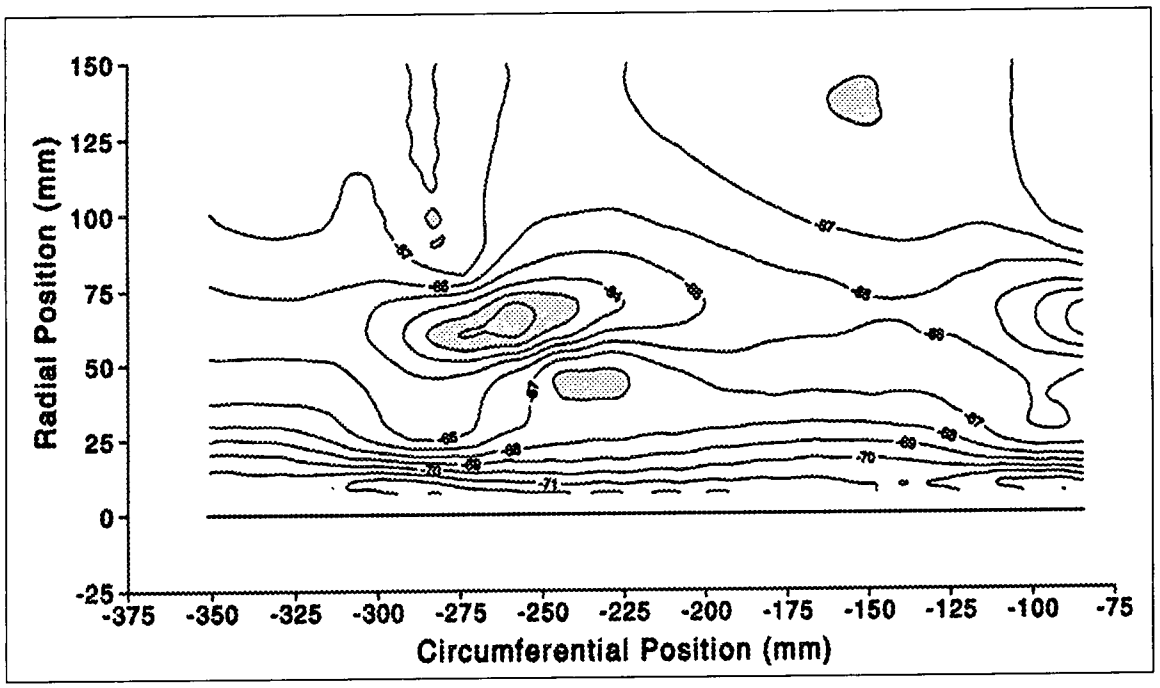

Profile 2 End Wall

Figure 4.14 Pitch Averaged Plots For Slot 10

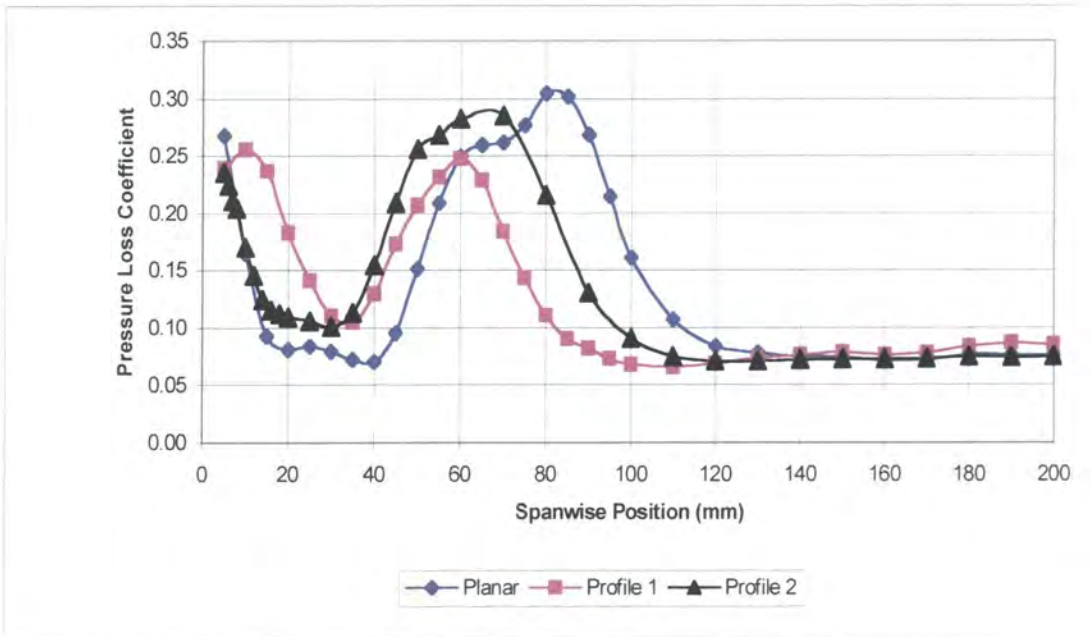

Figure 4.14 (a) Total Pressure Loss

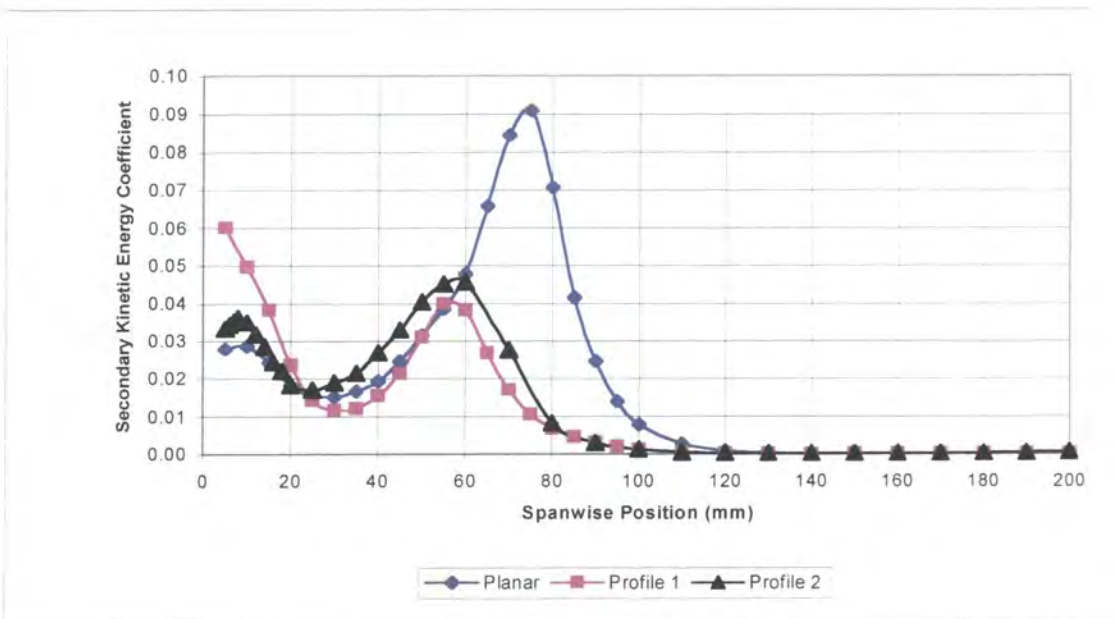

Figure 4.14 (b) Secondary Kinetic Energy

Figure 4.14 Pitch Averaged Plots For Slot 10 (cont.)

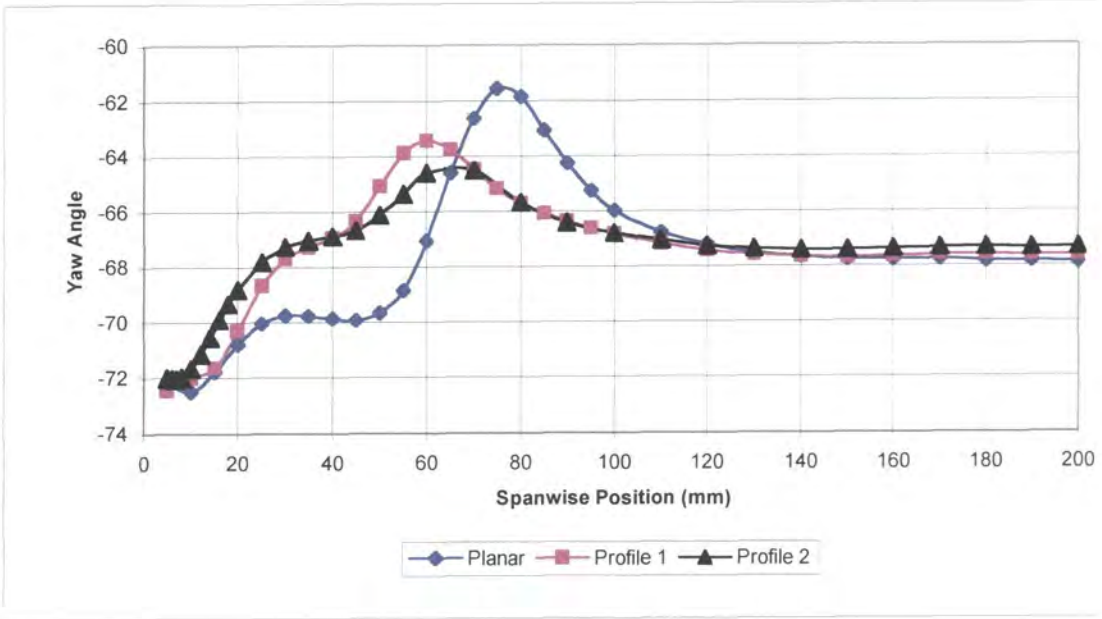

Figure 4.14 (c) Yaw Angle

Figure 4.15 Graphs For Net, Gross And Mixed-Out Loss For Slot 10

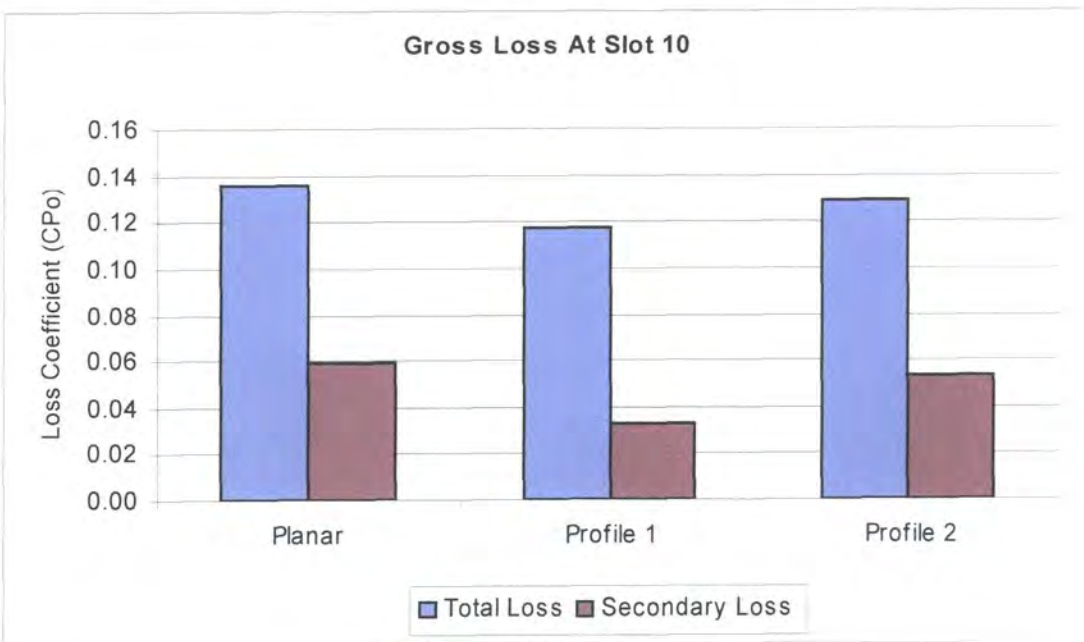

Figure 4.15 (a) Gross Loss At Slot 10

Figure 4.15 Graphs For Net, Gross And Mixed-Out Loss For Slot 10 (cont.)

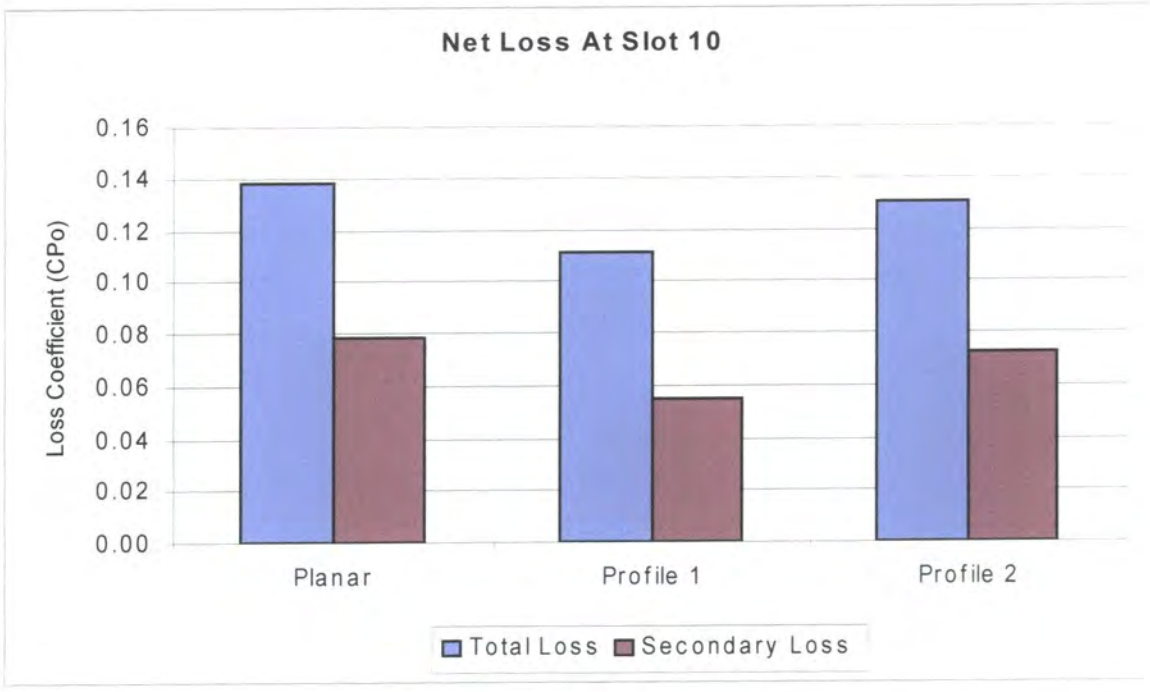

Figure 4.15 (b) Net Loss At Slot 10

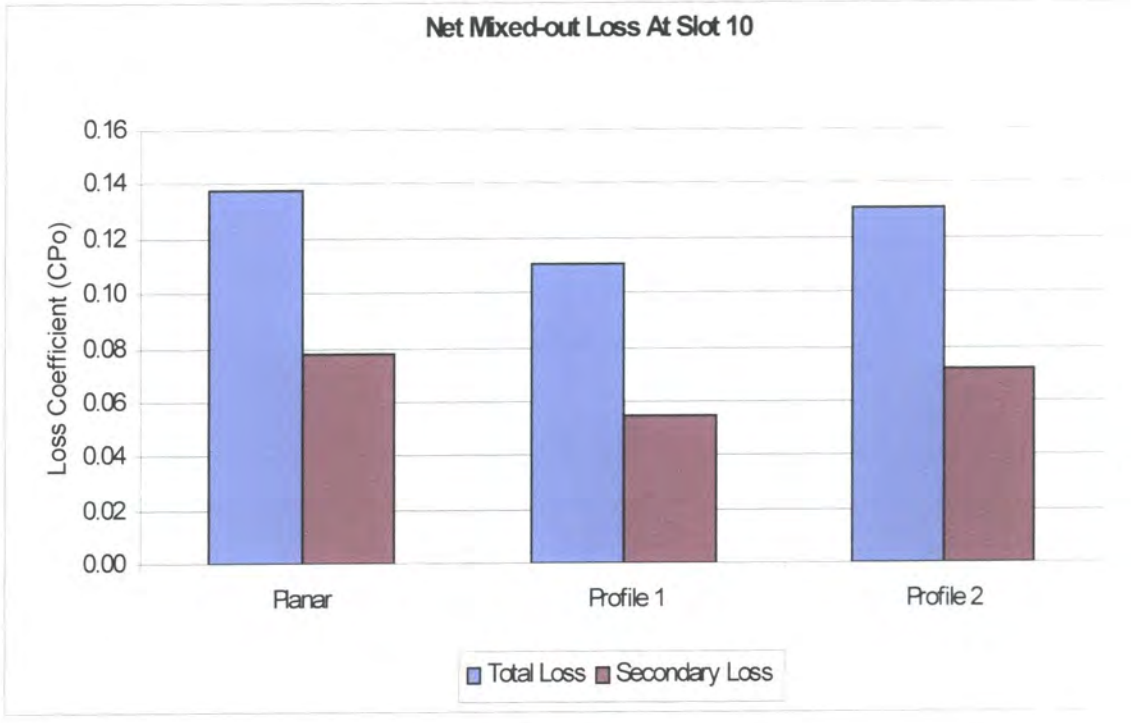

Figure 4.15 (c) Net Mixed-Out Loss At Slot 10

Figure 4.16 Location of Slots used for Flow Visualisation

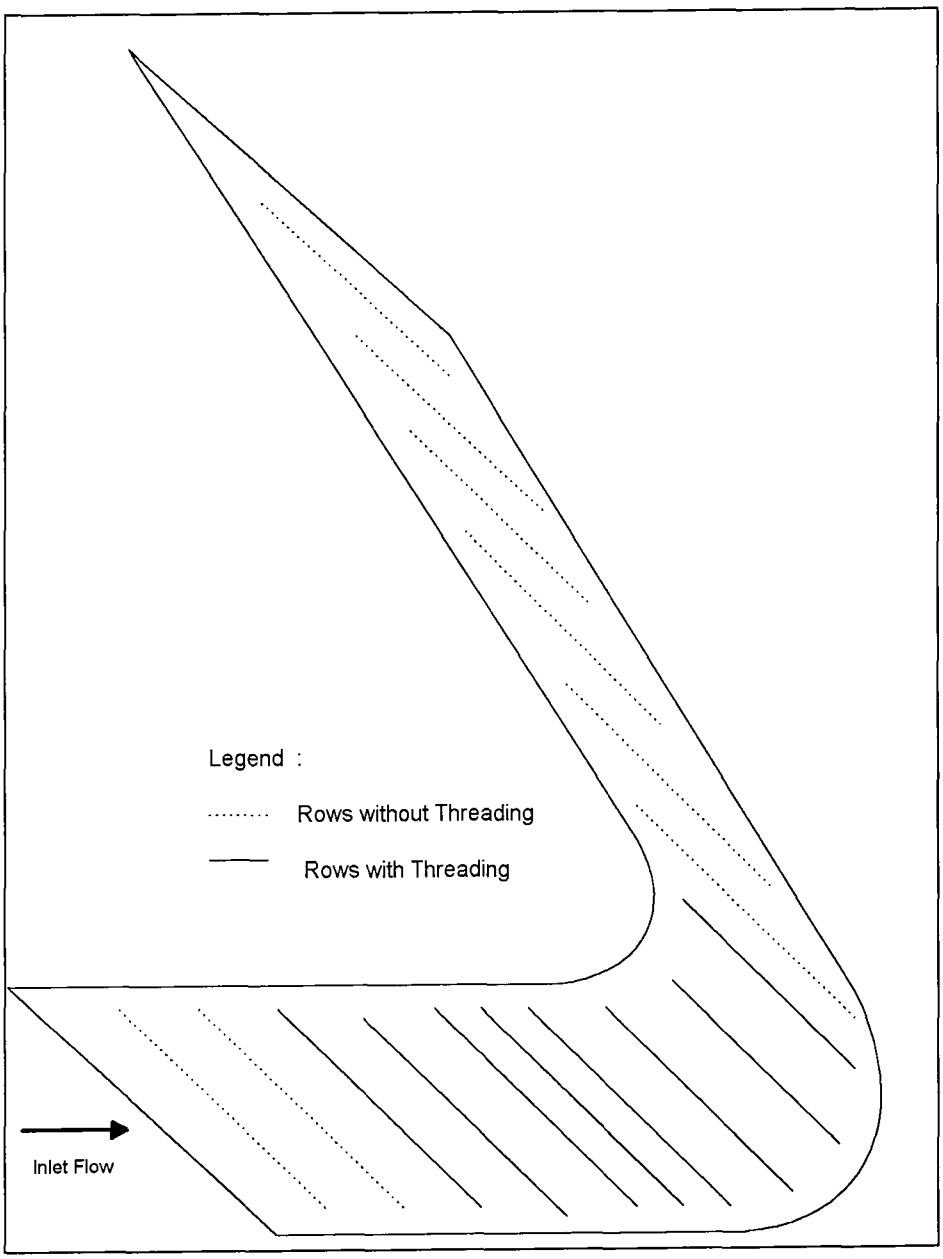

Figure 4.17 Video Clippings Of The Flow Visualisation

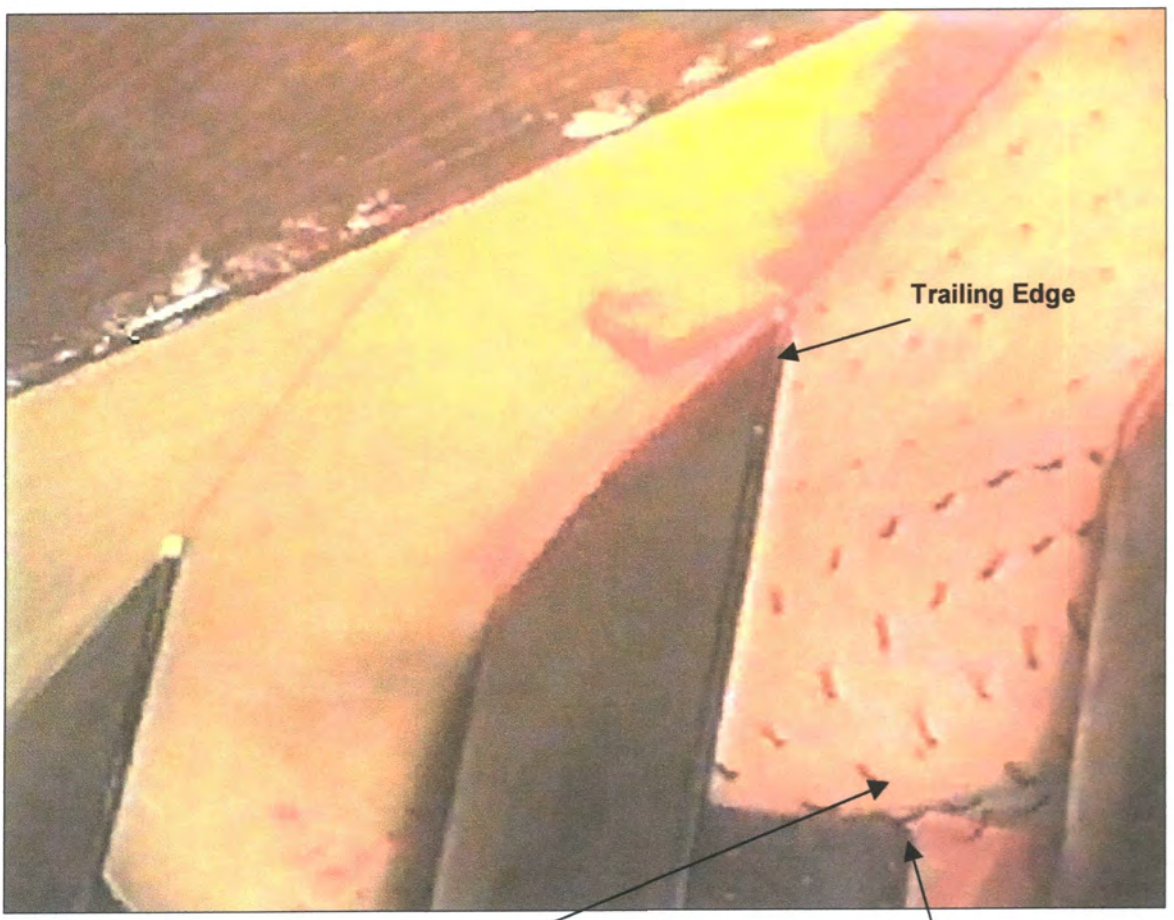

View from Downstream of Trailing Edge

Figure 4.17 Video Clippings Of The Flow Visualisation (cont.)

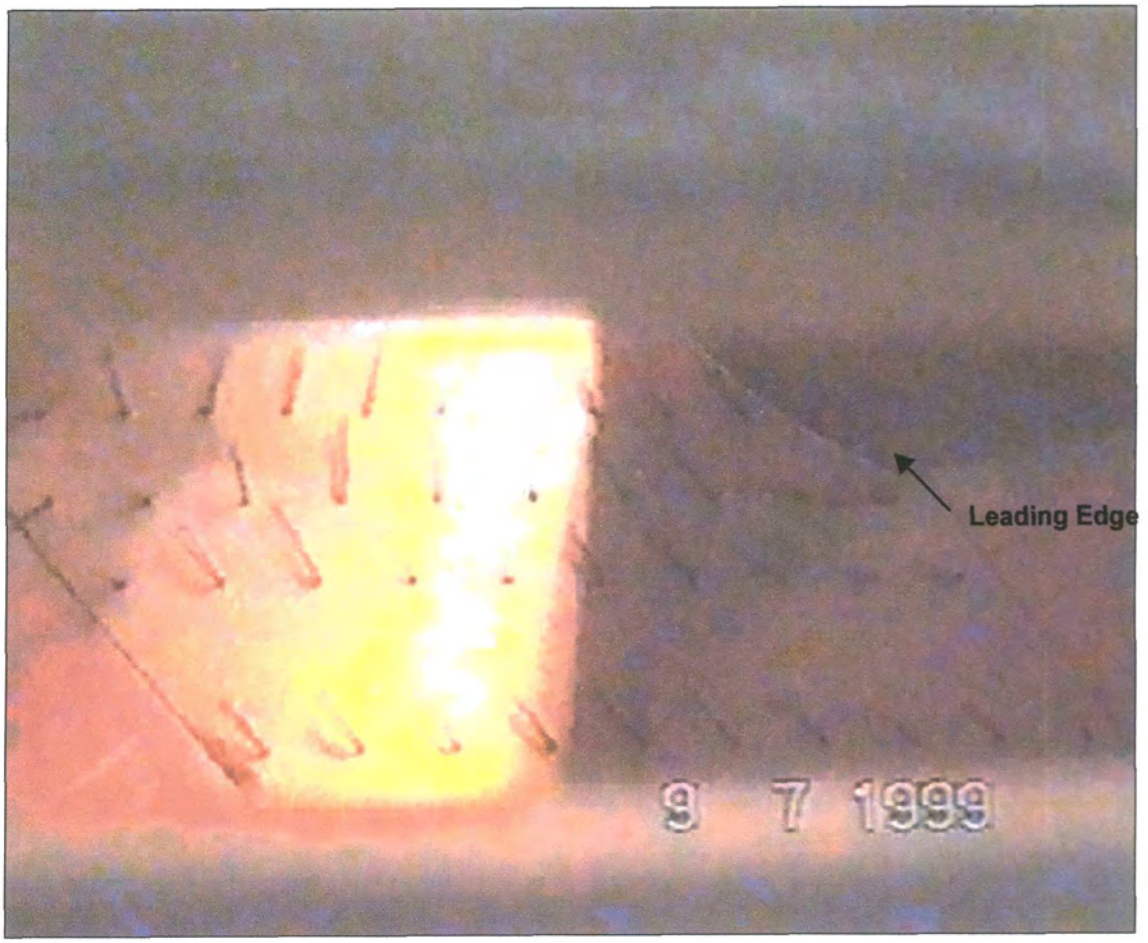

View Through Slot 1

Figure 4.17 Video Clippings Of The Flow Visualisation (cont.)

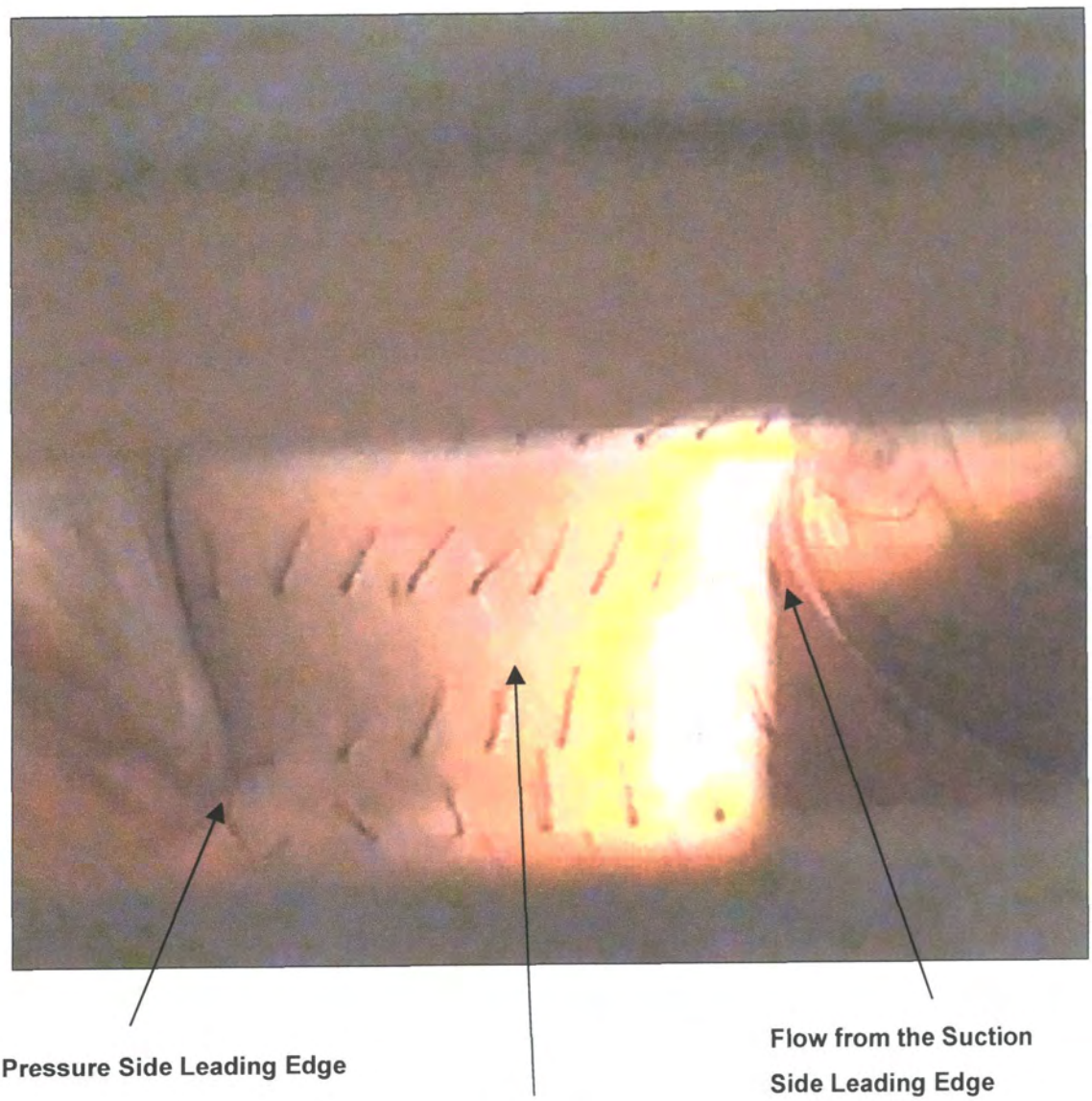

View Before Convex Curvature from Slot 1

Figure 4.18 **A Quantitative Picture of the Flow Visualisation**

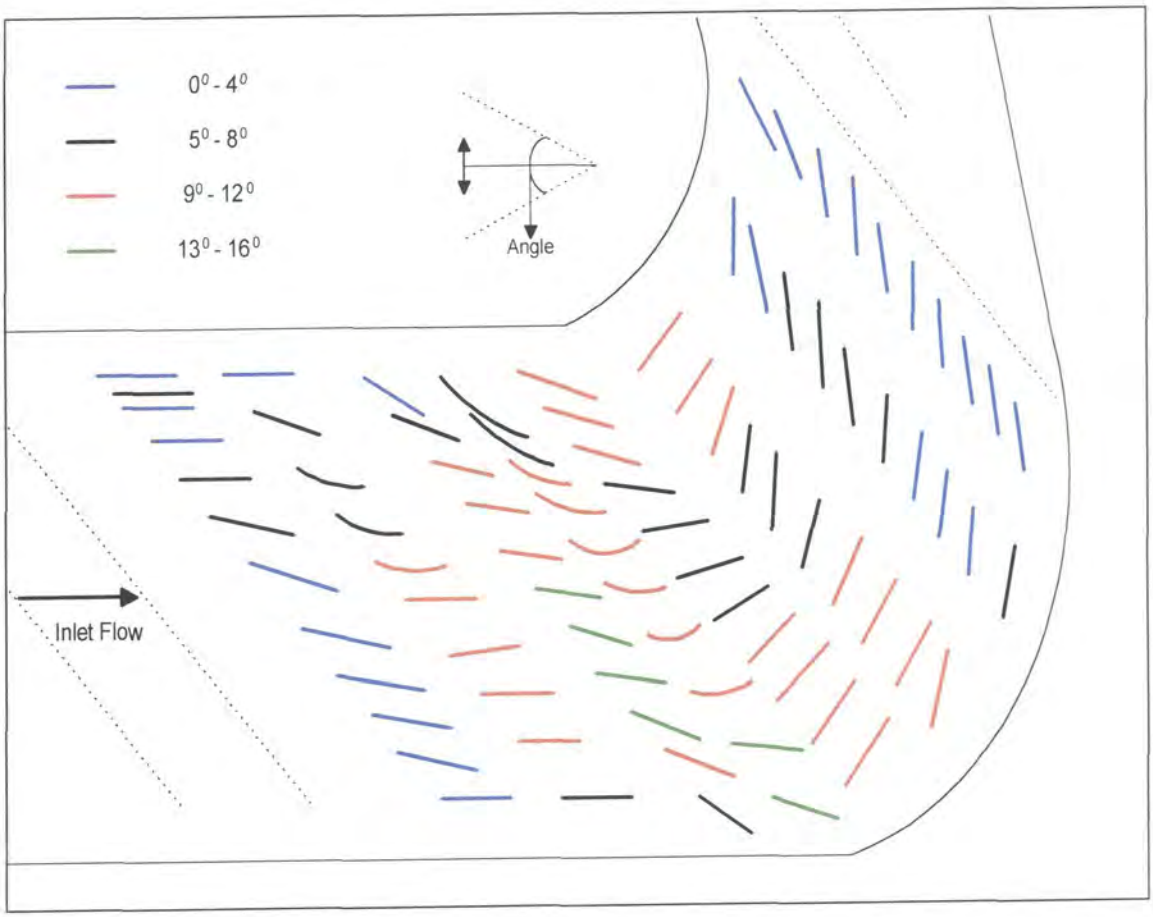

Chapter 5 Overview And Discussion

The primary aim of this work has been to investigate the effect of Profile 2 end wall on the secondary flows and losses downstream of the blades. This profile is designed with more practical features compared to its predecessor, Profile 1 end wall. It is intended to compare the performance of this new profile to Profile 1 and the Planar end wall. Profile 2 end wall is designed with a curvature that begins just downstream of the leading edge and ends just upstream of the trailing edge, so that it has practical application to real turbines.

Profile 2 end wall was manufactured out of polyurethane foam which has physical properties of being firm and durable. This profile was tested on the Durham linear cascade, which is a low speed, medium aspect ratio cascade. The cascade consists of 6 turbine rotor blades with a flow inlet angle of 42.5^0 and a blade exit angle of -68.7^0. The data acquisition system including the traverse gear, transducer and control software was designed and assembled. A five-hole probe was calibrated and used for the purpose of taking the pressure measurements. Static pressure tappings were also placed on the end wall surface.

An estimate on experimental errors was made. The most significant were $\pm$ 1^0 on angle and $\pm$ 0.005 on pressure coefficient. The angle error accounts for mid-span difference for Profile 2 end wall as seen in Figures 4.9c and 4.14c. However the differences in under and over turning are much more, which is an effect of the profile. Similarly, differences in pressure loss coefficient shown in Figures 4.9a and 1.14a are effects of the profile. This is much more than the

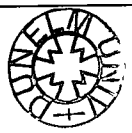

experimental uncertainty. Thus the overall conclusions are not significantly affected, except that the precise values of loss reduction figures which is discussed later (page 108 and 109) might need to be qualified.

Once the end wall was fixed onto the cascade, the inlet flow of the cascade was investigated. This was tested at a slot located –108% of the axial chord length which is slightly upstream of the leading edge. The results were presented in term of total pressure coefficient as in Figure 4.4. The results show that there is a hump in total pressure near the end wall, which gives shape to the graph seen. This is due to the wide gap between the last bar of the turbulence grid and the end wall. Although this gap is approximately 25 mm from the end wall, it appears that there is a jet flow with high energy produced which results in the unusual boundary layer profile. Nevertheless, the inlet profile is effectively identical for all three end walls signifying identical inlet flow conditions. It must also be noted that the small hump will not affect the secondary flow significantly.

The surface structure of Profile 2 end wall was then analysed through the static pressure measurements. Based on this analysis it would be expected that Profile 2 would cause less flow movement from the pressure surface to the suction surface downstream of the passage due to the more uniform static pressure observed on the suction surface. It is possible to raise the pressure on the suction surface and reduce that at the pressure surface by implementing the idea of non-axisymmetric end wall. Therefore, it is expected at this stage to achieve secondary flow reduction based on the more uniform pressure field that is observed in Profile 2 contour plot.

Downstream traverses of the profile were only done at Slot 8 and Slot 10. These two slots are located at the trailing edge and downstream of the trailing edge respectively. For this reason, it was not possible to analyse the flow from the leading edge up to the point measured. This has given some uncertainties regarding the flow evolution throughout the blade passage based on just the results of Slot 8 and 10. However, using the available data for the Planar and Profile 1 end wall and theoretical knowledge, it is possible to understand and estimate the flow progression from the leading edge to the trailing edge.

For both the traverses done for Slot 8 and Slot 10, the pitch averaging calculations were carried out over the range of the data. Within the blade passage the area extends from surface to surface while experimental data does not cover this whole area. This makes the data not strictly a representation of the three dimensional flow in the cascade. This effect can be quite considerable as can be seen from Figure 4.5, for example, where the velocity vectors close to the suction surface indicate high secondary kinetic energy, which is not included in the pitch averaging calculation. Since small variations in the data range can have a big effect on the pitch average, this may give misleading results.

Slot 8, which is located at 97% of the axial chord length, is just at the tip of the trailing edge. Here at the suction surface, the high velocity of the flow generates a great deal of secondary flow. At this stage, the passage vortex has already enlarged to its maximum size producing a loss core near the end wall suction surface corner. The vortex centre of the passage vortex has moved closer to the suction surface due to the strong pressure gradient between the two surfaces. The maximum values of secondary kinetic energy lie near the

suction surface corner. The same trend is seen with the total pressure loss contours.

The pitch average total pressure loss shows a high degree of loss from the end wall up to 80 mm to the mid span. After 80 mm, the loss is approximately zero indicating the decay of the three-dimensional flow and the beginning of the fully two-dimensional flow. In the range of 55 mm to 80 mm in radial position, there appears to be a negative loss on the graph. This is a flow characteristic that originated from the inlet boundary layer. It is thought that this negative value is due to some of the inlet boundary layer that has not migrated into the vortex but instead remains at its original spanwise position. As for the secondary kinetic energy, there is high amount of energy associated with the strong over-turning of the flow near the end wall. The yaw angles also show the strong under-turning and over-turning of the flow due the vortex movement.

The above general description applies to all three profiles. However, when the flow progression is compared between the profiles, there appears to be significant differences in the secondary flow development. Between Profile 1 and Profile 2 end wall, the two vortices near the end wall rotate much closer to each other in Profile 2 end wall compared to Profile 1 end wall. With Profile 2 end wall, it would seem that the passage vortex is almost merging with the smaller vortex seen on the left near the suction surface. The vortices in the profiled end walls are generally located much closer to the end wall compared to that in the Planar end wall. The other distinct difference seen in Profile 2 end wall is the presence of a very strong radial flow that is not seen in either of the Planar or

Profile 1 end wall. This has given rise to the high levels of secondary kinetic energy seen near the suction surface.

Profile 2 end wall also generates much lower under-turning and over-turning of the vortex compared to the Planar or Profile 2 end wall. One might expect that with the higher secondary kinetic energy due to the vortices in Profile 2 end wall, a large variation will be seen in yaw angle. This is not true because the secondary kinetic energy coefficient includes both the radial and circumferential flow, while the yaw angle only represent circumferential flows. The radial flow contributes rather largely towards the secondary kinetic energy contours and this is not reflected in the yaw angle contours. However, compared to the Planar end wall, both profiled end walls produce less under-turning and over-turning of the flow.

At Slot 10, the wake of the blade trailing edge becomes a dominant effect at the mid-span position. The development of the new boundary layer on the end wall and the convection effect of the secondary flow push the loss peak further away from the end wall for the Planar and Profile 2 end wall compared to Profile 1 end wall. The secondary flow here is much weaker than that at Slot 8 but it covers a larger area. This is more obvious with the Planar end wall than with the profiled end walls, owing to the reduced secondary flow with the profiled end walls. Profile 1 also appears to have a strong counter vortex near the end wall close to the suction surface. This is due to the low pressure region on the ridge of the surface.

Slot 10 is also the stage where the flow will experience the mixing process, where dissipation and diffusion are the dominant effects. Turbulent mixing causes the velocity differences to smooth out further downstream, thus giving rise to additional loss. Compared to the Planar end wall, the mixing process was slower in the profiled end walls. Profiled 1 end wall has moved the vortex slightly closer to the end wall while in Profile 2 end wall, there is not much difference in location. The secondary kinetic energy has also been significantly reduced with both the profiled end walls compared to the Planar end wall. However, between Profile 1 and Profile 2 end wall, Profile 2 end wall has actually generated a loss core that is further away from the end wall than in Profile 1 end wall. There is also a new boundary layer that is well developed on the end wall for the Profile 2 end wall. This boundary layer appears to have high levels of secondary kinetic energy, which is clearly reflected on the pitch-averaged secondary kinetic energy graph. However, since the secondary flow has been reduced due to the mixing, it was not possible to sweep this boundary layer into the vortex. Profile 2 has also produced less under-turning and over-turning of the flow.

Perhaps at this point one will raise the question 'Why did the loss appear to be higher in Slot 8 for Profile 2 end wall than in Slot 10 compared to the other two profiles?'. This misunderstanding could be due to the interpretation of the results. Slot 8 as has been mentioned before, is located just upstream of the trailing edge. It has not been possible to traverse the whole area, from blade surface to surface due to the size of the probe. The data has been processed and analysed only over the measured area and not extrapolated to the blade surface. It could be a possibility that the regions of high loss in the Planar and

Profile 1 end wall are actually located in the region not measured by the probe. Whereas with Profile 2 end wall, it is possible that there are higher secondary velocities in some areas that are convecting loss to a region where measurements are taken. Hartland [1999] who utilised CFD to predict the loss for the Planar and Profile 1 end wall, showed that the CFD calculation obtained more loss than that through experimental calculation. For Slot 8 the CFD calculation showed almost twice the total pressure loss calculated for the Slot 8 and 1.5 times compared to Slot 10.

The loss measured in Slot 10 is usually high due to the mixing process that occurs which in turn converts the available secondary kinetic energy of the flow into pressure loss. It could be also a possibility for Profile 2 end wall that most of the mixing has already occurred just before and during the Slot 8 stage. This is shown as high total pressure loss in the area averaged value. Then as the flow is mixed out, most of the high energy present in the fluid has already dissipated by the time it flows downstream of the trailing edge. At this point the area averaged total pressure loss value has relatively decreased and lies in between the Planar and Profile 1 end wall. This could also be another possible explanation to the question raised above.

One should also ponder on the question' Why is the secondary kinetic energy for Profile 1 and Profile 2 end wall similar and much less than the Planar end wall (i.e. reduced secondary flow) and yet the secondary loss for the Profile 2 end wall is much larger than Profile 1 end wall and nearly as much as the Planar end wall? '. This is contradictory to some loss correlations, which assume that the loss and secondary flows are linked. This could be largely due to the

profiling of Profile 2 end wall that starts with a sharp curvature at the inlet with restricted profiled length, which may be the region where separation could take place, causing extra loss. The flow visualisation shows that the flows are turned sharply at an angle near the convex curvature but do not indicate any reversed flow. There could probably be a three-dimensional separation, which requires further investigation. This could be a feature that was overlooked during the design stage.

Profile 2 has proved to reduce secondary flows and total pressure loss compared to the Planar end wall. It has reduced the mixed out loss by over 8% and the secondary loss by over 13%. However, Profile 1 has still appeared to be better than Profile 2. It has achieved a total and secondary loss reduction by over 15% and 34% respectively.

Chapter 6 Conclusions And Future Work

At present there are various techniques available aimed at reducing secondary flows in turbines from which end wall profiling has remained the most promising method. This research is focussed upon secondary flow reduction through end wall profiling. A new generation end wall, Profile 2 end wall, was designed at Rolls Royce plc. This end wall was then manufactured and tested. Following are the conclusions that can be drawn from the analysis of the results.

- The inlet boundary layer traverse results show that the inlet conditions of the flow for the three end walls are almost identical. Also, the range of measurement area for Profile 2 end wall is almost the same with the Planar and Profile 1 end wall, using a similar grid if not much finer. This shows that the results obtained from the testing of Profile 2 end wall are directly comparable to the Planar and Profile 1 end wall. Furthermore, testing at each Slot for the Profile 2 end wall has been repeated at least three times to ensure consistency of the results are maintained.

- Profile 2 end wall was designed using CFD within an inverse design method. It was thought that reducing the secondary flows and angle variations would certainly reduce the total loss. This is a reasonable assumption since it has been applied by previous workers. However, the experimental results have shown to be contradictory in some ways. The primary aim of reducing the secondary flows and angle variations compared to the Planar end wall has been achieved but it has

generated more loss when compared Profile 1 end wall. This could be due to a three dimensional flow separation at inlet near the pressure surface, which might be a contributor to the high total pressure loss seen with Profile 2 end wall and not with Profile 1 end wall.

- Profile 2 was tested at Slot 8 and Slot 10. Based on the results obtained, there was a question raised about the total pressure loss value from Slot 8 to Slot 10 for Profile 2 end wall compared to the Planar and Profile 1 end wall. This could be explained by a possible convection of loss by high secondary velocities to the region measured by the probe for the Profile 2 end wall. In the case of Planar and Profile 1 end wall, the loss may not have been convected to the region of measurement. Another possible explanation is the mixing process that begins to take place further upstream of the trailing edge and continues slightly downstream of the trailing edge, which gives rise to the high pressure loss value seen at Slot 8. Then as the flow progresses along, the mixing decreases and thus causing relatively reduced loss by the time it reaches Slot 10.

So far with the results at hand, it has only been possible to estimate the flow evolution from the leading edge to the trailing edge to a certain extent. These explanations have been supported by observations through CFD predictions made for the Planar and Profile 1 end wall and the flow visualisation carried out for Profile 2 end wall. However, it would be more advantageous if there were more results that could be used to analyse the flow in more detail.

The following lists possible future work that might be carried out to further understand the effects of Profile 2 end wall contour on the flow field.

- Testing should be carried out at Slots 1 to 7 and Slot 9. This would definitely provide a very detailed understanding of the flow in the blade passage. It could even shed some light on if there is any flow separation occurring at the pressure surface which is located further upstream of Slot 8. Similarly, flow visualisation using dye and diesel oil or a better technique should be repeated to provide a better picture of the flow in the passage.

- The experimental investigation of Profile 2 end wall or even the Planar and the Profile 1 end wall by Hartland only provides a partial picture of the flow field. This is due to the size of the probe used which limited the measurement area especially near the blade surfaces. The distance from the blade surface to the measurement area ranges between 20 mm to 35 mm. This distance is rather large compared to the size of the flow field that is being measured. There could be some flow activity that takes place in those regions. It would be an additional advantage if these left out areas were traversed using a more suitable probe of a smaller size. This is an important factor because similar situations will also be encountered upstream of Slot 8.

- It would also be beneficial to know how the CFD predictions for Profile 2 end wall will compare for those of Planar and Profile 1 end wall. This

will also shed some light on the possibility of loss being convected from the unmeasured region.

On the whole, Profile 2 end wall appears to stand between Planar and Profile 1 end wall in terms of its ability to reduce secondary flow and the related losses. As far as end wall profiling is concerned, it still shows promise for secondary flow reduction. However, this factor is also dependent upon the end wall profile shape. Profile 2 end wall has reduced secondary flows to some extent but still not quite as efficiently as its predecessor, Profile 1 end wall. Nevertheless, Profile 2 end wall can be further studied to understand how the curvature has effected the flow field. This information will be beneficial for future end wall profile designs.

References And Bibliography

Ainley D.G. and Mathieson G.C.R. [1951], *'An Examination of the Flow and Pressure Losses in Blade Rows of Axial Flow Turbines'*, N.G.T.E. Report R.86.

Arts T [1986], *'Effect of Tip End Wall Contouring on the Three-Dimensional Flow Field in an Annular Turbines Nozzle Guide Vane: Part 2 – Numerical Investigation'*, Journal of Engineering for Gas Turbines and Power, Vol. 108, pg. 426-428.

Atkins M J [1987], *'Secondary Losses and End Wall Profiling In A Turbine Cascade,'* Proceedings of the IMechE, Paper C255/87, pg. 29-42.

Barber T J, Langston L S [1979], *'Three Dimensional Modelling of Cascade Flows'*, 17th Aerospace Sciences Meeting.

Biesinger T E [1993], *' Secondary Flow Reduction Techniques in Linear Turbine Cascades'*, PhD Thesis, University of Durham.

Binder A [1985], *'Turbulence production Due to Secondary Vortex Cutting in a Turbine Rotor', Journal of Engineering for Gas Turbines and Power'*, Vol. 107, Pg. 1039-1046.

Binder A, Forster W, Mach K, Rogge H [1986],' *Unsteady Flow Interaction Caused by Stator Secondary Vortices in a Turbine Rotor'*, ASME Paper 86-GT-302.

Boletis E [1985], *'Effects of Tip End Wall Contouring on the Three- Dimensional Flow Field in an Annular Turbine Nozzle Guide Vane: Part 1 – Experimental Investigation'*, Journal of Engineering for Gas Turbines and Power, Vol. 107, pg. 983-990.

Came P.M., Marsh H. [1974], '*Secondary Flow In Cascades: Two Simple Derivations For The Components Of Vorticity*', Journal Of Mechanical Engineering Science, Vol. 16, pg. 391-401.

Cleak J G E [1989], '*Validation of Viscous, Three-Dimensional Flow Calculations in an Axial Turbine Cascade*', PhD Thesis, University of Durham.

Deich M E, Zaryankin A E, Filippov G A, Zatsepin M F [1960], *'Method Of Increasing The Efficiency of Turbine Stages With Short Blades*', AEI (Manchester) Ltd, Translation No 2816.

Denton J D [1993], '*Loss Mechanisms In Turbomachines*', Journal of Turbomachinery, Vol. 115, pg. 621-656.

Denton J D [1973], '*A Survey and Comparison of Methods for Predicting the Profile Loss of Turbine Blades*', Institution of Mechanical Engineers Conference Publication 3, pg. 204-212.

Duden A., Raab I., Fottner L. [1998],' *Controlling the Secondary Flow in a Turbine Cascade by 3d Airfoil Design and End Wall Contouring*', ASME Paper 98-GT-72.

Dunham J [1970],' *A Review of Cascade Data on Secondary Losses in Turbines*', Journal of Mechanical Engineering Science, Vol. 12, pg. 48-59.

Gaugler R E, Russell L M [1982],' *Flow Visualization Study of the Horseshoe Vortex in a Turbine Stator Cascade',* NASA Technical Paper 1884.

Glynn D.R. and H. Marsh [1980],' *Secondary Flow in Annular Cascades',* International Journal of Heat and Fluid Flow, Vol. 2, pg. 29-33.

Graves C P [1985], *'Secondary Flow And Losses In GasTurbines* ', PhD Thesis, University of Durham.

Gregory-Smith D G [1982], ' *Secondary Flows and Losses in Axial Flow Turbines*', Journal of Engineering for Power Vol. 104, pg. 819-822.

Gregory-Smith D G [1997], '*Secondary And Tip Clearance Flows In Axial Turbines, Lecture 1: Physics Of Secondary Flows*, Von Karman Institute for Fluid Dynamics course notes.

Gregory-Smith D G and Cleak J G E [1990],' *Secondary Flow Measurements in a Turbine Cascade with High Inlet Turbulence*', ASME Paper 90-GT-20.

Gregory-Smith D G and Graves C P [1983], *'Secondary Flows and Losses in Turbine Cascade*,' AGARD CP-351, 'Viscous Effects in Turbomachines', Paper no. 17.

Gregory-Smith D G and Biesinger [1993],'*Reduction In Secondary Flows and Losses in Turbine Cascade by Upstream Boundary Blowing*', ASME Paper 93-GT-114.

Gregory-Smith D G and Okan B M [1995], *'The Estimation of Secondary Flows and Losses in Turbines*', Proceedings of 1st European Turbomachinery Conference Turbomachinery-Fluid Dynamic and Thermodynamic Aspects, Germany.

Gregory-Smith D G and Walsh J A [1985],' *The Effect of Inlet Skew on the Secondary Flow and the Losses in a Turbine Cascade'*, Journal of Turbomachinery- Efficiency Production and Improvement, C275/87, pg. 15-28.

Gregory- Smith D G and Walsh J A [1989],'*Inlet Skew and the Growth of Secondary Losses and Vorticity in a Turbine Cascade',* ASME Paper 89-GT-65.

Gustafon B A [1977],' *Some Observation from Low Speed Cascade Tests Concerning Side Wall Boundary Layer Suction'*, AGARD –CP-214, Paper No. 19.

Han W, Wang Z, Tan C, Shi H, Zhou M [1994],*'Effects Of Leaning and Curving of Blades With High Turning Angles on the Aerodynamic Characteristics Of Turbine Rectangular Cascades'*, Journal of Turbomachinery, Vol. 116, Pg. 417-424.

Harrison S [1985], *'Secondary Loss Generation in a Linear Cascade of High-Turning Turbine Blades'*, ASME Paper 89-GT-47.

Harrison S [1990], *'The Influence of Blade Lean on Turbine Losses'*, ASME Paper 90-GT-55.

Hartland J C, Gregory-Smith D G, Rose M G [1998],' *Non-Axisymmetric End Wall Profiling in a Turbine Rotor Blade',* ASME Paper 98-GT-525.

Hartland J C, Rose M G, Harvey N W, Taylor M D, Shahpar S [1999],' *Non-Axisymmetric Turbine End Wall Design, Part 1: 3-Dimensional Linear Design System',* ASME Paper 99-GT-338.

Heinemann H J [1977],' *Influence Of Secondary Flow Effects on Blade Surface Pressure Measurements in Two-Dimensional Transonic Turbine Cascades'*, 12.1-12.14, AGARD-CP-214.

Hodson H P [1985], *'Boundary Layer Transition and Separation Near the Leading Edge of a High Speed Turbine Blade'*, Journal of Engineering for Gas Turbines and Power Vol. 107, pg. 127-134.

Hodson H P and Dominy R G [1986],' *Three-Dimensional Flow in a Low Pressure Turbine Cascade at its Design Condition'*, ASME 86-GT-106.

Horlock J.H. [1967], *'Some Recent Research in Turbomachinery'*, Proceedings of Institution of Mechanical Engineers, Vol. 182, pg. 571-594.

Horlock J.H and Lashiminarayana B [1963],' *Review: Secondary Flows and Losses in cascades and Axial Flow Turbomachines'*, International Journal of Mechanical Science, Vol. 5, pg. 287-307.

Joslyn H D, Dring R P, Sharma O P [1983], *'Unsteady Three-Dimensional Turbine Aerodynamics' Journal of Engineering for Power*, Vol.105, pg. 322-331.

Kawai T, Shinoki S, Adachi T [1989], *'Secondary Flow Control and Loss Reduction in a Turbine Cascade Using End Wall Fences'*, GSME International Journal, Vol. 32, No. 3, pg. 375-387.

Ken-ichi F, Yoshinori S, Tadashi T [1997],' *Experimental Studies on Unsteady Aerodynamic Loss of a High-Pressure Turbine Cascade'*, ASME Paper, 97-GT-52.

Langston L S [1980],' *Crossflows in a Turbine Cascade Passage'*, Journal of Engineering for Power, Vol. 102, pg. 866-874.

Langston L S, Nice M C, Hooper R M [1977],' Three-Dimensional Flow Within a Turbine Cascade Passage', Journal of Engineering for Power, pg. 21-28.

Marchal P, Sieverding C H [1977], *'Secondary Flows Within Turbomachinery Bladings'*, AGARD-CP-214 Paper No. 11.

Michelassi V, Martelli F, Corradini U [1998],' *Secondary Flow Decay Downstream of Turbine Inlet Guide Vane with End Wall Contouring*', ASME Paper 98-GT-95.

Mitchell J P, Huber F W [1993],' *Investigation of the Aerodynamic Performance of a Small Axial Turbine*', ASME Paper 93-GT-3.

Moore H [1995], *'Experiments in a Turbine Cascade for the Validation of Turbulence and Transition Models'*, PhD Thesis, University of Durham.

Moore J and Ransmayr A [1984],' *Flow in a Turbine Cascade: Part 1- Losses and Leading Edge Effects*', Journal of Engineering for Gas Turbines and Power, Vol. 106, pg. 400-408.

Moore J and Smith B L [1984],' *Flow in a Turbine cascade: Part 2- Measurement of Flow Trajectories by Ethylene Detection'*, Journal of Engineering for Gas Turbines and Power, Vol. 106, g 406-413.

Morris A W H, Hoare R G [1975], *'Secondary Loss Measurements in a Cascade of Turbine Blades with Meridional Wall Profiling'*, 75-WA/GT-13.

Moustapha S H, Paron G J, Wade J H T [1985], '*Secondary Flows in Cascades of Highly Loaded Turbine Blades*', Journal of Engineering for Gas Turbines and Power Vol. 107, pg. 1031-1038.

Prumper H [1988],' *Application of Boundary Layer Fences in Turbomachinery'*, Agard-AG-164,'Boundary Layer Effects in Turbomachines', pg. 311-331.

Rose M G [1994], *'Non-Axisymmetric End Wall Profiling in the HP NGV's of an Axial Flow Gas Turbine'*, ASME Paper 94-GT-249.

Schlichting H [1968],' *Boundary Layer Theory'*, 6th edition, Mc-Graw-Hill, New York.

Sieverding C H [1985], '*Recent Progress in the Understanding of Basic aspects of Secondary Flows in Turbine Blade Passages*', Journal of Engineering for gas Turbines and Power Vol. 107, pg. 248-257.

Sieverding CH [1975], '*Reduction of Secondary Losses in Turbines*', Von Karman Institute for Fluid Dynamics course notes.

Squire H B and Winter K G [1951], '*The Secondary Flow In A Cascade of a Airfoils in a Non-Uniform Stream'*, Journal of Aeronautical Science, pg. 271-277.

Tall W A [1977], '*Understanding Turbine Secondary Flow*', AGARD-CP-214.

Treaster A L and Yocum A M [1979],' *The Calibration and Application of Five-Hole Probes*, ISA Transactions, Vol. 18, pg. 23-34.

Wang Z, Lu W.L., Song Y, Xu W.Y. [1999],' *Effect of Blade Curving on the Flow Field Structure in an Annular Turbine Cascade*', ASME Paper 99-GT-69.

Yan J, Gregory-Smith D G, Ince N [1999(1)], ' *Profiled End Wall Design for a Turbine Nozzle Row*', Proceedings of the 3rd European Turbomachinery Conference, London.

Yan J, Gregory-Smith D G, Walker P J [1999(2)], ' *Secondary Flow Reduction in a Nozzle Guide Vane Cascade by Non-Axisymmetric End Wall Profiling*' ASME Paper 99-GT-339.

Yamamoto A and Nouse H [1988],' *Effects of Incidence on Three-Dimensional Flow in a Linear Turbine Cascade*', ASME Paper 88-GT-110.

Yamamoto A, Kondo Y, Muraq R [1990],' *Cooling Air Injection into Secondary flow and Loss Fields within a linear Turbine Cascade'*, ASME Paper 90-GT-141.

Appendix A Mixed-Out Loss Equations

By using the continuity and momentum equations, the area on any plane outside of the blade row may be extrapolated to a plane located at infinity. Here the flow would have 'mixed-out' to give a uniform velocity and pressure field and so 'mixed-out' total pressure loss coefficient may be calculated.

Assuming $V_{3\infty}$ = 0, by continuity

$$\int_0^h \int_0^s \rho V_1 dydz = \rho V_1 sh \text{ and therefore } V_{1\infty} = \frac{1}{sh} \int_0^h \int_0^s V_1 dydz$$

Equation A .1

By equating the tangential momentum

$$\int_0^h \int_0^s \rho V_1 V_2 dydz = \rho V_{1\infty} V_{2\infty} sh \text{ gives } V_{2\infty} = \frac{\int_0^h \int_0^s V_1 V_2 dydzz}{\int_0^h \int_0^s V_1 dydz}$$

Equation A .2

Equating the axial momentum gives

$$\int_0^h \int_0^s P dydz - P_\infty sh = \rho V_{\infty 1}^2 sh - \int_0^h \int_0^s \rho V_1^2 dydz$$

Equation A .3

Also,

$$\int_0^h \int_0^s C_{PS}\, dydz = \frac{1}{\frac{1}{2}\rho V_U^2} \int_0^h \int_0^s (P_U - P) dydz \qquad \text{Equation A .4}$$

Since P_U is a constant value, Equation A .4 becomes

$$\frac{1}{2}\rho V_U^2 \int_0^h \int_0^s C_{SU}\, dydz = P_U sh - \int_0^h \int_0^s P dydz \qquad \text{Equation A .5}$$

Combining Equation A .3 and A .5, will give

$$P_U sh - P_\infty sh = \rho V_{1\infty}^2 sh + \frac{1}{2}\rho V_U^2 \int_0^h \int_0^s C_{SU}\, dydz - \rho \int_0^h \int_0^s V_1^2 dydz$$

Equation A .6

Now after rearranging,

$$P_U - P\infty = \rho V_{1\infty}^2 + \frac{\frac{1}{2}\rho V_{U\infty}^2}{sh} \int_0^h \int_0^s C_{SU}\, dydz - \frac{\rho}{sh} \int_0^h \int_0^s V_1^2 dydz$$

Equation A .7

By applying the Bernoulli and defining the mixed out total pressure loss, $C_{TU\infty}$

$$C_{TU\infty} = \frac{P_{TU} - P_{T\infty}}{\frac{1}{2}\rho V_U^2} \qquad \text{Equation A .8}$$

will finally give

$$C_{TU\infty} = 1 + \frac{1}{V_U^2}\left[V_{1\infty}^2 - V_{2\infty}^2 + \frac{1}{sh}\left(V_U^2 \int_0^h \int_0^s C_{SU}\, dydz - 2\int_0^h \int_0^s V_1^2\, dydz\right)\right]$$

Equation A .9

Appendix B CNC Machining Details

The CFD grid provided by Rolls Royce plc. was converted to a grid file consisting of x, y and z co-ordinates. Once this was completed it was found that the grid file produced was too large in terms of memory consumption on the PC connected to the machine. Thus the grid file was broken into sections systematically according to their location and blade cutter requirements. This machining equipment is the CNC machine that is connected to an IBM PC, which utilises a software to facilitate the downloading of ASCII files. This software was written by Hartland for both the PC and CNC machine using C Programming.

This machine is capable of cutting light density materials using a grid file consisting of x, y, z co-ordinates representing the axial direction, tangential direction and the depth of movement respectively and an additional row containing a two digit command code. The three columns of the x, y and z co-ordinates must be of three real numbers with the command code being either 11, 22 or 33. This is shown in Table 3.4. The number 123001 must be added at the beginning of the file to initiate the machining cycle of the CNC machine. This is a security measure to avoid spurious co-ordinates from any data buffers from being read. Comments can also be added to the data file and these will be echoed on the PC screen but not transmitted to the CNC machine. These inserted comments have to be enclosed with the '#' symbols which must be separated from other test or numbers by a space or tab mark.

Command Code	Function
11	Move rapidly to x, y, z
22	Machine to x, y, z at a pre-set feed rate
33	Move rapidly to x, y, z then stop the tool and terminate the CNC program.

Table B.1 Data File Command Codes

The C program written reads the ASCII files as described above, echoing the data and comments on the screen. The comments are then ignored and the data is sent to the serial port on the PC. When the CNC program is started, the program continuously reads in the number from the serial port until it receives the numbers 123001. The program then starts the machine tool spinning, then reads in an integer from the serial port until it reads in an integer followed by the three coordinate figures. At the end of the file, the program automatically stops itself. The last command on the ASCII file has to be 33 to switch of the CNC machine once the work is completed. An example of the grid file used for the machining of the end wall is shown in the next page.

Example Of An End Wall Machining Grid File

```
  #     123001      starts      cycle #
  123001
  #     Move up to clear surface then move to start     #
11      0           0           10
11      165.595     60.000      10
  #     Start machining   cycle #
  #     Start pass  70    #
22      165.595     60.000      -25.000
22      164.595     60.000      -25.000
22      159.595     60.000      -25.000
22      154.595     60.000      -25.000
22      149.595     60.000      -25.000
22      144.595     60.000      -25.000
22      139.595     60.000      -25.000
22      134.595     60.000      -25.000
22      129.595     60.000      -25.000
22      124.595     60.000      -25.000
22      119.595     60.000      -25.000
22      114.595     60.000      -25.000
22      109.595     60.000      -25.000
22      104.595     60.000      -25.000
22      99.595      60.000      -25.000
22      94.595      60.000      -25.000
22      89.595      60.000      -25.000
22      84.595      60.000      -25.000
22      79.595      60.000      -25.000
22      74.595      60.000      -25.000
22      69.595      60.000      -25.000
22      64.595      60.000      -25.000
22      59.595      60.000      -25.000
22      54.595      60.000      -25.000
22      49.595      60.000      -25.000
22      44.595      60.000      -25.000
22      39.595      60.000      -25.000
22      34.595      60.000      -25.000
22      29.595      60.000      -25.000
22      24.595      60.000      -25.000
22      19.595      60.000      -25.000
22      14.595      60.000      -25.000
22      9.595       60.000      -25.000
22      4.595       60.000      -25.000
22      -0.405      60.000      -25.000
22      -5.405      60.000      -25.000
22      -10.405     60.000      -25.000
22      -15.405     60.000      -25.000
22      -20.405     60.000      -25.000
22      -25.405     60.000      -25.000
  #     Move up to clear surface then stop  #
33      25.031      1.010       10.000
```

Appendix C Probe Calibration Map

An example of a calibration map produced for the five-hole probe. The angle intervals are 5°, ranging from –25° to 25° in both pitch and yaw direction.

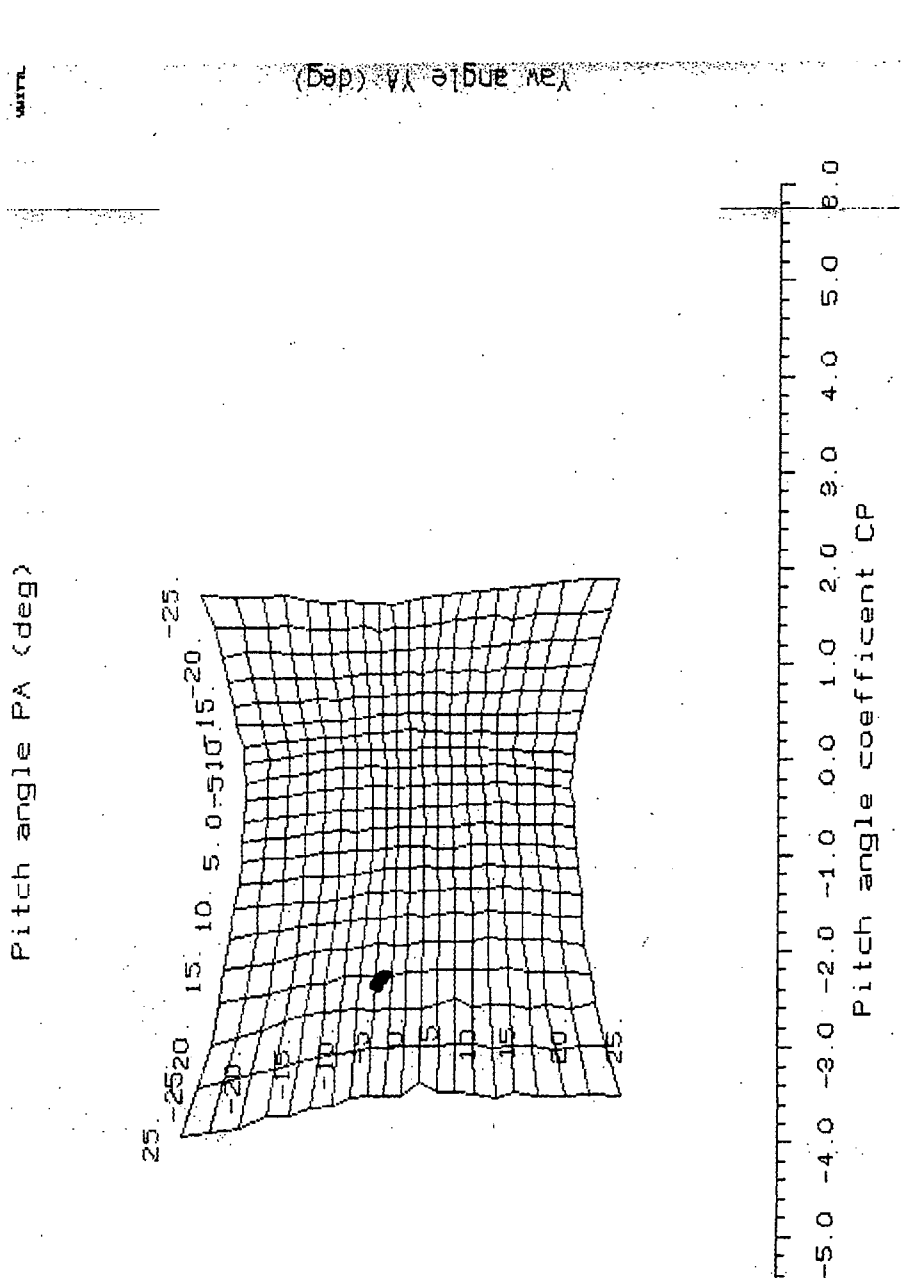

Appendix D Net, Gross and Mixed-Out Results

Gross Loss at Slot 10

Loss at Slot 10	Total Loss	Profile Loss	Secondary Value	% Planar
Planar End Wall	0.1355	0.0761	0.0595	100
Profile 1 End Wall	0.1044	0.0711	0.0333	56.1
Profile 2 End Wall	0.1286	0.0750	0.0536	90.1

Loss at Slot 1	Total Loss	Profile Loss	Secondary Value
Planar End Wall	-0.0022	0.0163	-0.0185
Profile 1 End Wall	-0.0063	0.0154	-0.0218
Profile 2 End Wall	-0.0022	0.0163	-0.0185

Net Loss at Slot 10

	Total Loss	Profile Loss	Secondary Value	% Planar
Planar End Wall	0.1377	0.0598	0.0780	100
Profile 1 End Wall	0.1108	0.0557	0.0551	70.7
Profile 2 End Wall	0.1308	0.0587	0.0721	92.5

Gross Mixed-Out Values at Slot 10

Loss at Slot 10	Total Loss	Profile Loss	Secondary Value	% Planar
Planar End Wall	0.1572	0.0790	0.0782	100
Profile 1 End Wall	0.1273	0.0834	0.0439	56.2
Profile 2 End Wall	0.1442	0.0782	0.0660	84.4

Loss at Slot 1	Total Loss	Profile Loss	Secondary Value
Planar End Wall	-0.0017	0.0163	-0.0179
Profile 1 End Wall	-0.0072	0.0125	-0.0197
Profile 2 End Wall	-0.0017	0.0163	-0.0179

Net Mixed-Out Values at Slot 10

	Total Loss	Profile Loss	Secondary Value	% Planar
Planar End Wall	0.1588	0.0627	0.0961	100
Profile 1 End Wall	0.1345	0.0709	0.0636	66.2
Profile 2 End Wall	0.1458	0.0619	0.0839	87.3